CENTRAL AND PERIPHERAL MECHANISMS OF PAIN AND ITCH

by
Shuohao Sun

A thesis submitted to Johns Hopkins University in conformity with the requirements for the degree of Doctor of Philosophy

Baltimore, Maryland

October, 2016

ABSTRACT

Pain and itch are two distinct yet related sensations. Here we present a series of experiments elucidating mechanisms of pain and itch in central and peripheral nervous systems. Coding of itch versus pain has been hotly debated for decades. However, the current coding theories (labeled line, intensity and selectivity theory) cannot accommodate all experimental observations. We identified a subset of spinal interneurons, labeled by gastrin releasing peptide (*Grp*), that receive direct synaptic input from both pain and itch primary sensory neurons. When activated, these Grp^+ neurons generated rarely-seen *simultaneous* robust pain and itch responses that were intensity-dependent. Accordingly, we propose a "leaky gate" model, in which Grp^+ neurons transmit both itch signals and weak pain signals (ensuring pain sensitivity) through the "gate", but recruit endogenous opioid systems to close the "gate" upon strong painful stimuli to prevent overwhelming pain. Consistent with our model, loss of these Grp^+ neurons increased pain responses while itch was decreased. Our new model incorporates currently underappreciated non-monotonic coding in the spinal cord and better explains observations in human psychophysical studies. We also explored peripheral mechanisms mediating protease induced itch. Various endogenous and exogenous proteases can trigger intense itch sensation, presumably via Protease-Activated-Receptor, PAR2. Here we demonstrate that in contrary to the current hypothesis, cysteine proteases including cathepsin S, activate dorsal root ganglion neurons and elicit scratching through Mas-related G protein coupled receptor, MrgprC11, but not PAR2. In contrast to its activation of conventional protease-activated receptors, cathepsin S-mediated activation of MrgprC11 did not involve the generation of a tethered ligand. This expansion of our understanding by which proteases interact with G-protein-coupled receptors (GPCRs) redefines the concept of what constitutes a protease-activated receptor. The findings also implicate

proteases as endogenous ligands to members of this orphan receptor family while providing new insights into how cysteine proteases contribute to itch.

Thesis Advisor

Xinzhong Dong, Ph.D.

Thesis Committee

Michael J. Caterina, M.D., Ph.D.

Dwight E. Bergles, Ph.D.

Jeremy Nathans, M.D., Ph.D.

ACKNOWLEDGEMENTS

I would first like to thank my advisor, Dr. Xinzhong Dong for his guidance and encouragements. He is always so energetic and so enthusiastic about science. His enthusiasm and optimism warmed me up in bad days and his wise judgment kept me on track in good days. He is also so nice and patient. His wonderful personalities forge this lab to be such a friendly and collegial place, which I will always cherish. Being both an extraordinary scientist and a wonderful mentor, Xinzhong was, is and always will be a role model for my scientific career.

I would also like to express my appreciation for my collaborators: lab mate, Dr. Qian Xu and Dr. Ethan Lerner and Dr. Vemuri Reddy from Mass General Hospital. My success in graduate school is due in no small part to the fruitful collaborations with them. My thesis committee, Dr. Mike Caterina, Dr. Dwight Bergles and Dr. Jeremy Nathans provided continuous inspiration and advices, which I'm thankful to.

I also want to recognize my former and current lab mates, Dr. Qin Liu, Dr. Zongxiang Tang, Dr. Liang Han, Yixun Geng, Dr. Hao-jui Weng, Dr. Zhe Li and Dr. Colleen Lavinka for their friendship, opinions and contributions. They have made my time in the lab memorable and fun.

Last but not least, I will always be indebted to my parents Lianyuan Sun and Yanping Zhang and my fiance Shuaiqi Yuan, whom I met during graduate school for their unconditional love and support, without which I could never manage to accomplish this.

TABLE OF CONTENTS

LIST OF TABLES

LIST OF FIGURES

CHAPTER 1: INTRODUCTION

Itch, also known as pruritus, is defined as an "unpleasant sensation that elicits the desire or reflex to scratch"(Ikoma et al., 2006) and can be distinguished as acute and chronic forms with the latter lasting more than six weeks(Ständer et al., 2007). Itch can be caused by various stimuli including those that are mechanical, electrical and chemical, with exogenous and endogenous chemical stimuli ranging from amines, proteases, neuropeptides to inflammation mediators and certain drugs (see Table 1.1)(Akiyama and Carstens, 2013). Acute itch, such as that caused by a mosquito bite, is commonly experienced in daily life and has a protective role as to remove irritants and avoid future insults. Histamine mediated itch is well studied, while non-histaminergic itch attracts more and more attention in recent year. Histamine and non-histamine itch seem to activate largely non-overlap projection neurons in the spinal cord(Akiyama et al., 2009; Davidson et al., 2007) and non-histaminergic projection neurons were found to terminate in more thalamic nuclei(Davidson et al., 2012). The mechanical pain generated by scratching can usually suppress acute itch, however chronic itch conditions commonly accompanied with co-morbidities, such as depression and sleep disorders, can be debilitating and remain unmet clinical needs. Chronic itch conditions are generally divided into four categories: dermatological, systemic, neurological and psychogenic. Dermatological itch comes from skin conditions such as atopic dermatitis, psoriasis and urticaria. Systemic itch can be caused by pathology of other organs, for example liver cholestasis and kidney dialysis. Neurological itch is caused by direct damage to the nervous system either peripherally or centrally. Finally, psychogenic itch is associated with psychological and psychiatric disorders. This chapter is modified from previous publication(Sun and Dong, 2016).

Pain and itch are two distinct yet related sensations. Itch sensation is initiated in the skin while pain sensation in muscles and internal organs in addition to skin. Both pain and itch are

detected by peripheral afferents of similar small diameter primary sensory neurons, with cell bodies located in dorsal root ganglia (DRG) and trigeminal ganglia. These sensory signals are then carried by small unmyelinated C fibers and lightly myelinated Aδ fibers with slow conduction velocities to the spinal dorsal horn and further to the brain. Yet pain and itch trigger distinct behavioral responses. Pain generates a withdrawal response to avoid tissue damage, while itch elicits scratching to remove irritants. Pain can suppress itch, which is demonstrated when the mechanical pain generated by scratching relieves the itchy feeling (Davidson et al., 2009). Itch, however, can rarely suppress pain.

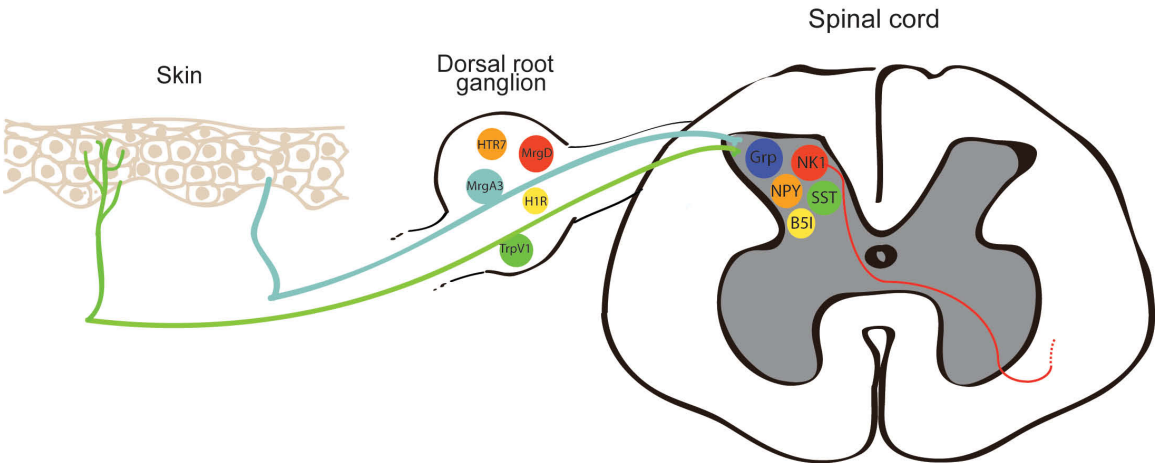

Figure 1.1 Diagram of pain and itch pathways in DRG and the spinal cord

Pain and itch signals from periphery transmit to DRG, spinal cord and then further to the brain. Representative subsets of DRG neurons: TrpV1 and MrgD marks subsets of peptidergic and non-peptidergic nociceptors respectively; H1R, MrgA3 and HTR7 marks pruriceptive subsets responsive to histamine, chloroquine and serotonin respectively. Representative subsets of spinal cord neurons: NK1 marks projection neurons sending output to higher brain areas; Grp and SST marks excitatory interneuron populations involved in pain and itch transmission; B5I and NPY marks inhibitory interneuron populations responsible for inhibition of chemical and mechanical itch by pain respectively.

DRG neurons have pseudo-unipolar morphologies, sending output to spinal cord. In addition to the classic distinction of peptidergic and non-peptidergic nociceptors, for example as labeled by TrpV1 and MrgD(Cavanaugh et al., 2009; Mishra et al., 2011), respectively in Figure 1.1, new markers for pruriceptive subsets have recently been established. Multiple Mas-related G protein coupled receptors (Mrgs) were found to be itch receptors, including MrgA3 responsive to chloroquine(Liu, 2009), MrgC11 to BAM and SLIGRL(Liu, 2009, 2011) and subset of MrgD to β-alanine(Liu et al., 2012). Unlike DRG neurons, which all serve output functions, only a small subset of dorsal horn neurons transmit signals further to the brain(Spike et al., 2003), as marked by NK1(Todd et al., 1998) in Figure 1.1. The remaining majority are interneurons forming interlacing spinal circuitries. Interneurons in superficial lamina have been carefully characterized based on their morphologies and firing patterns(Grudt and Perl, 2002), yet their functions remain largely elusive. In the past few years, several genetically labeled populations(Bourane et al., 2015a; Duan et al., 2014; Kardon et al., 2014), including SST, B5I and NPY as shown in Figure 1.1, have been defined with functions relating to pain and itch, promoting the functional dissection of complex spinal cord circuitries.

On the cellular level, neurons responsive to itchy stimuli in both DRG and the spinal cord can also be activated by pain (Akiyama et al., 2009; Davidson et al., 2007; Jansen and Giesler, 2015; Liu et al., 2009; Schmelz et al., 2003), begging the question how these two sensations are distinguished (Figure 1.1). Indeed, itch used to be regarded as a sub-modality of pain because of their similarities. One related theory is called intensity theory, stating that weak and strong activation of the same group of neurons generates itch and pain sensations respectively(Von frey, 1922; Lewis et al., 1927; Patel and Dong, 2010). Another competing theory is called labeled line theory, which, in contrast, proposes mutually exclusive populations for the detection of itch and

pain(Norrsell et al., 1999). It is clear now that itch is a distinct sensation from pain. Loss of the gastrin releasing peptide receptor (GRPR) population in the spinal cord resulted in a profound defect of itch behaviors, but pain responses remained intact unequivocally demonstrating the existence of separable itch and pain pathways(Sun et al., 2009). However itch neurons are almost exclusively poly-modal. They respond to painful stimuli such as capsaicin or mustard oil in addition to itchy stimuli(Liu et al., 2009; Schmelz et al., 2003; Wilson et al., 2011). The coding puzzle of itch and pain is better explained by selectivity theory. When the itch population is selectively activated, an itchy sensation is generated, regardless of the stimuli. In contrast, when an algogen activates a larger population, including both pain and itch sensing neurons strong enough, itch is occluded by inhibition from pain neurons, just as scratching induced pain inhibits itch and therefore only pain sensation is perceived. Although being two separate sensations, itch and pain share common downstream pathways, such as Trp (transient receptor potential) channels.

Table 1.1 Pruritogens and related itch transduction mechanisms

	Pruritogen	Receptor	Channel	Signaling
G protein couple receptors	Histamine	H1R, H4R(Bell et al., 2004; Dunford et al., 2007)	TrpV1(Imamachi et al., 2009)	PLCβ3(Han et al., 2006; Imamachi et al., 2009), IP3(Nicolson et al., 2002),Ca^{2+}(Kim et al., 2004; Thurmond et al., 2008),PLA2/LO(Kim et al., 2004)
	Chloroquine	MrgprA3(Liu et al., 2009)	TrpA1(Wilson et al., 2011)	Gβγ(Wilson et al., 2011)
	BAM	MrgprC11(Liu et al., 2009)	TrpA1(Wilson et al., 2011)	PLC(Wilson et al., 2011)
	Cathepsin S	MrgprC11(Reddy et al., 2015)		
	Tryptase	PAR2, IL7α(Wilson et al., 2013)		
	Serotonin	5-HT2(Yamaguchi et al., 1999), 5-HT7(Morita et al., 2015)	TrpA1(Morita et al., 2015)	PLCβ3(Imamachi et al., 2009), AC, Gβγ(Morita et al., 2015)
	12(S)-HPETE	LTB4 receptor 2(Kim et al.,		

Cytokine receptors		2008b), 5-HT1, 5-HT2(Kim et al., 2008a)		
	Endothelin	ETa(Trentin et al., 2006)	TrpA1(Gomes et al., 2012)	PKC, AC(Liang et al., 2010)
Toll like receptors	Cathepsin E	ETa(Andoh et al., 2012)		
	Bradykinin	B2R(Bandell et al., 2004; Wang et al., 2008)	TrpV1(Bautista et al., 2006; Kim et al., 2004), TrpA1(Bandell et al., 2004; Bautista et al., 2006; Wang et al., 2008)	PLA2/LO(Kim et al., 2004), PLC(Bautista et al., 2013)
Direct channel activation	Substance P	NK1R(Andoh et al., 1998)		NO(Andoh and Kuraishi, 2003), LTB4(Andoh et al., 2001)
	Bile acids	TGR5(Alemi et al., 2013)	TrpA1(Lieu et al., 2014)	PKC, Gβγ(Lieu et al., 2014)
	LPA	LPA1, LPA3(Shimizu et al., 2014)		Rho/ROCK(Hashimoto et al., 2004)
	LTB4	LTB4 receptor 2(Fernandes et al., 2013)	TrpV1, TrpA1(Fernandes et al., 2013)	RO(Fernandes et al., 2013)
	LTD4	Cysltr2(Usoskin et al., 2014)		
	TXA2	TP receptor(Andoh et al., 2007)		
	β-alanine	MrgprD(Liu et al., 2012)		
	TSLP	TSLPR, IL7α(Wilson et al., 2013)	TrpA1(Wilson et al., 2013)	PLC(Wilson et al., 2013)
	IL31	IL31RA(Cevikbas et al., 2014), OSMR(Cevikbas et al., 2014; Kasraie et al., 2011)	TrpV1, TrpA1(Cevikbas et al., 2014)	ERK(Cevikbas et al., 2014)
	IL13		TrpA1(Oh et al., 2013)	
	Imiquimod	TLR7?(Liu et al., 2010)		K2P, Kv1.1, Kv1.2(Lee et al., 2012)
	LPS (no direct itch)	TLR4(Min et al., 2014)		
	Oxidants		TrpA1(Andersson et al., 2008; Liu and Ji, 2012)	

Abbreviation: RO, reactive oxygen.

CHAPTER 2: LEAKY GATE MODEL: INTENSITY-DEPENDENT CODING OF PAIN AND ITCH IN THE SPINAL CORD

Introduction

Pain and itch trigger distinct behaviors, yet itch responsive neurons in both DRG and spinal cord also respond to painful signals (Akiyama et al., 2009; Davidson et al., 2007; Liu et al., 2009; Schmelz et al., 2003), begging the question how these two sensations are distinguished. Debates about pain and itch coding have been on-going for decades. The intensity theory (Figure 2.1A) claims that poly-modal neurons can be stimulated strongly or weakly to generate pain or itch sensations respectively(Von frey, 1922; Lewis et al., 1927). However, weaker painful stimuli or stronger itchy stimuli fail to turn into a different sensation, as predicted by the intensity theory, rendering it untenable(Handwerker et al., 1991; Ochoa and Torebjörk, 1989; Tuckett, 1982). The labeled line theory (Figure 2.1B) argues that different senses are coded by mutually exclusive populations(Norrsell et al., 1999; Schmelz et al., 1997), but cannot explain the existence of poly-modal neurons. A modified labeled line theory, termed selectivity theory (Figure 2.1C) (Handwerker, 1992; McMahon and Koltzenburg, 1992), suggests that itchy stimuli specifically activate itch-selective neurons to generate itch sensation, while painful stimuli activate both itch-selective neurons and a larger nociceptive population whose activation inhibits itch to produce only pain sensation.

Recent studies largely support selectivity theory(Bourane et al., 2015b; Han et al., 2013; Kardon et al., 2014; Mishra and Hoon, 2013; Sun et al., 2009). In DRG, Han et al. confirmed the existence of "itch-selective" neurons by showing that the activation of the *MrgprA3*$^{+}$ primary sensory neurons generated itch but not pain responses, while its ablation impaired itch and spared pain(Han et al., 2013). Further along this same labeled line, the "itch-selective" neurons in the spinal cord are proposed to be the gastrin releasing peptide receptor (GRPR) positive population.

The loss of the GRPR^{+} neurons abolished most itch responses but spared pain(Sun et al., 2009). In addition, brain natriuretic peptide (BNP) is suggested to be the itch-specific neurotransmitter, signaling between itch-selective cells in DRG and itch-selective cells in the spinal cord(Mishra and Hoon, 2013). However, in human psychophysical studies, most chemical-induced itch sensations are accompanied by weaker nociceptive sensations (burning, pricking, stinging etc.) (LaMotte et al., 2014). These mixed sensations raise questions about the "selectivity" of itch pathways.

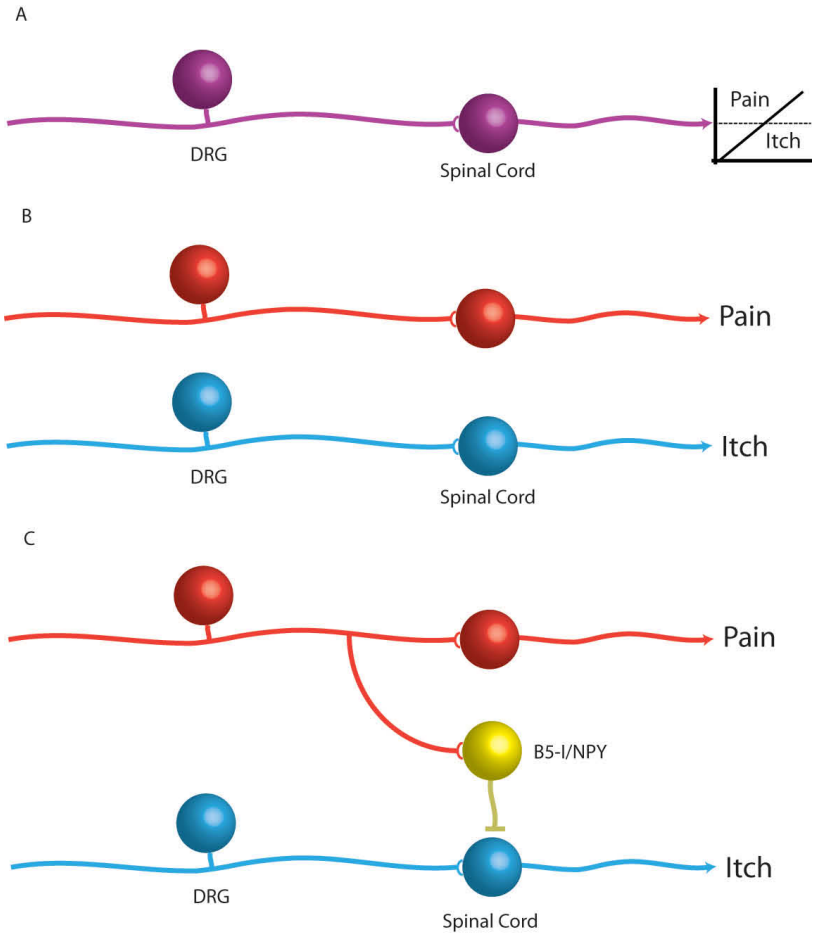

Figure 2.1 Diagrams of pain and itch coding theories.

Diagrams showing (A) intensity theory, (B) labeled line theory and (C) selectivity theory of pain and itch coding.

Although we cannot deny the beauty of simplicity, the anatomical structure of the spinal cord dorsal horn seems to suggest a more complicated and integrative organization of sensory circuits than labeled lines. Unlike pseudo-unipolar DRG neurons, which all serve output functions, only a small subset of superficial dorsal horn neurons transmit signals further to the brain(Spike et al., 2003). The remaining majority are interneurons forming interlacing local circuitries. Lamina I neurons can be categorized as fusiform, pyramidal, multipolar and etc. according to morphology, with the first two categories representing nociceptive and thermoreceptive neurons respectively(Han et al., 1998). Lamina II neurons can be morphologically sorted into islet, central, radial, vertical and etc. types(Grudt and Perl, 2002). Largely, the functions of these local circuitries remain unknown. Here we attempted to reveal the functions of dorsal horn circuits as they related to pain and itch. Secondary neurons are the first step in the spinal circuitry, receiving direct synaptic input from DRG neurons. We identified a subset of secondary neurons, positive for *Grp*, that receive direct synaptic inputs from both pain and itch primary sensory neurons. Surprisingly, the activation of the Grp^{+} neurons generated both pain and itch responses with the pain coding being intensity dependent. These data led us to propose a "leaky gate" model which provides a refined theory for pain and itch coding in the spinal cord.

Methods

Mouse lines

Grp^{Cre} and Grp^{EGFP} mouse lines were acquired from MMRRC. $MrgprA3^{Cre}$ mouse line was previously generated by our group. $ROSA26^{LSL\text{-}tdTomato}$, $ROSA26^{LSL\text{-}ChR2}$, $ROSA26^{LSL\text{-}DTR}$, $ROSA26^{LSL\text{-}TrpV1}$, $vGlut2^{Cre}$, $GAD1^{EGFP}$ and $TrpV1^{-/-}$ mouse lines were acquired from the Jackson laboratory. We used Grp^{Cre}, Grp^{EGFP}, and $MrgprA3^{Cre}$ as hemizygotes or heterozygotes for all the experiments.

Immunofluorescence

Adult mice were anesthetized with pentobarbital and perfused with 20 ml 0.1 M PBS (pH 7.4, 4 °C) followed with 25 ml of fixative (4% formaldehyde (vol/vol) and 14% sat. picric acid (vol/vol) in PBS, 4 °C). Spinal cord and DRG were dissected from the perfused mice. DRG was post-fixed in fixative at 4 °C for 30 min, and spinal cord were fixed for 1 h. Tissues were cryoprotected in 30% sucrose (wt/vol) for more than 12 h and were sectioned with a cryostat. The sections on slides were dried at 37 °C for 40 min, and fixed with 4% paraformaldehyde at room temperature for 10 min. The slides were pre-incubated in blocking solution (10% normal goat serum (vol/vol), 0.2% Triton X-100 (vol/vol) in PBS, pH 7.4) for 1 or 2 h at room temperature, then incubated overnight at 4 °C with primary antibodies. Secondary antibody incubation was performed at room temperature for 2 h.

For primary antibodies, we used rabbit α-CGRP (T-4239, Peninsula, 1:1,000), rabbit α-NF200 (AB1982, Chemicon, 1:1,000), rabbit α-PKCγ (sc-211, Santa Cruz Biotechnology, 1:1,000), rabbit α-GFP (A-11122, Molecular Probes, 1:1,000), mouse α-Neuronal nuclei (MAB377, Chemicon, 1:200), mouse α-PSD95 (K28/43, NeuroMab, 1:500), rabbit α-PSD95 (EP1183Y, Millipore, 1:500), guinea pig α-TrpV1 (AB5566, Millipore, 1:200), rabbit α-MrgprC11 (made by our lab, 1:200) and mouse α-Enkephalin (NOC1, Millipore, 1:100). For secondary antibodies, we used goat α-rabbit (A11008, Alexa 488 conjugated; A11011, Alexa 568 conjugated; A21245, Alexa 647 conjugated, Thermo Fisher), goat α-mouse (A11001. Alexa 488 conjugated; A11004, Alexa 568 conjugated; A21245, Alexa 647 conjugated, Thermo Fisher) and goat α-guinea pig (A11075, Alexa 568 conjugated). All secondary antibodies were diluted 1:500 in blocking solution. To detect IB4 binding, sections were incubated with Griffonia simplicifolia isolectin GS-IB4 (1:500; I21411, Alexa 488 conjugated; I21412, Alexa 568 conjugated, Thermo Fisher).

Electrophysiological recordings

To prepare spinal cord slices, 4 to 6 week-old mice were deeply anesthetized with 2% isoflurane (Abbott Laboratories, North Chicago, IL, USA). Spinal cord with dorsal root or DRG was rapidly removed and placed in ice-cold, low-sodium Krebs solution which contained: 95mM NaCl, 2.5mM KCl, 26mM $NaHCO_3$, 1.25mM NaH_2PO_4-H_2O, 6mM $MgCl_2$, 1.5mM $CaCl_2$, 25mM glucose, 50mM sucrose, 1mM kynurenic acid bubbled with 95% O_2/5% CO_2. Sagittal spinal cord slices (400μm) with dorsal roots or DRG attached were cut by a Vibratome (VT1200, Leica Biosystems, Buffalo Grove, IL, USA) and transferred to low-sodium Krebs solution without kynurenic acid for recovery at 34°C for 45 minutes and then at room temperature for an additional 1 hour before being used for recordings.

For electrophysiology recording, slices were stabilized with a nylon harp and submerged in a low-volume recording chamber (SD Instruments, San Diego, CA, USA), which was perfused with Krebs solution (125mM NaCl, 2.5mM KCl, 26mM $NaHCO_3$, 1.25mM NaH_2PO_4-H_2O, 1mM $MgCl_2$, 2mM $CaCl_2$, 25mM glucose) at a rate of 5ml/min bubbled with 95% O2/5% CO2. Whole-cell patch-clamp recording of Grp^+ neuron was carried out under oblique illumination with an Olympus fixed-stage microscope system (BX51, Melville, NY, USA). Using a puller (P1000, Sutter, Novato, CA, USA), we fabricated thin-walled glass pipettes (World Precision Instruments, Sarasota, FL, USA) that had a resistance of 3-6 MΩ and were filled with internal solution (120mM K-gluconate, 20mM KCl, 2mM $MgCl_2$, 0.5mM EGTA, 2mM Na_2-ATP, 0.5mM Na_2-GTP, and 20mM HEPES). The cells were voltage clamped at –70 mV. Membrane current signals were sampled at 10kHz and low-pass filtered at 2 kHz. We monitored R series and R input and discarded cells if either of these values changed by more than 20%.

DRGs were collected from mice, which were deeply anesthetized with 2% isoflurane (Abbott Laboratories, North Chicago, IL, USA) and put in cold DH10 medium (DMEM/F-12 with 10% fetal bovine serum and 1% penicillin/streptomycin, Gibco) and treated with enzyme solution (5mg/ml dispase and 1mg/ml collagenase Type I in HBSS without Ca^{2+} and Mg^{2+}, Gibco) at 37°C. After trituration and centrifugation, cells were resuspended in DH10 with nerve growth factor (50ng/ml, Upstate) and glial cell line-derived neurotrophic factor (25ng/ml, R&D Systems), plated on glass coverslips coated with poly-D-lysine (100 μg/ml, Biomedical Technologies) and laminin (10μg/ml, Invitrogen), cultured at 37°C, and used after 20–40 hours. Whole-cell recording of MrgprA3 positive DRG neurons were performed with Axon 700B amplifier and pClamp 10 software (Molecular Devices, Sunnyvale, CA). The thin-walled glass pipettes were pulled by a puller (P1000, Sutter, Novato, CA, USA) with the resistance of 2-4 MΩ.

Dorsal roots stimulation was applied by a suction electrode at 500μA, sufficient to activate C-fibers, using a Master-9 Pulse Stimulator and Iso-Flex Stimulus Isolator (AMPI, Jerusalem, Israel). For light stimulation mediated by channelrhodopsin, the LED blue light (465 nm, 300 mW/cm2) was elicited by a high power LED illumination system(LEX2-B, Brainvision) through the Olympus fixed-stage microscope system (BX51, Melville, NY, USA). The LED illumination system was connected to an A/D converter (Digidata 1440, Axon CNS, Molecular Devices), and controlled by the pClamp10 software (Axon CNS). For DRG attached spinal cord slice Grp neurons recording, drugs were directly puffed on the DRG tissue using the DVD-8VC superfusion application system (ALA Scientific Instruments, Farmingdale, NY, USA). To differentiate monosynaptic and polysynaptic connections, 20 C-fiber-strength electrical stimulation or light stimulation at 1Hz were delivered, neurons with no failure in EPSCs were monosynaptically connected according to established criteria(Nakatsuka et al., 2000).

Biocytin Labeling

After 20 min in the whole-cell patch-clamp configuration, the biocytin-filled (0.5%) electrodes were withdrawn from the targeted neuron, and the slices were immersed in 4% paraformaldehyde for 15 min. Spinal slices were then washed with PBS (3 X 20 min) and incubated with Alexa-488 conjugated streptavidin (1:200, Life technologies) at 4°C overnight. After washing with PBS (3 X 20 min), the fluorescent signals of the spinal cord sections were collected as z-series images using a confocal microscope.

Rabies viral tracing

Mice were anesthetized by isoflurane and a laminectomy was performed at the T13-L1 level. A fine glass capillary was inserted into dorsal spinal cord. AAV helper virus, AAV8-LSL-TVA-EGFP-B19G (UNC vector core), was first injected (500nl, 50nl/min). AAV1-LSL-tdTomato virus (Upenn vector core) was similarly injected to visualize *Grp*$^{+}$ neurons. EnvA pseudotyped rabies glycoprotein deficient GFP rabies virus (Courtesy of Dr. Fan Wang's group, Duke University) was injected in the same spot three weeks later. Animals were perfused 7 days after rabies virus injection and processed for immunostaining.

Behavioral testing

All behavioral tests were performed with an experimenter blind to genotype. The mice were 2–4-month-old males that had been backcrossed to C57Bl/6 mice for at least six generations. All experiments were performed using protocols approved by the Animal Care and Use Committee of Johns Hopkins University School of Medicine. The day before the behavioral tests, all mice were acclimated for at least 30 min to their testing environment. We housed 4-5 mice in each cage in the vivarium with 12h light/dark cycle and all the behavioral tests were performed in the morning.

For ablation experiments, we injected 8-week-old Grp^{Cre}; $ROSA26^{LSL\text{-}DTR;LSL\text{-}tdTomato}$ mice and $ROSA26^{LSL\text{-}DTR;LSL\text{-}tdTomato}$ littermates with diphtheria toxin (intra-peritoneal, 35 μg per kg of body weight, Sigma) twice, separated by 72 h. Behavioral experiments were performed 4 weeks after the first toxin injection.

Back injections were performed as previously described(Han et al., 2013). Briefly, pruritic compounds were subcutaneously injected into the nape of the neck (50μl). Behavioral responses were video recorded for 30 min. The video recording was subsequently played back in slow motion and the number of bouts of scratching with the hindpaw and directed toward the injection site, were counted.

For the hot plate test, a clear plexiglass cylinder was placed on the plate and the mice were placed inside the cylinder. The onset of brisk hindpaw lifts and/or flicking/licking of the hindpaw was assessed at different temperatures.

For the tail immersion test, mice were gently restrained in a 50ml conical tube into which the mice voluntarily entered. The protruding one-third of the tail was then dipped into a water bath of varying temperatures. The latency to respond to the heat stimulus with vigorous flexion of the tail was measured.

For the Hargreaves test, mice were placed under a transparent plastic box (4.5 × 5 × 10 cm) on a glass floor. The infrared source was placed under the glass floor and the infrared light was delivered to the hindpaw. The latency for the animal to withdraw its hindpaw was measured.

For the Von Frey filament test, mice were placed under a transparent plastic box (4.5 × 5 × 10 cm) on a metal mesh. Von Frey filaments, each delivering a different bending force, were applied to the hind paw using the up-down method and the threshold force corresponding to 50% withdrawal was determined.

For the chemically induced pain test, cheek injection was used to administer a total volume of 10μl of capsaicin and the numbers of front paw wipes were counted in 10 minutes.

For the rotarod test, each mouse was trained for 5 min at a constant speed of 4 rpm on the rotarod (Rotamex, Columbus Instruments). The first trial started at least 1h after training. Every day, each mouse received three trials, separated by 30 min, at speeds accelerating from 4 to 40 rpm (with a 4 rpm increase every 30 s). Each mouse was tested for three consecutive days. The trial was finished when the mouse fell off the rotarod. The latency to falling off the rotarod was recorded and used in subsequent analyses.

For capsaicin mediated activation experiments, Grp^{Cre}; $ROSA26^{LSL\text{-}TrpV1}$; $TrpV1^{-/-}$ mice were intrathecally injected with 10μl capsaicin of different concentrations or capsaicin with naloxone (0.1mg/ml), naltrindole (0.2mg/ml), CTAP (0.5mg/ml), CTOP (1mg/ml), cycloSOM (0.1mM) and bicuculline (10μM). High definition videos were recorded from the top for 30 minutes with four mirrors to enable views of all angles. Video recordings were subsequently played back at 1/5 normal speed. The durations of licking directed to lower back region with a characteristic frequency of 5Hz were quantified in the first four minutes and bouts of scratching were counted in 30 minutes. $ROSA26^{LSL\text{-}TrpV1}$; $TrpV1^{-/-}$ littermates were used as controls. Wild type and $TrpV1^{-/-}$ mice were also intrathecally injected with GRP, BNP and capsaicin. Licking and scratching behaviors quantified as reference.

Light activation of $MrgprA3^{+}$ neurons: $MrgprA3^{Cre}$; $ROSA26^{LSL\text{-}ChR2}$ mice with shaved nape regions were given 100 ms blue light at 1Hz or 5Hz and litter mate $ROSA26^{LSL\text{-}ChR2}$ mice were used as controls. Scratching bouts were counted in 5 minute time period. Sham operations without blue light were used to determine baseline scratch numbers.

ELISA

Grp^{Cre}*; ROSA26*$^{LSL\text{-}TrpV1}$*; TrpV1*$^{-/-}$ mice and *ROSA26*$^{LSL\text{-}TrpV1}$*; TrpV1*$^{-/-}$ littermate controls were deeply anesthetized with isoflurane, decapitated and the lumbar spinal cord was quickly removed to ice-cold, low-sodium Krebs solution which contain: 95mM NaCl, 2.5mM KCl, 26mM $NaHCO_3$, 1.25mM NaH_2PO_4-H_2O, 6mM $MgCl_2$, 1.5mM $CaCl_2$, 25mM glucose, 50mM sucrose, 1mM kynurenic acid bubbled with 95% O_2/5% CO_2. Spinal cords were cut into three sagittal sections and then recovered in oxygenated ACSF for about 1h at 37°C. Three sections were subsequently incubated with 200µl oxygenated Krebs solution (125mM NaCl, 2.5mM KCl, 26mM $NaHCO_3$, 1.25mM NaH_2PO_4-H_2O, 1mM $MgCl_2$, 2mM $CaCl_2$, 25mM glucose) with capsaicin (2mg/ml, 5µg/ml and 0µg/ml, respectively) and proteinase inhibitor mix (1µM phosphoramidon, 1µM captopril and 0.1% BSA) for 15 minutes at 37°C. 100µl of ACSF from each sample was then used for the detection of Enkephalin release. ELISA detections of enkephalin were performed following manufacturer's protocol (FEK02421, Phoenix Pharmaceuticals). Results were normalized to the weight of the tissue. At least six mice were used for each condition.

Statistical analysis

Data are presented as mean ± s.e.m. n represents the number of mice analyzed. The distribution of the variables in each experimental group was approximately normal. Most statistical comparisons were conducted by two-tailed, unpaired Student's t test. Extended Welch's t test was used for the comparison of ratios of ablated responses and control responses. Power analysis was used to justify the sample size. Differences were considered to be statistically significant for $P < 0.05$. Representative data are from experiments that were replicated biologically at least three times with similar results.

Extension of Welch's t test: µ1h: mean of log value of ablated responses, high dose; µ1l

mean of log value of ablated responses, low dose; μ2h: mean of log value of control responses, high dose; μ2l: mean of log value of control responses, low dose. Null hypothesis H_0: (μ1h − μ2h) − (μ1l − μ2l) = 0. Alternative H_1: (μ1h − μ2h) − (μ1l − μ2l) > 0. Test statistics:

$t = \frac{(\overline{\mu 1h} - \overline{\mu 2h}) - (\overline{\mu 1l} - \overline{\mu 2l})}{s}$, where $\bar{\mu}$ detonates the sample means of the subgroup.

$s = \sqrt{\frac{s1h^2}{n1h} + \frac{s1l^2}{n1l} + \frac{s2h^2}{n2h} + \frac{s2l^2}{n2l}}$, where s^2 denotes the sample variance and n is the sample size.

Under H_0, the test statistics follows t-distribution and the degrees of freedom,

$$df = \frac{\left(s1h^2/n1h + s2h^2/n2h + s1l^2/n1l + s2l^2/n2l\right)^2}{\left(s1h^2/n1h\right)^2/(n1h-1) + \left(s2h^2/n2h\right)^2/(n2h-1) + \left(s1l^2/n1l\right)^2/(n1l-1) + \left(s2l^2/n2l\right)^2/(n2l-1)}.$$

Dose response curve fitting for capsaicin mediated activation:

Itch dose responses were fit with Hill equation: $y = 7.946 + \frac{154.854}{1+10^{(0.495-x)\times 0.5577}}$

Pain dose responses were fit with polynomial equation: $y = 0.469 - 3.882x + 11.38x^2 - 1.904x^3 + 0.08229x^4$

Results

Genetic labeling of itch secondary neurons in the spinal cord

Previously we found that *MrgprA3*$^+$ itch selective primary sensory neurons terminate their axons in lamina II of spinal cord(Han et al., 2013). To identify genetic markers of secondary neurons which form synapses directly with *MrgprA3*$^+$ neurons, we utilized transgenic mouse lines with Cre recombinase expression under specific neuronal gene promoters, generated using bacterial artificial chromosome (BAC)-based transgenic technology by the Gene Expression Nervous System Atlas (GENSAT) project(Gong et al., 2003). Upon screening all GENSAT Cre

lines with expression in the spinal cord dorsal horn, we focused on a promising target, *Grp*. *Grp* has previously been implicated in itch transmission. *Grp* was reported to express in DRG but not spinal cord and proposed to provide input to $GRPR^{+}$ neurons(Sun and Chen, 2007). However, recent studies suggest that *Grp* instead expresses in spinal cord dorsal horn, not the DRG(Fleming et al., 2012; Solorzano et al., 2015).

Consistent with the recent studies, we found Grp^{Cre} expression was restricted to the superficial lamina of the spinal cord and we could not detect Grp^{Cre} expression in DRG (Figure 2.2 A and B), when visualized with $ROSA26^{LSL\text{-}tdTomato}$ reporter line. To further determine the laminar distribution of the Grp^{+} neurons in the dorsal horn, we performed immunostaining on Grp^{Cre}; $ROSA26^{LSL\text{-}tdTomato}$ spinal slides. Grp^{+} neurons were located deeper than the CGRP-labeled lamina II outer layer (Figure 2.2E), co-localized with IB4 positive fibers in lamina II dorsal inner layer (Figure 2.2F) and partially overlapped with PKCγ neurons in ventral inner layer(Braz et al., 2014; Solorzano et al., 2015) (Figure 2.2G). Since there are no projection neurons in lamina II(Todd, 2010), *Grp* thus labels a subset of interneurons in the lamina II inner layer. Regarding neurotransmitter types, more than 90% of Grp^{+} neurons expressed the glutamatergic excitatory marker (Figure 2.2H and K), vesicular glutamate transporter (*vGlut2*), as labeled by $vGlut2^{Cre}$(Vong et al., 2011). Less than 10% of Grp^{+} neurons overlapped with the GABAergic inhibitory marker, *GAD1* (Figure 2.2I), when visualized with $GAD1^{EGFP}$(Chattopadhyaya et al., 2004). Therefore, *Grp* labels a subset of excitatory interneurons in lamina II inner layer.

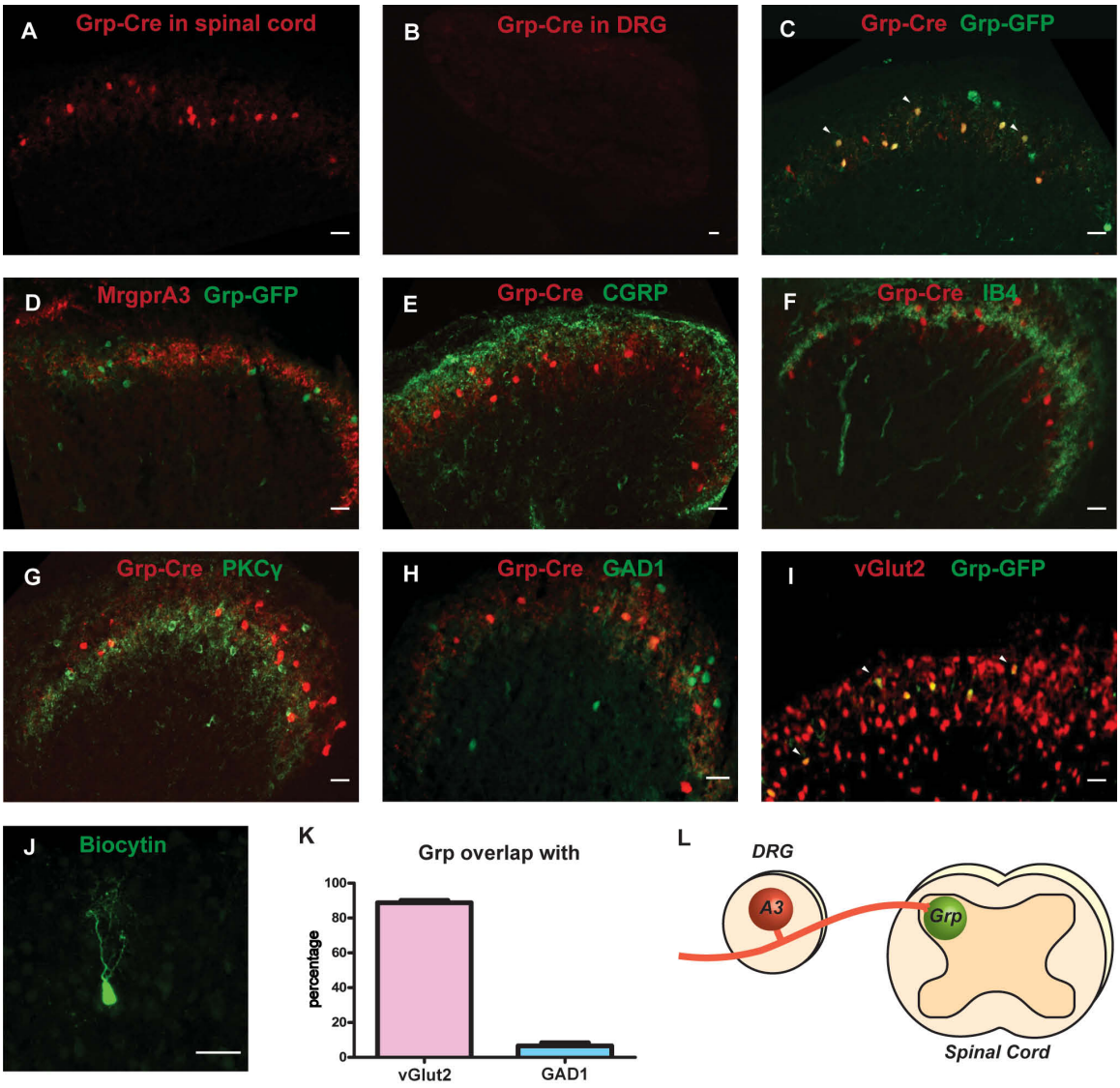

Figure 2.2 Genetic labeling of itch secondary neurons in the spinal cord

(A and B) Spinal cord and DRG sections from Grp^{Cre}; $ROSA26^{LSL\text{-}tdTomato}$ mice, tdTomato fluorescence were visualized directly without staining. (C and D) Grp^{Cre}; $ROSA26^{LSL\text{-}tdTomato}$;$Grp^{EGFP}$ and $MrgprA3^{Cre}$; $ROSA26^{LSL\text{-}tdTomato}$; Grp^{EGFP} spinal sections stained with GFP antibody. (E-G) Grp^{Cre}; $ROSA26^{LSL\text{-}tdTomato}$ spinal sections stained with antibodies to CGRP, IB4 and PKCγ respectively. (H and I) Grp^{Cre}; $ROSA26^{LSL\text{-}tdTomato}$; $Gad1^{EGFP}$ and $vGlut2^{Cre}$; $ROSA26^{LSL\text{-}tdTomato}$; Grp^{EGFP} spinal sections stained with GFP antibody. (J) Representative image of biocytin

labeled individual *Grp*$^{+}$ neurons. (K) Percentage of *Grp*$^{+}$ neurons expressing *vGlut2* and *Gad1*. n= 15 hemisections from three mice per group. Data are represented as mean ± SEM. All scale bars represent 20 μm. Arrowhead indicates overlap. (L) Diagram summarizing the potential synaptic connections between *MrgprA3*$^{+}$ DRG neurons and *Grp*$^{+}$ neurons in the spinal cord.

To check the prevalence of *Grp*$^{+}$ neurons in the spinal cord, we stained for pan-neuronal marker, NeuN. *Grp* labeled only 4.24% of neurons in lamina II (Figure 2.3), estimated to be about 1% of total dorsal horn neurons(Todd et al., 1998). Moreover, *Grp*$^{+}$ neurons were all characterized as vertical neurons according to morphology(Grudt and Perl, 2002) (Figure 2.2J, n=19). Such a small group of genetically labeled neurons with uniform morphologies more likely have uniform functions. Thus the *Grp*^{Cre} line from GENSAT serves as a great tool to investigate this small subset of spinal interneurons.

GENSAT had another *Grp* line with EGFP expression under the same promoter. We crossed the EGFP line with *Grp*^{Cre}*; ROSA26*$^{LSL\text{-}tdTomato}$. *Grp*^{Cre} expression largely overlapped with *Grp*^{EGFP} (Figure 2.2C and 2.3), confirming that the two BAC lines label the same subset of dorsal horn neurons. We found that *Grp*^{EGFP} overlapped with *MrgprA3* central terminals in the spinal cord. Moreover, *Grp*^{EGFP} co-localized with both *MrgprA3* and post-synaptic marker PSD95 (Figure 2.3), suggesting that *Grp*$^{+}$ neurons likely form synaptic contacts with *MrgprA3*-labeled (diagramed in Figure 2.2L), itch-selective neurons in DRG(Han et al., 2013).

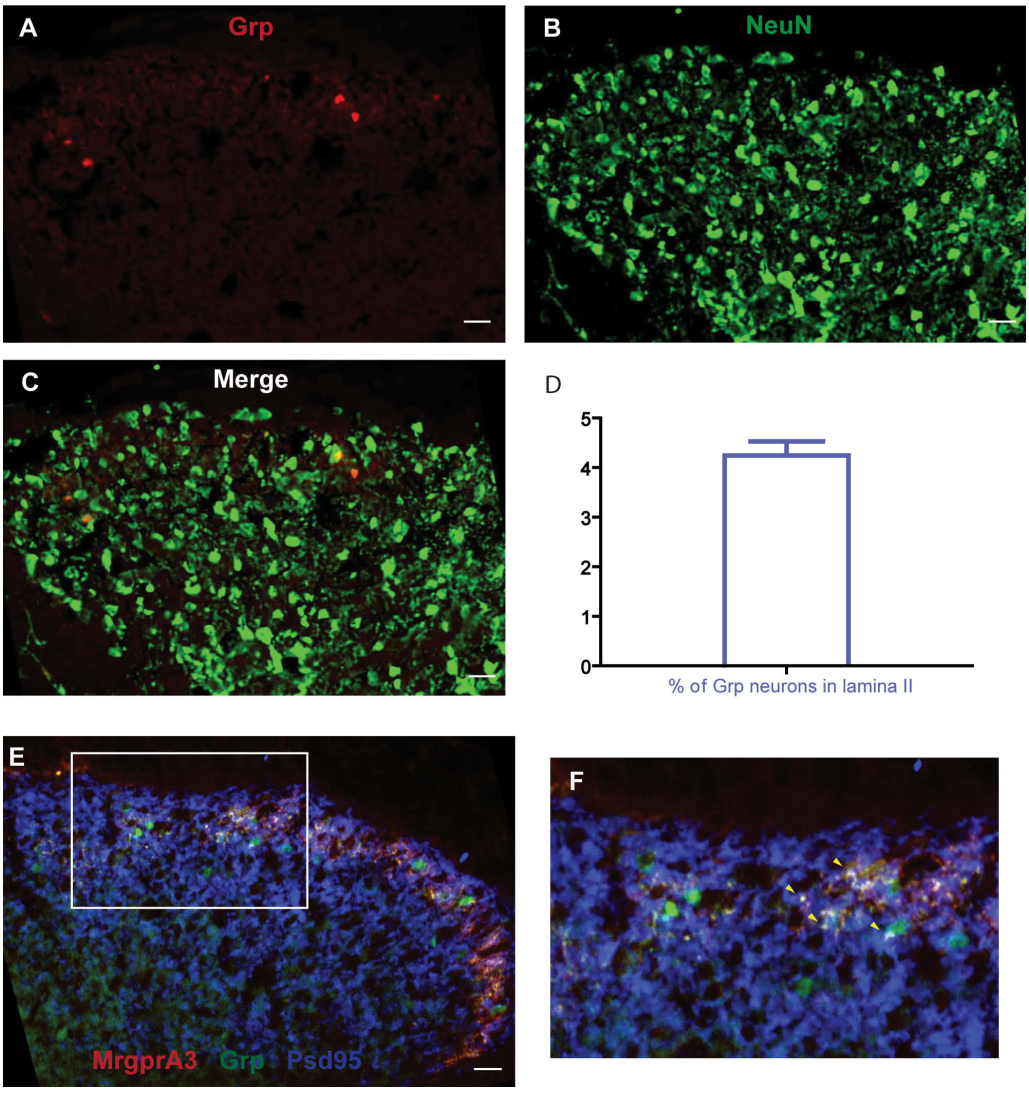

Figure 2.3 Further characterization of *Grp*$^{+}$ neurons

(A) Spinal cord sections from *Grp*^{Cre}*; ROSA26*$^{LSL\text{-}tdTomato}$ mice, tdTomato fluorescence were visualized directly without staining. (B) NeuN staining. (C) Co-localization of *Grp*$^{+}$ neurons and NeuN staining. (D) *Grp*$^{+}$ neurons represent 4.24% lamina II neurons (n = 25 hemisections from five mice). (E) Co-localization of *Grp*$^{+}$ neurons with *MrgprA3* and PSD95. (F) Representative neurons in boxed region in E shown at greater magnification. Arrowheads indicate co-localization of *Grp*$^{+}$ neurons with *MrgprA3* central terminals and synaptic marker PSD95. Data are represented as mean ± SEM. All scale bars represent 20 μm.

Grp$^+$ neurons receive direct synaptic inputs from itch-selective primary neurons

Next, to examine the synaptic inputs to *Grp*$^+$ neurons, we recorded from *Grp*$^+$ neurons in spinal slides while electrically stimulating the dorsal root. All *Grp*$^+$ neurons had monosynaptic inputs from C fibers with short synaptic delays (Figure 2.5), demonstrating that *Grp* exclusively labels secondary neurons with direct synaptic input from DRG. We then tried to further determine the source of C fiber inputs onto *Grp*$^+$ neurons. To directly test whether *Grp*$^+$ neurons receive direct synaptic input from *MrgprA3*$^+$ neurons, we crossed *MrgprA3*^{Cre} with Cre dependent Channelrhodopsin reporter line *ROSA26*$^{LSL\text{-}ChR2}$ to selectively activate *MrgprA3* fibers with blue light (as diagramed in Figure 2.4A).

To examine the behavioral effect of light-mediated activation of the *MrgprA3*$^+$ neurons, we shone blue light on the shaved nape regions of *MrgprA3*^{Cre}*; ROSA26*$^{LSL\text{-}ChR2}$ mice (as diagramed in Figure 2.4A). 1Hz 100ms light stimulation generated significant scratching compared with controls (Figure 2.4B). Similar to chemical activation(Han et al., 2013), optogenetic activation generated only scratching behavior, which confirmed the role of *MrgprA3*$^+$ neurons as itch-selective neurons. 5Hz light stimulation, however, failed to elicit scratching above baseline (Figure 2.4B and 2.5). Consistently, 1Hz light stimulation reliably evoked action potentials in *MrgprA3*$^+$ neurons, while 5Hz light stimulation failed to do so (Figure 2.5), suggesting that these neurons might not be able to fire at this higher frequency.

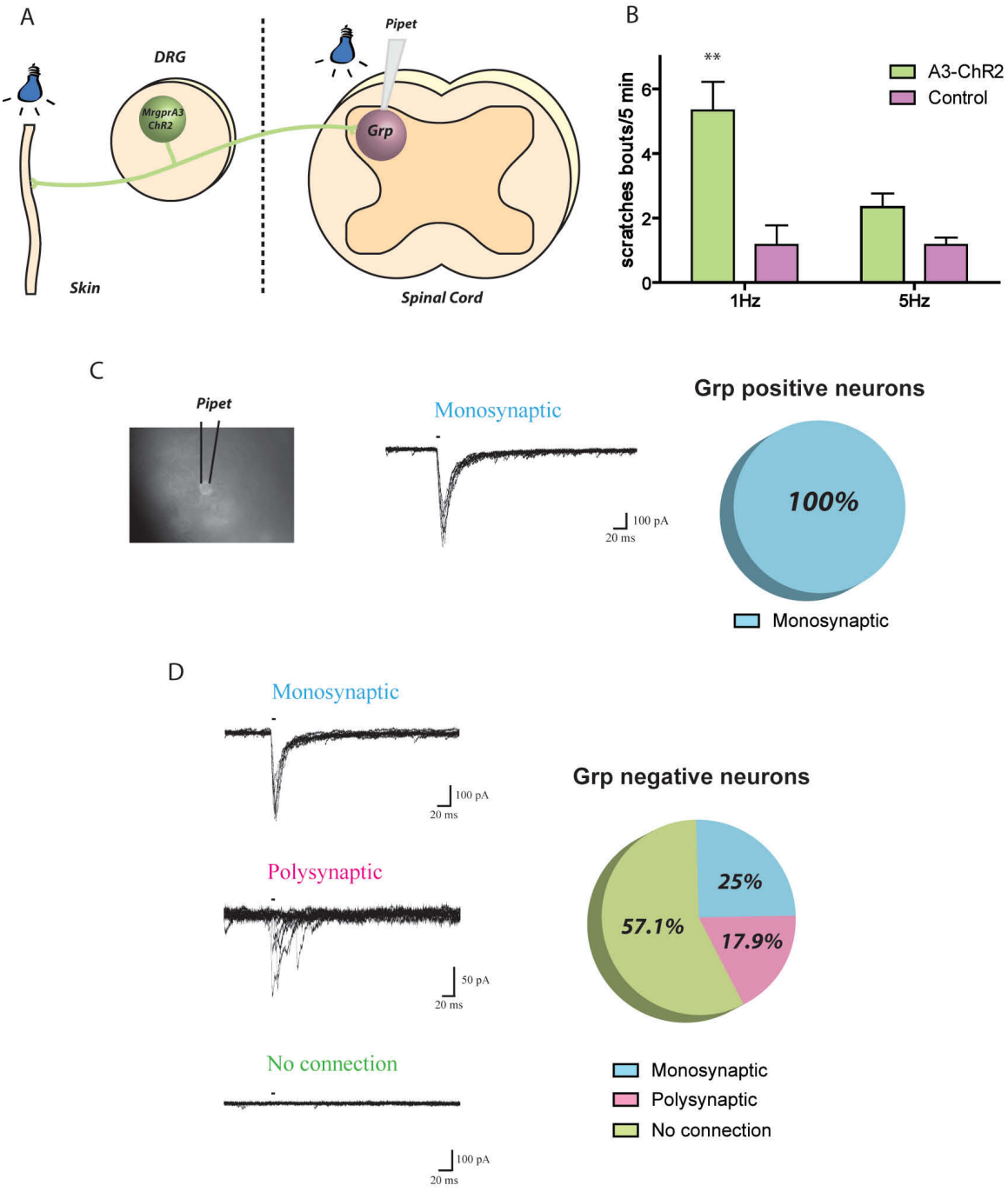

Figure 2.4 *Grp*$^+$ neurons receive monosynaptic itch input

(A) Left: diagram showing light activation of *MrgprA3* peripheral fibers in behavioral tests; right: diagram showing light activation of *MrgprA3* central terminals and recording of *Grp*$^+$ neurons in

the spinal cord. (B) 1Hz and 5Hz 100ms light stimulation triggered scratching bouts in five minutes. *MrgprA3*^{Cre}*; ROSA26*$^{LSL\text{-}ChR2}$ and *ROSA26*$^{LSL\text{-}ChR2}$ control mice with light delivered to shaved nape regions (n=6). Data are represented as mean ± SEM. (C) From left to right: image of *Grp*$^{+}$ neurons in spinal slice with electrode (black lines), representative traces of light-induced EPSCs in *Grp*$^{+}$ neurons with monosynaptic input from *MrgprA3*$^{+}$ neurons and percentage of *Grp*$^{+}$ neurons with monosynaptic input from *MrgprA3*$^{+}$ neurons. (D) Left: representative traces of light-induced EPSCs in lamina II *Grp* negative neurons with monosynaptic input, polysynaptic input and no synaptic input from *MrgprA3*$^{+}$ neurons. Right: percentage of lamina II *Grp* negative neurons with monosynaptic input, polysynaptic input and no synaptic input from *MrgprA3*$^{+}$ neurons. Recordings done by Dr. Qian Xu.

When we recorded from the *Grp*$^{+}$ neurons while stimulating the *MrgprA3* central terminals with light, 100% of the *Grp*$^{+}$ neurons (16/16) received monosynaptic input from *MrgprA3*$^{+}$ neurons (Figure 2.4C and 2.5), suggesting that *Grp*$^{+}$ neurons labeled a functionally unified population of secondary neurons that all receive direct itch input from the periphery. When we recorded from surrounding *Grp* negative neurons, 25% of them (7/28) also received monosynaptic input, an additional 18% (5/28) received polysynaptic input and the remaining 57% (16/28) had no connection with *MrgprA3*$^{+}$ neurons (Figure 2.4D and 2.5), suggesting that *Grp* labels a major subset of itch secondary neurons in the spinal cord.

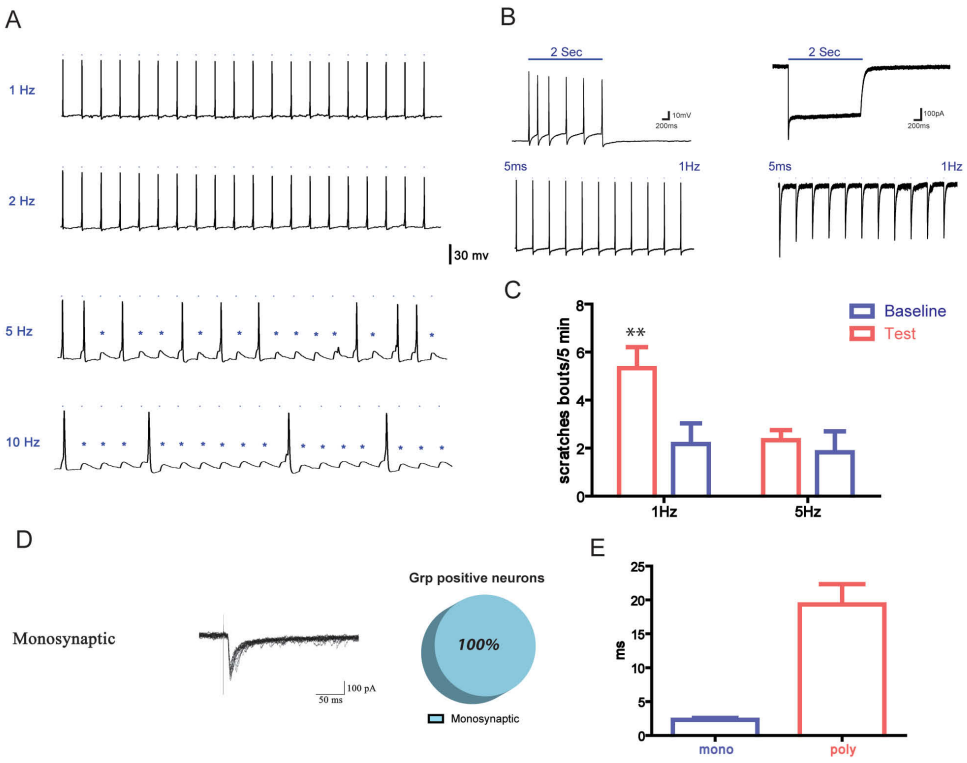

Figure 2.5 Light-mediated *MrgprA3* activation and monosynaptic input to *Grp*$^{+}$ neurons

(A) Light-evoked action potentials in cultured *MrgprA3*^{Cre}*; ROSA26*$^{LSL\text{-}ChR2}$ DRG neurons. * indicates failure of action potential. (B) Continuous and 1Hz light induced responses in current clamp and voltage clamp mode. Blue bars indicate 5ms light stimulation. (C) Light-induced scratching bouts in *MrgprA3*^{Cre}*; ROSA26*$^{LSL\text{-}ChR2}$ (test, n=6) compared with sham responses with no light (baseline, n=6). **: P<0.01, two-tailed unpaired Student's t test. (D) 100% of *Grp*$^{+}$ neurons (n=14) received C fiber monosynaptic input. Representative traces shown in middle. (E) EPSC jitters of *Grp*$^{+}$ neurons and *Grp* negative neurons with polysynaptic connections with MrgprA3^{+} neurons (n=16 vs. 5). Data are represented as mean ± SEM. Recordings done by Dr. Qian Xu.

***Grp*$^{+}$ neurons receive monosynaptic input from both itch and pain primary sensory neurons**

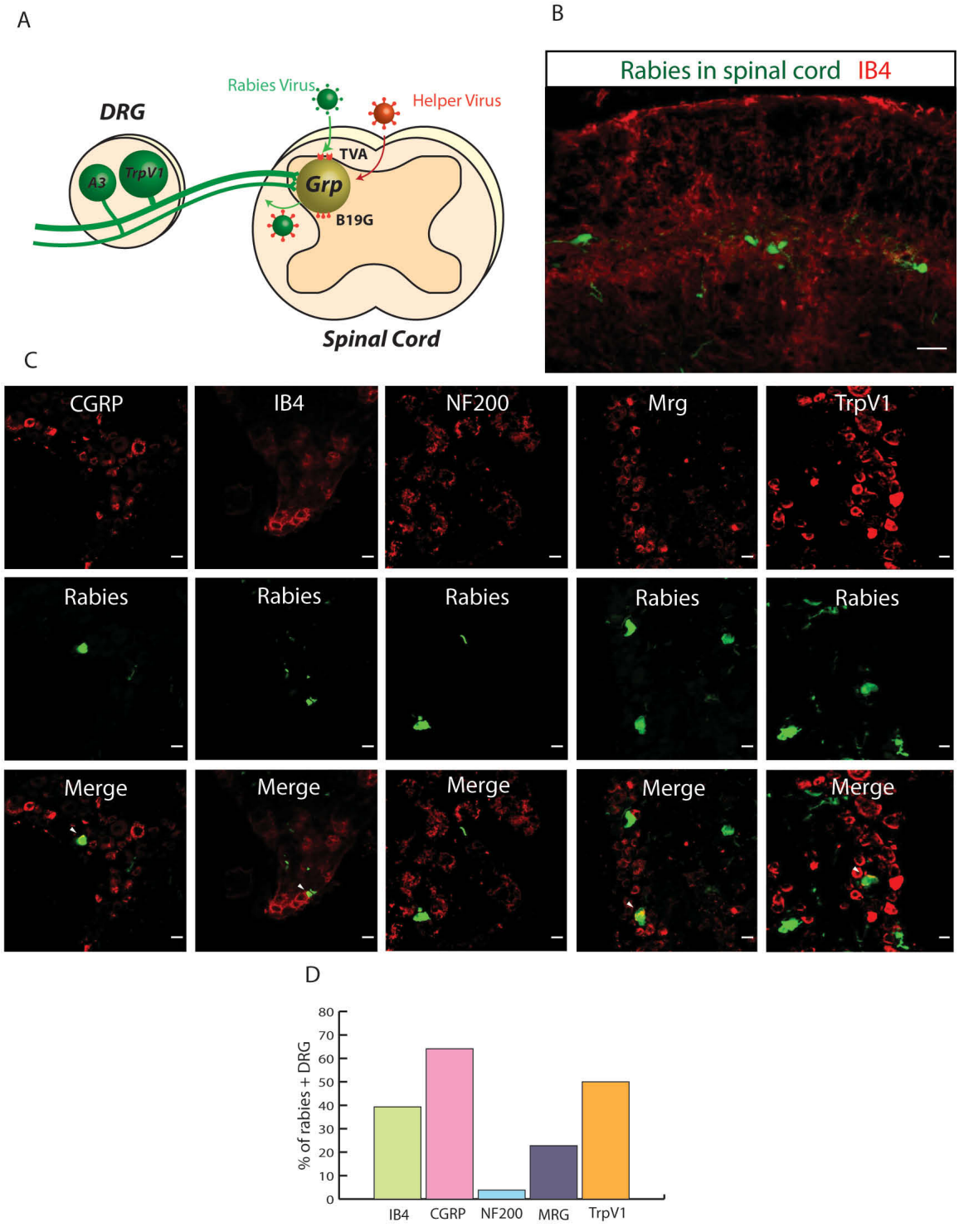

Figure 2.6 Monosynaptic retrograde tracing from *Grp*$^{+}$ neurons

(A) Diagram showing monosynaptic retrograde tracing strategy from *Grp*$^{+}$ neurons. (B) Rabies-labeled neurons overlap with IB4 in spinal cord. (C) Top panels: L4-6 DRG sections labeled with different markers (CGRP, IB4, NF200, MrgprC11 and TrpV1). Middle panels: rabies virus trans-synaptically labeled DRG neurons. Bottom panels: merge images. Arrowhead indicates overlap of markers and rabies-labeled DRG neurons. All scale bars represent 20 μm. (D) Percentage of rabies trans-synaptically labeled DRG neurons co-localize with different markers. Pooled results from more than 30 DRG sections of at least five mice for each marker.

We then tried to determine whether *Grp*$^{+}$ neurons receive other somatosensory input, such as input from nociceptors in DRG. However, it is hard to selectively activate nociceptors without also targeting the itch-selective neurons, given that they share many genetic markers. Therefore we decided to use mono-synaptic rabies tracing(Wickersham et al., 2007) to systemically quantify the inputs to the *Grp*$^{+}$ population. AAV helper virus (AAV8-LSL-TVA-EGFP-B19G) was injected into the spinal cord to enable expression of TVA receptor and rabies glycoprotein in Cre expressing neurons. Deficient rabies virus (ΔG-RV-GFP) specifically infected the *Grp*$^{+}$ neurons which expressed TVA. The *Grp*$^{+}$ neurons also contained the rabies glycoprotein that allowed the virus to be transported from the *Grp*$^{+}$ neurons only to their presynaptic targets (as diagramed in Figure 2.6A).

Deficient rabies virus successfully infected neurons in spinal cord lamina II of *Grp*^{Cre} mice (Figure 2.6B) but not in Cre negative mice or when injected without the helper virus (Figure 2.7), showing the specificity of viral tracing. In DRG, rabies virus trans-synaptically labeled mostly small to medium diameter neurons. 64.1% of rabies labeled DRG neurons expressed

peptidergic marker calcitonin gene-related peptide (CGRP), 39.3% of rabies labeled DRG neurons expressed non-peptidergic marker IB4, while very few (3.85%) expressed myelinated neuronal marker NF200 (Figure 2.6C and D). We utilized an available MrgprC11 antibody, which marks an itch population containing most *MrgprA3*$^{+}$ neurons(Han et al., 2013) and showed that these neurons are indeed trans-synaptically labeled, confirming that *Grp*$^{+}$ neurons received monosynaptic input from itch-selective neurons. However, only 22.3% of rabies-labeled neurons were *MrgprC11* positive, while 50.0% of rabies-labeled neurons were positive for nociceptive marker, TrpV1(Figure 2.6D). Even though most *Mrgpr*$^{+}$ neurons also expressed CGRP, IB4 and TrpV1, the fact that these markers labeled much more rabies-infected neurons demonstrated that not only itch-selective neurons, but also nociceptive populations provide monosynaptic inputs to *Grp*$^{+}$ neurons.

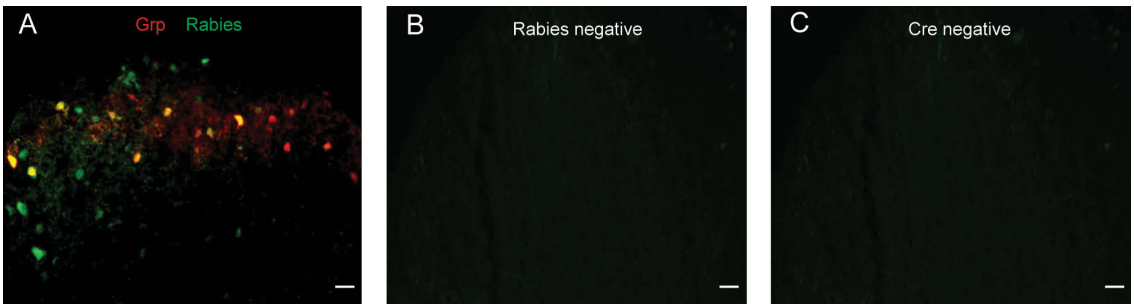

Figure 2.7 Single synapse retrograde tracing from *Grp*$^{+}$ neurons

(A) Rabies virus (green) infected *Grp*$^{+}$ neurons labeled by tdTomato fluorescence and surrounding neurons representing presynaptic targets of *Grp*$^{+}$ neurons. (B and C) Rabies virus cannot infect spinal cord neurons without helper virus or in Cre negative control mice. All scale bars represent 20 μm.

Painful stimuli strongly while itchy stimuli weakly activate *Grp*$^+$ neurons

Since *Grp*$^+$ neurons receive direct synaptic inputs from both itch and pain primary sensory neurons, we next tried to determine whether *Grp*$^+$ neurons can distinguish between pain and itch inputs. We performed DRG-attached spinal slice recordings and applied drugs on DRG cell bodies to mimic natural painful and itchy stimuli coming from the periphery (Figure 2.8A). Both pain- and itch-producing drugs applied directly on DRG triggered action potentials in *Grp*$^+$ neurons (Figure 2.8C-E). Capsaicin evoked high frequency firing in *Grp*$^+$ neurons; while the pruritogen SLIGRL produced only weak firing. To confirm that limited penetration of peptide SLIGRL did not affect the responses of *Grp*$^+$ neurons, we applied a small molecule pruritogen, histamine. Similarly, histamine generated only weak firing in *Grp*$^+$ neurons, which suggests that these neurons fire strongly in response to painful stimuli but weakly in response to itchy stimuli (diagramed in Figure 2.8B).

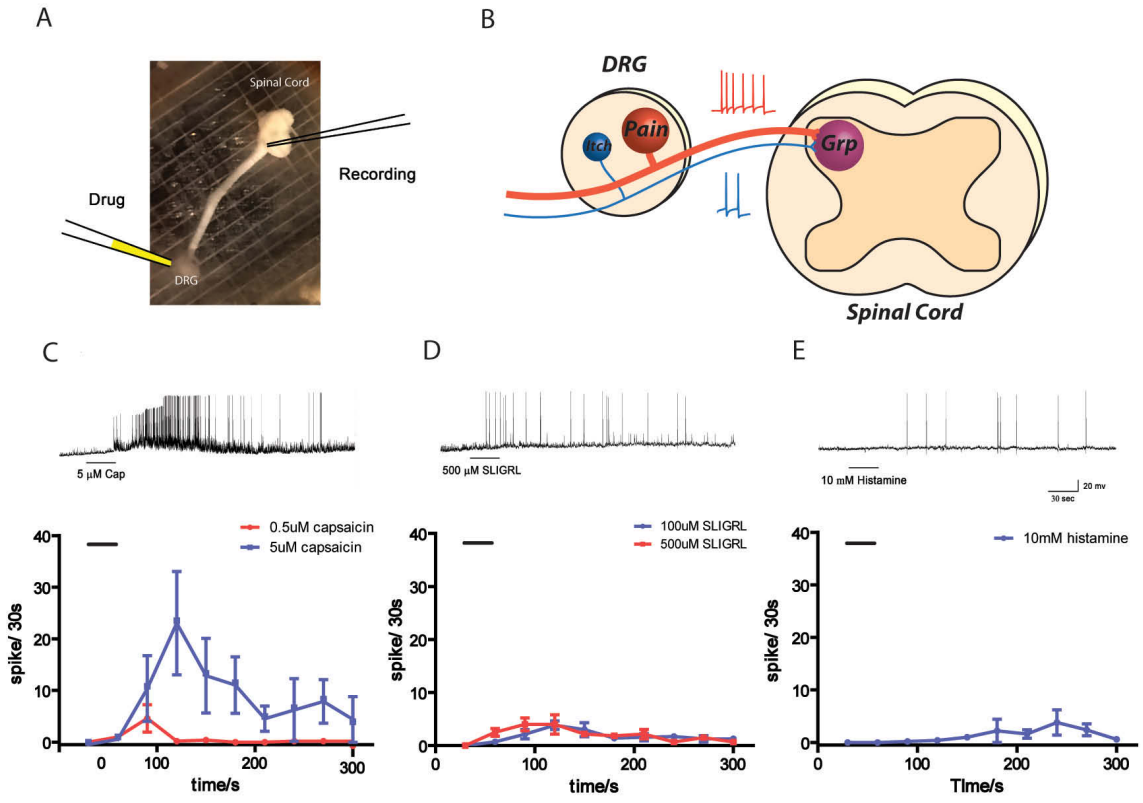

Figure 2.8 Painful stimuli strongly activate while itchy stimuli weakly activate *Grp*$^+$ neurons

(A) Image of DRG attached spinal cord slice. Recording electrode on right and drug application electrode on left. (B) Diagram summarizing painful stimuli from DRG can strongly activate *Grp*$^+$ neurons while itchy stimuli can only weakly activate *Grp*$^+$ neurons. (C-E) Top panels: representative traces of action potentials from *Grp*$^+$ neurons in responses to drugs. Bottom panels: *Grp*$^+$ neurons in response to capsaicin, histamine and SLIGRL application on DRG. Black bar indicates duration of drug application (n=6). Data are represented as mean ± SEM. Recordings done by Dr. Qian Xu.

Coding of both pain and itch by *Grp*$^+$ neurons

Although the itch neurons in DRG are responsive to both painful and itchy stimuli, activation of these neurons generates itch, not pain responses(Han et al., 2013). Similarly, *Grp*$^+$ neurons receive direct synaptic inputs from both pain and itch primary neurons. Using behavioral assays, we next determined what sensations are generated by the activation of *Grp*$^+$ neurons. To specifically activate *Grp*$^+$ neurons, we crossed Grp^{Cre} to $ROSA26^{LSL\text{-}TrpV1}$ in a global TrpV1 knockout background (Grp^{Cre}; $ROSA26^{LSL\text{-}TrpV1}$; $TrpV1^{-/-}$). In Grp^{Cre}; $ROSA26^{LSL\text{-}TrpV1}$; $TrpV1^{-/-}$ *mice*, TrpV1 agonist capsaicin selectively activated *Grp*$^+$ neurons, the only cells with TrpV1 expression (as diagramed in Figure 2.8A). To test the functional expression of TrpV1, we injected AAV1-LSL-tdTomato virus into the spinal cord and recorded from tdTomato labeled *Grp*$^+$ neurons. Labeled neurons from Grp^{Cre}; $ROSA26^{LSL\text{-}TrpV1}$; $TrpV1^{-/-}$ but not from Grp^{Cre}; $TrpV1^{-/-}$ mice responded to capsaicin (Figure 2.10). *Grp*$^+$ neurons with ectopic TrpV1 expression showed lower sensitivity to capsaicin compared with TrpV1$^+$ DRG neurons. These neurons exhibited

monotonically increased responses to a wide range of capsaicin doses (Figure 2.10), confirming the functional expression of TrpV1 in *Grp*$^{+}$ neurons.

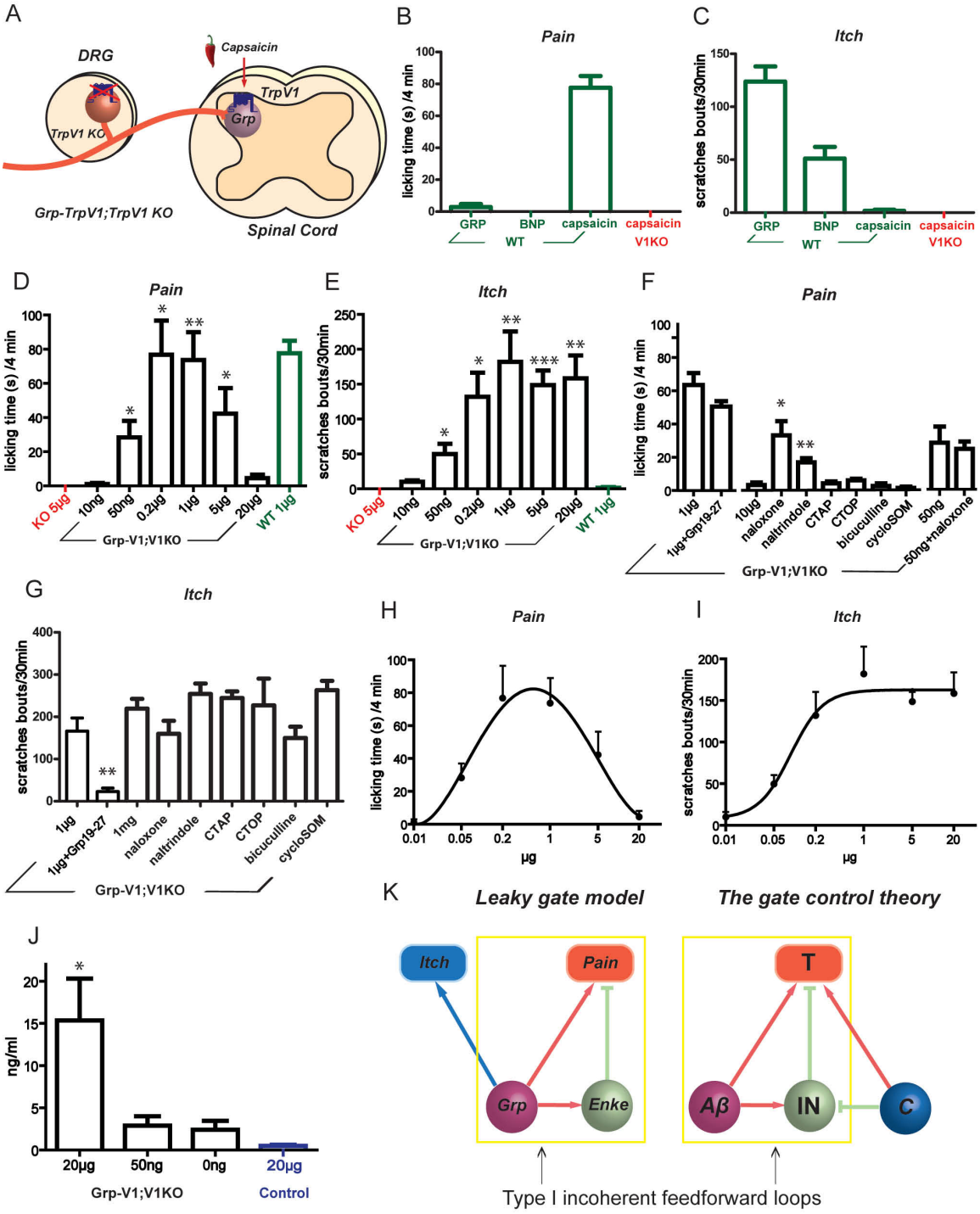

Figure 2.9 Intensity dependent coding of pain and itch by *Grp*$^{+}$ neurons

(A) Diagram showing the strategy of capsaicin-mediated specific activation of *Grp*$^{+}$ neurons in *Grp*^{Cre}*; ROSA26*$^{LSL\text{-}TrpV1}$*; TrpV1*$^{-/-}$ mice. (B and C) Pain-related licking time and itch-related scratching bouts in wild type (green bars) and *TrpV1*$^{-/-}$ mice (red bars) triggered by intrathecal delivery of 10μl capsaicin (1μg, n=6), BNP (25μg, n=8) and GRP peptides (200μM, n=8). (D and E) 10μl intrathecal capsaicin-triggered pain and itch responses in *Grp*^{Cre}*; ROSA26*$^{LSL\text{-}TrpV1}$*; TrpV1*$^{-/-}$ mice (black bars, from left to right: 10ng, n=9; 50ng, n=6; 0.2μg, n=5; 1μg, n=6; 5μg, n=10; 20μg, n=6) together with responses in wild-type (green bars, 1μg, n=6) and *TrpV1*$^{-/-}$ mice (red bars, 5μg, n=6) from (B and C). (F and G) 10μl intrathecal capsaicin-triggered pain and itch responses in *Grp*^{Cre}*; ROSA26*$^{LSL\text{-}TrpV1}$*; TrpV1*$^{-/-}$ mice with drugs. From left to right 1μg capsaicin without and with GRPR antagonist (Deamino-Phe^{19},D-Ala^{24},D-Pro^{26}-psi(CH_2NH)Phe^{27})-GRP (19-27), 200μM, n=6 and 5); 10μg capsaicin, n=8; 10μg capsaicin with naloxone (1μg, n=7), naltrindole (10μg, n=7), CTAP (5μg, n=6), CTOP (10μg, n=6), bicuculline (10μM, n=7), cycloSomatostatin (0.1mM, n=8) and for (F) 5μg/ml capsaicin without (n=6) and with naloxone (1μg, n=9). (H and I) Pain and itch dose-response curve fitting of (D and E). (J) Enkephalin release with different doses of capsaicin from *Grp*^{Cre}*; ROSA26*$^{LSL\text{-}TrpV1}$*; TrpV1*$^{-/-}$ mice (black bars) and *ROSA26*$^{LSL\text{-}TrpV1}$*; TrpV1*$^{-/-}$ control mice (blue bars) normalized to per g tissue used in ELISA. (K) Comparison of "leaky gate" model (left) and the gate control theory (right). Yellow rectangles indicate type I incoherent feed forward loop formed by *Grp*$^{+}$ neurons and Aβ fibers respectively. Data are represented as mean ± SEM. *: $P < 0.05$, **: $P<0.01$, ***: $P<0.001$, two-tailed unpaired Student's t test. Abbreviations: WT short for wild type. KO short for *TrpV1*$^{-/-}$. Grp-V1;V1KO short for *Grp*^{Cre}*; ROSA26*$^{LSL\text{-}TrpV1}$*; TrpV1*$^{-/-}$, Enke short for Enkephalin, T short for pain transmission neurons, IN short for inhibitory interneurons.

To better interpret the behavioral responses, we used wild-type mice to first test drugs known to produce pain (capsaicin) and itch (gastrin releasing peptide, GRP and brain natriuretic peptide, BNP) responses when given intrathecally. The behavior chamber was surrounded by four mirrors on opposing sides and behaviors were recorded with a high-definition camera located above the chamber. This enabled the behavior to be viewed and captured from all angles (Figure 2.10)(LaMotte et al., 2011). When we played back videos at 1/4 normal speed, distinct behavioral responses to pain- and itch-producing drugs were observed in wild-type mice. Capsaicin generated extensive licking directed to the lower back regions at a characteristic frequency of 5Hz, but no scratching. This licking behavior usually stopped within 5 minutes of injection and was absent in TrpV1$^{-/-}$ mice, suggesting the specificity of this licking response. GRP and BNP, however, produced scratching that lasted about 30 minutes after injection, but no licking.

Surprisingly, the activation of *Grp*$^{+}$ neurons in *Grp*^{Cre}*; ROSA26*$^{LSL\text{-}TrpV1}$*; TrpV1*$^{-/-}$ mice by intrathecal capsaicin generated both pain-related licking and itch-related scratching; capsaicin generated no response in Cre negative control mice (*ROSA26*$^{LSL\text{-}TrpV1}$*; TrpV1*$^{-/-}$) and only pain-related licking in wild-type mice (Figure 2.9B and C), which confirms the specificity of the activation responses. The licking responses lasted only about 4 minutes after injection (similar to the licking responses in wild-type mice) and were not affected by a GRPR antagonist (Figure 2.9D and F); the scratching responses lasted more than 30 minutes and were effectively blocked by GRPR antagonist (Figure 2.9E and G). This result confirms previous reports that neurons expressing GRPR are important for the transmission of itch sensation. Thus the activation of *Grp*$^{+}$ neurons can trigger both robust pain and itch responses, a phenomenon rarely observed. Unlike itch-selective neurons in DRG, *Grp*$^{+}$ neurons receive monosynaptic inputs from both itch and pain neurons and code for both itch and pain, showing unexpected convergence of two related sensations in the spinal cord.

Intensity dependent coding of pain by *Grp*$^+$ neurons

Next, we used a dose-response curve to examine the relationship between *Grp*$^+$ neuron activation and behavior. Increasing doses of capsaicin increased itch responses until a plateau was reached while pain responses, surprisingly, showed an inverted U relationship (Figure 2.9D and E). Increased capsaicin resulted in increased licking time that peaked and then decreased with higher capsaicin doses. Weak and strong activation produced little pain while medium range activation generated optimal pain responses. Given that high doses of capsaicin still caused robust itch responses, the inverted U pain responses were unlikely caused by desensitization. Thus *Grp*$^+$ neurons demonstrate intensity-dependent coding. Rather than generating itch sensation with weak activation and pain sensation with strong activation, as suggested by the original intensity theory, *Grp*$^+$ neurons monotonically code for itch while pain is coded only by a certain range of inputs.

When we tried to fit the *Grp* activation dose response curves, the itch responses fitted nicely to the Hill equation (R^2=0.97, Figure 2.9I), while the pain responses, perhaps not surprisingly, did not assume sigmoidal shape. Instead, the pain responses fitted well with a polynomial equation (R^2=0.99, Figure 2.9H). Non-monotonic dose responses, such as hormesis responses, are usually modeled with polynomial equations(Bailer and Oris, 1997, 1998). The typical inverted U dose response curve of hormesis is generated by low dose stimulation and high dose inhibition effect of the same drug(Calabrese and Baldwin, 2003), suggesting that similar antagonizing actions might underlie the pain response curve generated by the activation of *Grp*$^+$ neurons.

To further explore the mechanisms underlying this novel inverted U coding of pain, we tried to "rescue" pain responses during strong activation of the *Grp*$^+$ neurons. An opioid antagonist, naloxone, at a dose not eliciting pain itself, "rescued" the pain responses from almost

zero to about half of the maximal level. Both bicuculline , a GABA A antagonist, and cyclo-somatostatin, the antagonist of anti-nociceptive somatostatin highly expressed in the surrounding region, failed to "rescue" the pain responses (Figure 2.9F). Successfully rescuing pain responses again confirmed that *Grp*$^{+}$ neurons were not desensitized by high doses of capsaicin. Naloxone had no effect on itch responses (Figure 2.9G), demonstrating the specificity of the "rescue" effect. To demonstrate that naloxone was not simply blocking the basal activity of the endogenous opioid system, independent of *Grp* activation, we co-injected naloxone with a low dose of capsaicin which can produce both medium pain and itch responses. No effect was observed on pain responses (Figure 2.9F), showing that the endogenous opioid system is only recruited to inhibit pain during strong activation of the *Grp*$^{+}$ neurons. The data suggest that the endogenous opioid system is at least partially responsible for the pain inhibition associated with strong activation of the *Grp*$^{+}$ neurons and therefore, together with direct pain coding by the *Grp*$^{+}$ neurons, generates this inverted U response curve.

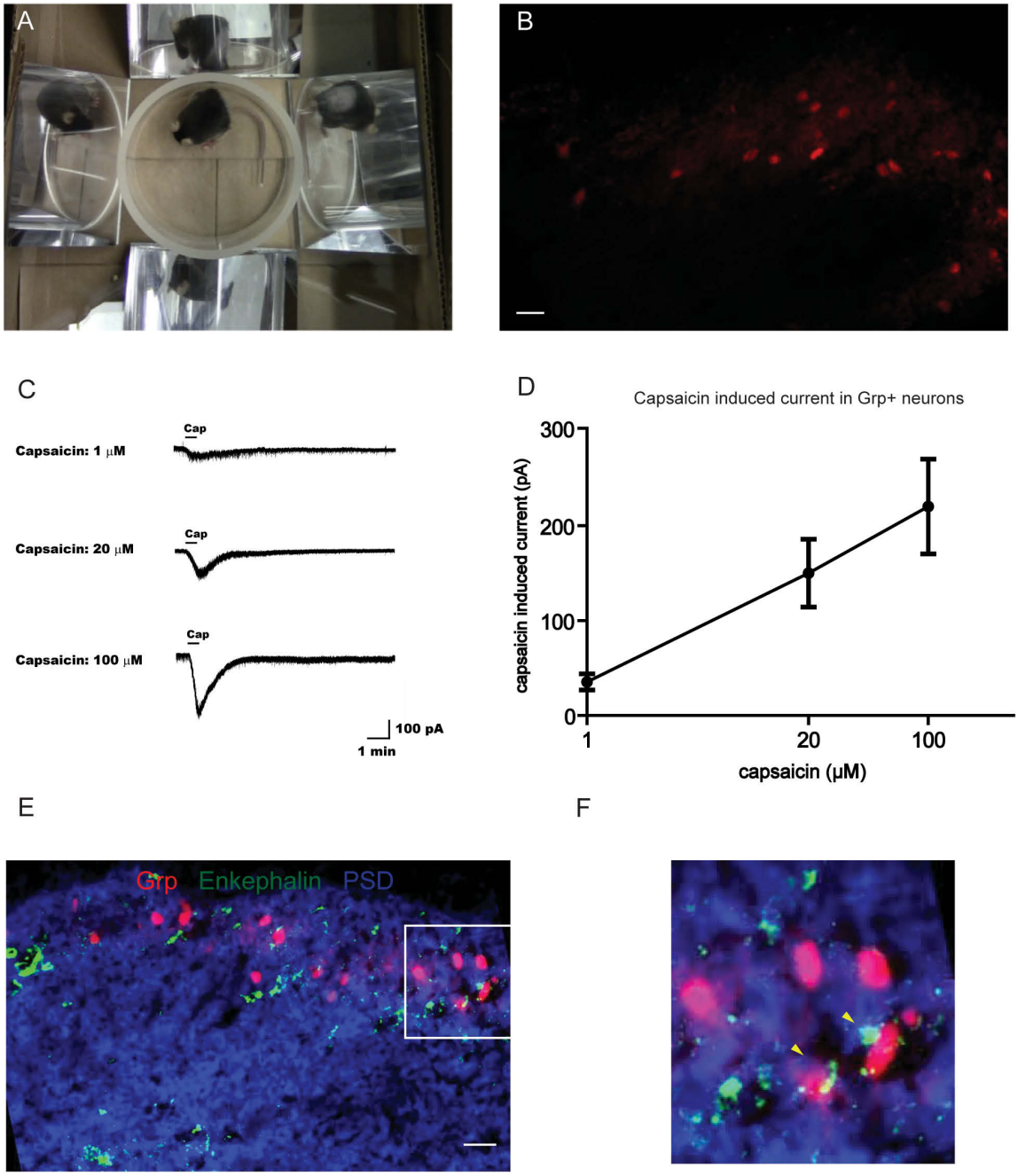

Figure 2.10 Capsaicin-mediated activation of *Grp*$^+$ neurons and co-localization of *Grp*$^+$ neurons and enkephalin-expressing neurons

(A) Photo showing behavior chamber with four mirrors on opposing sides with high-definition camera recording video from above. (B) AAV1-LSL-tdTomato virus labeled neurons from

Grp^{Cre}*; ROSA26*^{TrpV1}*; TrpV1*$^{-/-}$ spinal cord. (C) Representative traces of capsaicin-induced EPSCs in *Grp*$^{+}$ neurons of *Grp*^{Cre}*; ROSA26*$^{LSL\text{-}TrpV1}$*; TrpV1*$^{-/-}$ spinal slices. Black bars indicate capsaicin application. (D) Capsaicin dose responses of *Grp*$^{+}$ neurons ectopically expressing TrpV1 (n=6 each dose). Recordings done by Dr. Qian Xu. (E) Co-localization of *Grp*$^{+}$ neurons with Enkephalin-expressing neurons and PSD95. (F) Representative neurons in boxed region in E shown at greater magnification. Arrowheads indicate *Grp*$^{+}$ neurons co-localized with Enkephalin and synaptic marker PSD95. Data are represented as mean ± SEM. All scale bars represent 20 μm.

We determined which endogenous opioid peptide was employed to block pain by utilizing mu opioid antagonist CTAP and CTOP and delta opioid antagonist naltrindole. Naltrindole but not CTAP or CTOP induced a similar rescue effect as naloxone (Figure 2.9F), while none of the drugs affected itch responses (Figure 2.9G). These results link enkephalin, the endogenous ligand for delta opioid receptors, to this pain inhibition effect. Indeed, enkephalin release was detected with ELISA when *Grp*^{Cre}*; ROSA26*$^{LSL\text{-}TrpV1}$*; TrpV1*$^{-/-}$ spinal cords were treated with high dose capsaicin but not detected with low dose or no capsaicin (Figure 2.9J). Furthermore, spinal cord from Cre negative control mice (*ROSA26*$^{LSL\text{-}TrpV1}$*; TrpV1*$^{-/-}$) treated with high dose capsaicin released a minimal amount of enkephalin, which confirms that the release of enkephalin is dependent on strong activation of the *Grp*$^{+}$ neurons. To test whether *Grp*$^{+}$ neurons are synaptically connected with enkephalin-expressing interneurons in the spinal cord, we performed triple labeling of *Grp*$^{+}$ neurons (tdTomato), enkephalin and synaptic marker PSD95. Co-localizations of these three markers suggest that enkephalin-expressing interneurons may receive synaptic input from *Grp*$^{+}$ neurons (Figure 2.10). Moreover, enkephalin, like most neuropeptides, is stored in large dense core vesicles that require strong depolarization for

release(Cesselin et al., 1984; Neuman et al., 1984). This is consistent with the observation that only strong activation of the *Grp*$^+$ neurons triggers pain inhibition.

Grp$^+$ neurons form "leaky gate" to negatively regulate pain transmission

In short, activation of the *Grp*$^+$ neuron population codes for pain but also inhibits pain through the release of enkephalin, forming a type I incoherent feed forward loop (summarized in Figure 2.13B). Feed forward loop (FFL) is a common network motif highly represented in biological networks such as neuronal circuitries(Alon, 2007; Milo et al., 2002). The type I incoherent FFL, featuring direct activation and indirect inhibition of the same output, functions to generate non-monotonic responses, such as the inverted U response curve(Kaplan et al., 2008). A circuit with the inverted U response curve works as an amplitude filter to transmit signals only in a certain range(Entus et al., 2007), which is consistent with the pain behavioral responses associated with *Grp* activation.

A type I incoherent FFL that is related to pain is demonstrated in the gate control theory(Melzack and Wall, 1965; Wall, 1978). The gate control theory of pain proposes that nociceptive transmission neurons (T) receive both noxious input from C fibers and non-noxious input from Aβ fibers. Aβ input also indirectly inhibits nociceptive transmission neurons through inhibitory interneurons (IN). Thus Aβ fibers form a type I incoherent feed forward loop to control pain transmission (Figure 2.13A). The indirect inhibition through IN can close the "gate" (T) and suppress painful input.

Here, we propose a model to explain our experimental observations and then provide more data to support the model. Similar to Aβ fibers in the gate control theory, we propose that *Grp*$^+$ neurons can use the type I incoherent feed forward loop as a "gate" to regulate pain transmission. When strongly activated, *Grp*$^+$ neurons can trigger enkephalin release to close the

"gate" to painful signals from both *Grp*$^{+}$ neurons and potentially other pain- sensing neurons in the spinal cord, resulting in reduced pain sensation (summarized in Figure 2.13B). However, the Aβ and *Grp* gates have some fundamental differences. The Aβ FFL does not let any signals through the "gate", at least under physiological conditions, so that non-noxious input does not elicit pain sensations; the *Grp* FFL allows weak pain signals to pass through the "gate" but suppresses strong pain signals. Therefore, we named it a "leaky" gate. We think the advantage of this "leaky gate" is that passing on weak signals ensures sensitivity to weak painful stimuli while inhibiting strong signals prevents overwhelming pain sensations.

Increased pain and decreased itch after ablation of *Grp*$^{+}$ neurons

According to our "leaky gate" model, the *Grp* FFL functions as a "brake" to prevent strong pain signals from overwhelming the system. Therefore, we predicted that the loss of the *Grp*$^{+}$ neurons should lead to an increase of pain responses. To directly test this prediction, we ablated *Grp*$^{+}$ neurons with diphtheria toxin. Diphtheria toxin receptors (DTRs) were specifically expressed in *Grp*$^{+}$ neurons with Cre dependent *ROSA26*$^{LSL\text{-}DTR}$ line together with *ROSA26*$^{LSL\text{-}tdTomato}$ allele to monitor ablation efficacy (Figure 2.11A). Diptheria toxin treatments successfully ablated more than 95% of the *Grp*$^{+}$ neurons (Figure 2.11B and C). Cre negative mice (*ROSA26*$^{LSL\text{-}DTR/LSL\text{-}tdTomato}$) treated with same doses of diphtheria toxin were used as controls. Ablated mice were generally healthy and had normal motor coordination in the rotarod test (Figure 2.12). In addition, CGRP and IB4 labeled lamina II regions showed no change after ablation, suggesting that the loss of such a small population did not affect general organization of the local circuitries. The number of PKCγ positive neurons was reduced, consistent with the partial overlap between PKCγ and *Grp*$^{+}$ neurons while the number of Pax2^{+} interneurons were comparable between ablated and control mice, confirming that diphtheria toxin treatment did not produce non-specific neurotoxicity (Figure 2.12).

First, we tested acute pain responses. Chemical pain induced by capsaicin cheek injections greatly increased after ablation (Figure 2.11E, yellow shaded). *Grp*^{Cre}*; ROSA26*$^{LSL\text{-}DTR/LSL\text{-}tdTomato}$ mice also had significantly shorter response time in all thermal pain assays including hot plate, Hargreave and tail immersion when compared with control mice (Figure 2.11E). Mechanical sensitivity tested by Von Frey filaments remained the same in both genotypes (Figure 2.11F). Thus, loss of *Grp*$^{+}$ neurons enhanced chemical and thermal pain, as predicted by the "leaky gate" model. We next tested itch responses. Scratching responses to multiple pruritogens including histamine (100mM), Chloroquine (CQ, 4mM), SLIGRL (1mM) and serotonin (5-HT, 1mM) were all significantly reduced in *Grp*^{Cre}*; ROSA26*$^{LSL\text{-}DTR/LSL\text{-}tdTomato}$ mice, confirming the critical role of *Grp*$^{+}$ neurons in itch coding (Figure 2.11D).

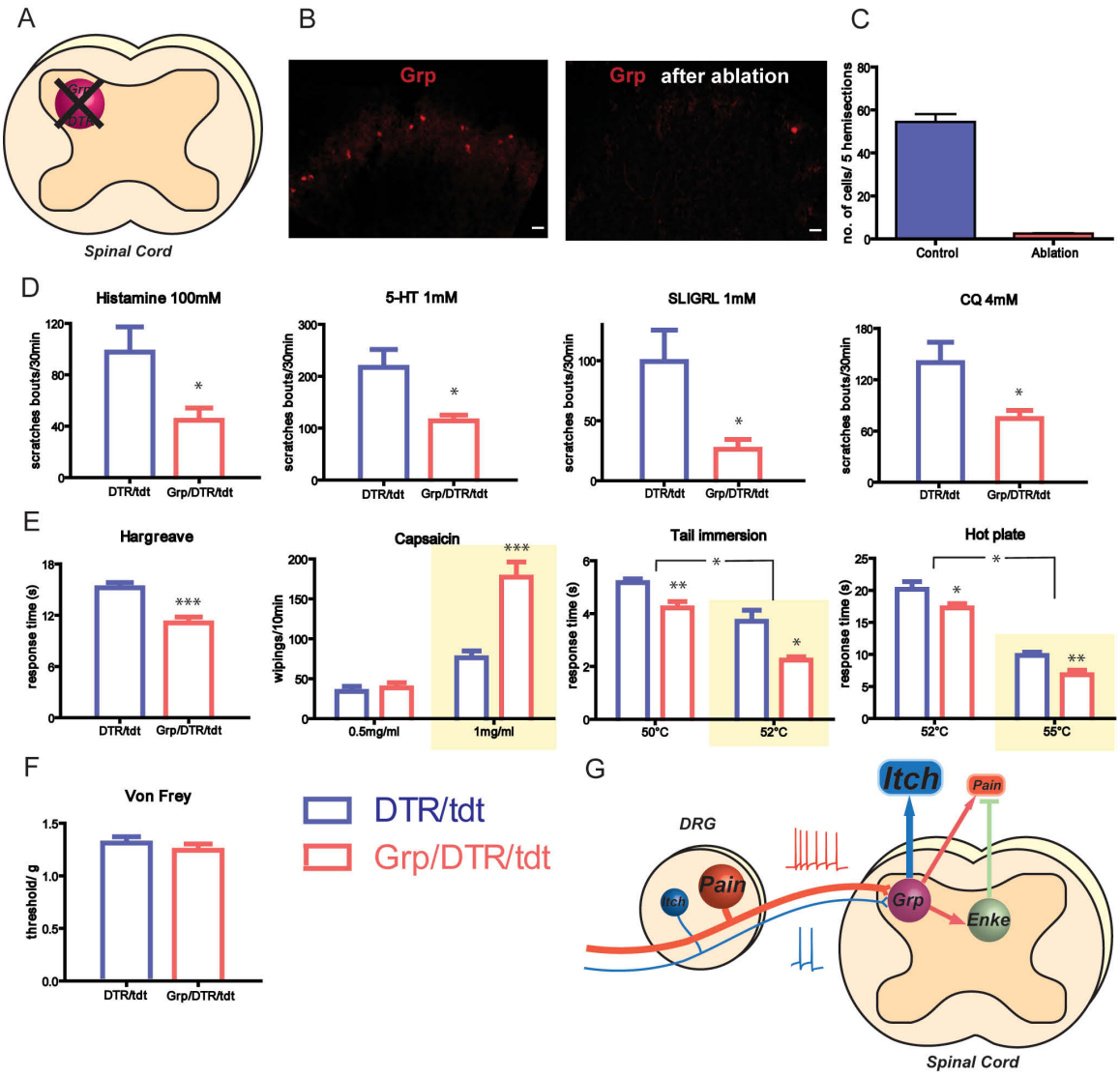

Figure 2.11 Increased pain and decreased itch responses after the ablation of *Grp*$^{+}$ neurons

(A) Diagram showing ablation of *Grp*$^{+}$ neurons in the spinal cord. (B) Representative images of *Grp*^{Cre}*; ROSA26*$^{LSL\text{-}DTR;\ LSL\text{-}tdTomato}$ spinal slices with and without diphtheria toxin treatments. All scale bars represent 20 μm. (C) Quantification of *Grp*$^{+}$ neurons per five 20μm hemisections in *Grp*^{Cre}*; ROSA26*$^{LSL\text{-}DTR;\ LSL\text{-}tdTomato}$ (red) and *ROSA26*$^{LSL\text{-}DTR;\ LSL\text{-}tdTomato}$ control mice (blue) after diphtheria toxin treatments (n=5 mice). (D) Scratching bouts induced by histamine (100mM, n=6 vs. 8), serotonin (1mM, n=7 vs. 8), SLIGRL (1mM, n=7) and chloroquine (4mM, n=11 vs. 9)

injection in the nape region (50µl) in *Grp*^{Cre}*; ROSA26*$^{LSL\text{-}DTR;\ LSL\text{-}tdTomato}$ (red) and *ROSA26*$^{LSL\text{-}DTR;\ LSL\text{-}tdTomato}$ control mice (blue). (E) Pain responses from Hargreaves test (n=8 vs. 7), capsaicin cheek injections (1mg/ml, n=8; 0.5mg/ml, n=7 vs. 6), hot plate test (52°C, n=10; 55°C, n=7 vs. 6) and tail immersion tail (50°C, n=7 vs. 6; 52°C, n=7 vs. 6) in *Grp*^{Cre}*; ROSA26*$^{LSL\text{-}DTR;\ LSL\text{-}tdTomato}$ (red) and *ROSA26*$^{LSL\text{-}DTR;\ LSL\text{-}tdTomato}$ control mice (blue). Yellow shaded regions represent responses with strong stimuli. (F) Von Frey test responses (n=11) in *Grp*^{Cre}*; ROSA26*$^{LSL\text{-}DTR;\ LSL\text{-}tdTomato}$ (red) and *ROSA26*$^{LSL\text{-}DTR;\ LSL\text{-}tdTomato}$ control mice (blue). (G) Diagram summarizing the role of *Grp*$^{+}$ neurons in pain and itch coding. *Grp*$^{+}$ neurons receive weak input from itchy stimuli and strong input from painful stimuli, and positively code for itch while negatively regulate pain transmission. Data are represented as mean ± SEM. *: $P < 0.05$, **: $P<0.01$, ***: $P<0.001$, extended Welch's t test for response ratio comparison between different temperatures in hot plate and tail immersion test and two-tailed unpaired Student's t test for the rest. Abbreviations: Grp/DTR/tdt short for *Grp*^{Cre}*; ROSA26*$^{LSL\text{-}DTR;\ LSL\text{-}tdTomato}$ and DTR/tdt short for *ROSA26*$^{LSL\text{-}DTR;\ LSL\text{-}tdTomato}$, CQ short for chloroquine, 5-HT short for serotonin.

Strong pain responses are more affected by the loss of *Grp*$^{+}$ neurons

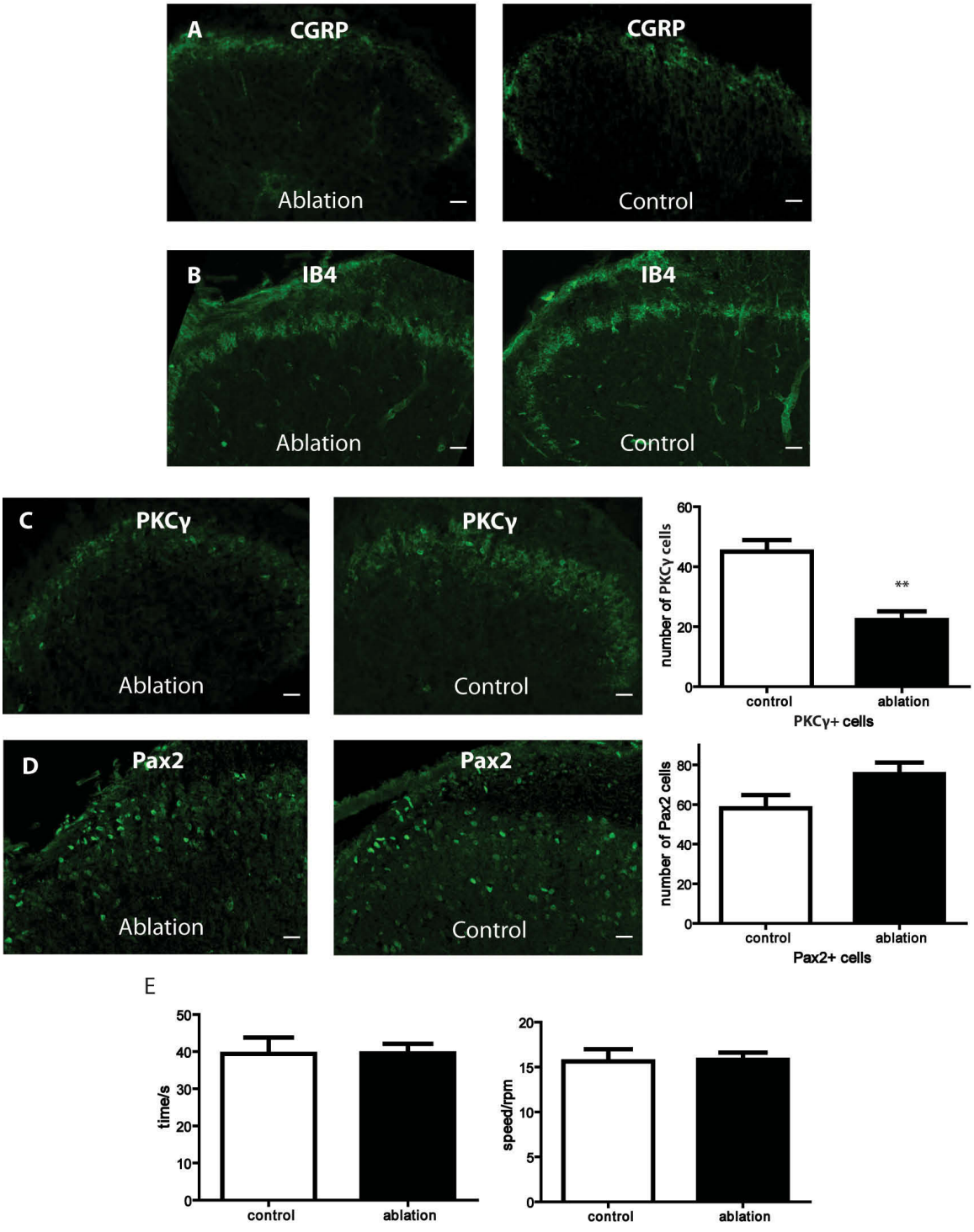

Figure 2.12 DTX treatment did not produce neurotoxic effects

(A and B) Representative images of *Grp*^{Cre}*; ROSA26*$^{LSL\text{-}DTR;\ LSL\text{-}tdTomato}$ (ablation) and *ROSA26*$^{LSL\text{-}DTR;\ LSL\text{-}tdTomato}$ (control) spinal cords stained with CGRP and IB4. (C and D) Representative images of PKCγ and Pax2 positive neurons in *Grp*^{Cre}*; ROSA26*$^{LSL\text{-}DTR;\ LSL\text{-}tdTomato}$ (ablation) and *ROSA26*$^{LSL\text{-}DTR;\ LSL\text{-}tdTomato}$ (control) spinal cords. Quantification on right panels. **: P<0.01, two-tailed unpaired Student's t test. (E) Ablation of *Grp*$^{+}$ neurons did not affect motor coordination in Rotarod test. Data are represented as mean ± SEM. All scale bars represent 20 μm.

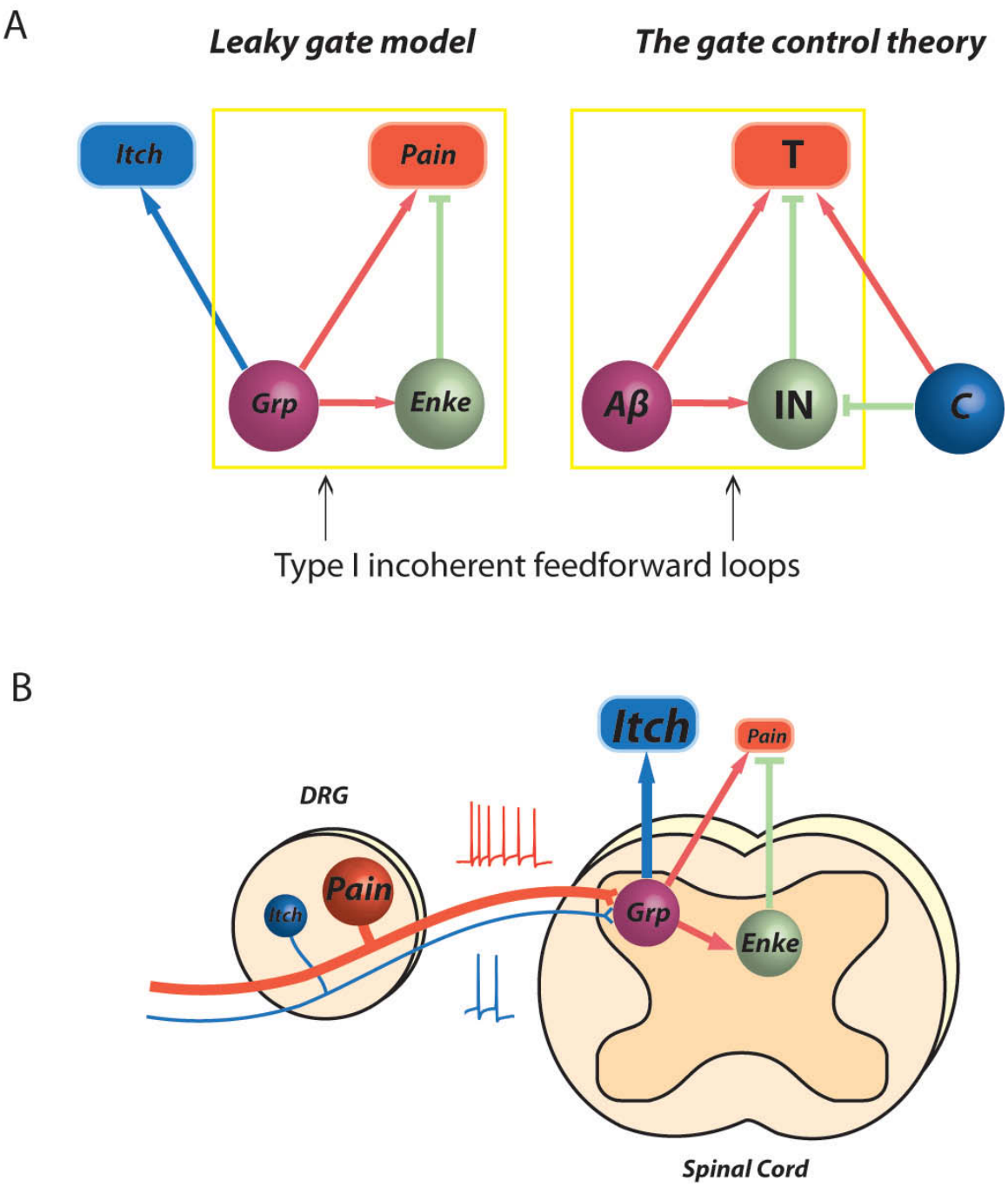

Figure 2.13 "Leaky gate" model in pain and itch transmission

(A) Comparison of "leaky gate" model (left) and the gate control theory (right). *Grp*$^+$ neurons directly code for pain and itch while inhibiting pain through Enkephalin-expressing interneurons. Aβ fibers activate pain transmission neurons and also indirectly inhibit pain transmission neurons via inhibitory interneurons. Yellow rectangles indicate type I incoherent feed forward loop formed by *Grp*$^+$ neurons and Aβ fibers respectively. (B) Diagram summarizing the role of *Grp*$^+$ neurons in pain and itch coding. *Grp*$^+$ neurons receive weak input from itchy stimuli and strong input from painful stimuli, and positively code for itch while negatively regulate pain transmission. Abbreviations: Enke short for Enkephalin, T short for pain transmission neurons, IN short for inhibitory interneurons.

We also compared dose effect on itch responses, which are normally coded by the *Grp*$^+$ neurons, between control and ablated mice. Ablated mice showed reduced itch responses to low doses of SLIGRL and CQ (Figure 2.11D), while high doses generated similar responses in both ablated and control mice (Figure 2.12). Thus in contrast to pain, stronger itch responses are less affected by the loss of *Grp*$^+$ neurons, potentially due to saturation or compensation from other itch secondary neurons. These results confirm that the *Grp* FFL has distinct roles in pain and itch coding.

Discussion

The selectivity theory depicts pain and itch coding in the spinal cord as the continuation of separate labeled lines from periphery with pain inhibiting itch through B5-I interneurons(Kardon et al., 2014) or NPY interneurons(Bourane et al., 2015c). We show that a subset of secondary neurons with uniform morphologies, the *Grp*$^+$ population, participates in the coding of both pain and itch sensations. We think this potentially represents the currently underappreciated crosstalk of these two sensations in the spinal cord. The difference of circuit organizations in DRG and the spinal cord is hinted at by their distinct anatomical structures. DRG neurons with pseudo-unipolar organizations and little crosstalk between each other resemble labeled lines, while neurons in the spinal cord dorsal horn form an interlacing network, enabling crosstalk of incoming information from different sensations.

Another feature of the *Grp*$^+$ population is the intensity dependent coding of pain. The *Grp*$^+$ neurons directly code for pain sensation and upon strong activation, indirectly inhibit pain via the recruitment of the endogenous opioid system. Only a certain range of input can trigger pain sensation via *Grp*$^+$ neurons. Contrary to the intensity theory, which suggests that different intensities differentiate different sensations, the intensity-dependent pain coding by the *Grp*$^+$ neurons reflects a way of pain signal processing in the spinal cord. Unlike classical monotonic coding of sensory information, this novel intensity-dependent coding serves as a good example of the currently overlooked non-monotonic signal processing by spinal circuits.

The *Grp*$^+$ population forms a type I incoherent feed forward loop to regulate pain transmission, similar to the role of Aβ fibers in the gate control theory. Both systems function as "brakes" for pain. Pain detection systems need to be sensitive enough to protect the body from potential harm, but when exposed to strong pain stimuli, high sensitivity could be troublesome.

High sensitivity may generate too much pain and interfere with proper behavioral responses. Thus brakes are necessary. Brakes triggered by signals from Aβ mechanosensitive fibers makes gentle rubbing an effective way to relieve pain, while brakes triggered by pain itself can provide negative feedback to prevent overwhelming pain responses. The pain inhibition mediated by *Grp*$^{+}$ neurons, however, cannot be triggered by itch, since itch stimuli only weakly activate *Grp*$^{+}$ neurons, consistent with the fact that itch can rarely inhibit pain.

Unlike the role of Aβ fibers in the gate control theory, the *Grp* FFL functions as a "leaky gate" to pass along weak pain signals and only close the gate to inhibit strong pain signals. Such a "leaky gate" can reduce strong pain responses without sacrificing the sensitivity to weak pain signals. The pain inhibition mediated by enkephalin is more prominent than the coding of pain by the *Grp*$^{+}$ population, since the inhibition effect could completely block pain responses from the *Grp*$^{+}$ population and further reduce pain coded by other pain-sensing neurons in the spinal cord. If such strong pain inhibition was triggered also by weak stimuli, it may likely affect pain sensitivity. Incoherent feed forward loops can provide diverse response patterns by varying the relative strength of the two arms with opposing effects on the output and, thus, are well suited for the fine-tuning of sensory responses, as illustrated by the gate control theory and the "leaky gate" model.

The ablation experiments showed that stronger pain responses had bigger increases after the ablation of the *Grp*$^{+}$ neurons, suggesting that the *Grp* FFL provides stronger inhibition on stronger painful input in physiological conditions, consistent with the "leaky gate" model. Theoretically, weak enough painful stimuli might evoke weaker pain responses after the ablation of *Grp*$^{+}$ neurons, as these painful stimuli do not trigger pain inhibition and thus are positively coded by the *Grp*$^{+}$ population. However, given that the *Grp*$^{+}$ neurons only represent a subset of pain responsive neurons in the spinal cord, the loss of these neurons may generate a more subtle

change in behavior when compared with the loss of the strong pain inhibition effect mediated by the *Grp* FFL and thus be much harder to detect with animal behavioral tests. In a previous study, Mishra et al. ablated 70% of NPR1$^+$ neurons, which were reported to be a subset of *Grp*$^+$ neurons, with BNP conjugated saporin and only found a significant change in histamine responses(Mishra and Hoon, 2013). We think the partial loss of *Grp*$^+$ neurons might not be sufficient to generate significant changes in pain responses; however, the response time in the hot plate test did seem to show a trend of reduction after the ablation of NPR1$^+$ neurons.

Evidence suggests that *Grp*$^+$ neurons are synaptically connected with enkephalin expressing neurons, so activation of *Grp*$^+$ neurons likely triggers enkephalin release from these local interneurons. Most enkephalin positive neurons in the spinal dorsal horn are GABAergic inhibitory interneurons(Fukushima et al., 2011; Todd et al., 1992). Enkephalin, like other typical neuropeptides, is stored in large dense core vesicles and released upon strong, not weak, depolarization(Cesselin et al., 1984; Neuman et al., 1984). Therefore, it is strong painful but not itchy or weak painful stimuli that can strongly activate *Grp*$^+$ neurons and further trigger enkephalin release in enkephalin positive inhibitory interneurons. This explains the selective recruitment of enkephalin by strong painful stimuli. Support of the *Grp* FFL recruitment of the enkephalin system was found by the increase of enkephalin release from spinal cord following nociceptive stimuli(Cesselin et al., 1985).

The *Grp*$^+$ neurons represent a subset of secondary neurons mediating pain and itch sensations in the spinal cord. Painful stimuli from the periphery can elicit both pain and itch responses via the *Grp*$^+$ neurons. The itch responses are likely blocked by feed forward inhibition from parallel pain pathways, as stated by the selectivity theory. Similarly, itchy stimuli from the periphery can also trigger both itch and pain responses via the *Grp*$^+$ neurons. The pain responses, we think, might be weak, given the weak activation of the *Grp*$^+$ neurons by itchy stimuli. Indeed,

in human psychophysical studies, most itchy substances induce itch sensation accompanied by weaker and shorter lasting noxious sensations, such as pricking and burning, while painful substances induced nociceptive but not itch sensations(LaMotte et al., 2014; Liu et al., 2012; Sikand et al., 2009, 2011a). Thus the "leaky gate" model can explain the nociceptive sensations generated by itchy chemicals in human psychophysics studies. However, we cannot rule out the possibility that mechanical or other forms of itch can bypass or block the weak pain responses and result in pure itch sensation.

In summary, Grp^{+} neurons positively code for itch while negatively regulating pain transmission with a "leaky gate." This study, to our knowledge, experimentally demonstrates intensity-dependent coding of pain in spinal cord for the first time. It better explains observations in human psychophysical studies and serves as a great example of non-monotonic coding and fine-tuning of sensory information in spinal cord. The new "leaky gate" model and related mechanistic understanding of pain and itch coding may provide valuable information for the treatment of devastating chronic pain and chronic itch conditions, as the influential gate control theory of pain did.

CHAPTER 3: REDEFINING THE CONCEPT OF PROTEASE-ACTIVATED RECEPTORS: CATHEPSIN S EVOKES ITCH VIA ACTIVATION OF MRGPRS

Introduction

The sensation of itch is relayed from the skin to the brain via a complex but orchestrated series of signals. Itch is initiated when exogenous or endogenous pruritogens activate receptors or channels on the peripheral projections of primary sensory neurons, the cell bodies of which reside in the dorsal root or trigeminal ganglia. Specific members of the family of Mas-related G-protein-coupled receptors (Mrgprs) are expressed by subsets of nociceptive fibres(Dong et al., 2001). These receptors have been shown to bind select pruritogens in the periphery and mediate non-histaminergic itch(Liu, 2009, 2011). For example, mouse MrgprA3 and human MRGPRX1 respond to chloroquine, an anti-malarial drug, and are responsible for relaying chloroquine-induced scratching in mice(Liu, 2009; Wilson et al., 2011). Mouse MrgprC11 and human MRGPRX1 respond to a different subset of pruritogens including bovine adrenal medulla peptide (BAM8–22). MrgprC11 is activated by SLIGRL and SLIGKV, the tethered ligand peptides of respective mouse and human protease-activated receptor-2 (PAR2), while MRGPRX2 is activated by SLIGKV(Lembo, 2002; Liu, 2009, 2011; Sikand et al., 2011b). Trypsin, a serine protease and conventional activator of PARs, does not activate Mrgprs(Liu, 2011; Ramachandran and Hollenberg, 2008).

In addition, β-alanine, a body-building supplement known to cause itch upon ingestion, activates the MrgprD receptor expressed by nociceptive fibres(Liu, 2012). In transgenic mice in which a cluster of Mrgprs has been ablated, cutaneous exposure to these pruritogens evokes significantly less scratching compared with wild-type (WT) controls. These findings underscore the importance of this family of receptors to peripheral detection of non-histaminergic itch stimuli

and the subsequent activation of itch-specific neural pathways. While several exogenous compounds trigger Mrgpr activation, endogenous ligands or modulators of MrgprA3 and MrgprC11 receptors have yet to be identified.

Both serine and cysteine proteases have been implicated in triggering itch and inflammation in the skin. The plant cysteine protease mucunain, derived from the tropical bean plant commonly known as cowhage, and the human cysteine protease, cathepsin S (cat S), elicit itch in human volunteers(Reddy et al., 2008, 2010). We demonstrated previously that cat S, mucunain and other plant cysteine proteases including papain, bromelain and ficin are capable of activating PAR2 and PAR4(Reddy and Lerner, 2010; Reddy et al., 2010). It has been presumed that cysteine protease-evoked itch was induced via PAR2 activation. The possibility that activation of receptors other than PARs could be responsible for this sensation has not been investigated. MrgprC11 is activated by SLIGRL, a synthetic peptide generated based on the tethered sequence of the PAR2 N terminus following cleavage by serine proteases(Liu, 2011). This observation is surprising because Mrgprs are not members of the PAR family. MrgprC11 does not have either arginine or lysine residues in its N-terminal extracellular domain. This receptor would neither be cleaved nor in theory activated, by serine proteases including trypsins and kallikreins. In contrast, the MrgprC11 receptor N terminus contains glycine and leucine residues, both cleavage targets for aspartyl and cysteine proteases(Rawlings et al., 2012).

Here, we formally investigated whether select cysteine proteases are capable of cleaving and activating MrgprC11 receptors in vitro, and determined the significance of MrgprC11 signalling in mediating cat S-induced scratching in vivo. The results demonstrate that cathepsin S provokes itching by cleavage of MrgprC11 at a specific site, resulting in activation of this receptor without generating either a tethered or diffusible ligand. Although cathepsin S can activate PAR2 receptors, such an activation is not necessary for itching provoked by this protease.

Hybrid receptors in which the N terminus of MrgprC11 was replaced with the N terminus from either the β2AR or MC1R were also activated by cathepsin S. These findings highlight the possibility that cysteine proteases may exert effects on other "non-PAR" GPCRs and further suggest that proteases are capable of modulating GPCRs by multiple mechanisms.

Methods

Reagents, peptides and antibodies

Recombinant cat S was generated as previously described(Reddy et al., 2010) and diluted in 1x PBS, pH 7.4, 5mM EDTA, 5mM dithiothreitol and 5mM cysteine chloride. Papain (Sigma-Aldrich) was diluted in 0.1x PBS, 50mM sodium acetate, pH 6.5, 5mM EDTA, 5mM dithiothreitol and 5mM cysteine chloride. Crystalline papain is more active and has a broader cleavage range than recombinant cat S. Different incubation times or concentrations were thus used as indicated. N-terminal peptides derived from the sequence of MrgprC11 were obtained from GenScript and diluted in PBS. The 28 amino-acid N-terminal peptide MDPTISSHDTESTPLNETGHPNCTPILT was made by Peptide 2.0 (Chantilly, VA). The cysteine protease inhibitor E-64 was obtained from Sigma-Aldrich. Similar results were obtained at either 5 or 10 mM of this compound. Anti-Gaussia luciferase, catalogue # E8023S from New England Biolabs was used at a dilution of 1:1,500. Anti-phospho-PKC (pan) (bII Ser660) catalogue #9371 from Cell Signaling Technology was used at a dilution of 1:1,000. Horseradish peroxidase (HRP)-labelled donkey anti-rabbit, catalogue # NB660–894, and anti-mouse antibodies, catalogue # NB7544, were from Thermo Fisher and used at 1:2,000 and 1:5,000, respectively. Molecular weight markers were Bioreagents EZ-run prestained rec protein ladder, cat # 3603500 from Thermo Fisher. All other reagents were purchased from Invitrogen, unless otherwise noted.

Mice

WT and PAR2 KO mice were obtained from Jackson Laboratories. Mrgpr cluster KO mice were generated by our lab as previously described(Liu, 2009). The mouse studies were performed at Johns Hopkins and approved by the IACUC at that institution.

Cell culture

HeLa cells were obtained from the ATCC and maintained in DMEM supplemented with fetal bovine serum, L-glutamine, penicillin and streptomycin (Fisher Biochemicals). Dissociated DRG neurons were prepared from WT, Mrgpr cluster KO, PAR2 KO and Pirt-GCaMP3 mice as reported previously(Liu, 2009). DRGs were collected from all spinal levels of 4-week-old mice, placed in cold medium and treated with enzyme solution at 37°C. Following titration and centrifugation, cells were suspended, plated on glass coverslips coated with poly-D-lysine and laminin, incubated at 37°C and used within 48 h.

Cloning of WT MrgprC11 and generation of mutants

The coding region of MrgprC11 was cloned by PCR from mouse genomic DNA using the forward and reverse primers: 50-GCGCTCGAGAGCATGGATCCAACCATCTCATC-30 and 50-GCGAAGCTTTCAATATCTGCTTTCTGAAATCTC-30. C11 N-terminal mutants were made by site-specific mutagenesis procedures to change the listed residues to isoleucine or arginine at the P2 site. Leucine at P2 is the preferred site for cleaved by cathepsin S as in native MrgprC11, with isoleucine less so and arginine not at all.

Preparation of G. luciferase–MrgprC11 fusion cDNAs

G. luciferase complementary DNA (cDNA) was cloned, without its termination codon, into pcDNA3.1 as an XbaI–XhoI fragment. MrgprC11 cDNA was fused as an XhoI–HindIII unit

at the 30 terminus of the luciferase cDNA to obtain LucMrgprC11. Preparation of MrgprC11 with β2AR and MC1R amino termini. The MrgprC11 coding region without its N terminus from amino-acid 34 to its C terminus was cloned as an EcoRI–HindIII cDNA into pcDNA3.1 to obtain the vector pMrgprC11NR. The N termini of b2AR and MC1R from amino acids 1–34 and 1–37, respectively, were isolated as XhoI–EcoRI fragments by PCR, and cloned into pMrgprC11NR to generate the vectors pARC11 and pMC1RC11 for expression of the chimeric receptors β2AR–MrgprC11 and MC1R–MrgprC11.

Calcium imaging

HeLa cells were grown to confluence, trypsinized and then transfected with the pcDNA vector carrying the G. luciferase–MrgprC11 fusion construct, MrgprC11 cDNA or salmon sperm DNA as a control using Lipofectamine 2000. Transfected cells were plated into 96-well glass-bottom plates at 50,000 cells per well and maintained at 37°C in 5% humidified CO_2 for 3 h after which time the medium was replaced. Twenty-four to 48 h after transfection, cells were incubated for 60 min at room temperature with 2 mM of Fura-2-acetoxymethyl ester (Fura-2) diluted in complete DMEM. Following Fura-2 loading, the medium was replaced with 90 ml of HEPES-buffered saline (20mM HEPES, 115mM NaCl, 5.4mM KCl, 2mM $CaCl_2$, 0.8mM $MgCl_2$ and 13.8mM glucose, pH 7.4) and cells were used immediately for calcium imaging. A luciferase–receptor construct was used in all tranfections to establish consistency of transfection efficiency. Ratiometric calcium imaging was performed using a Zeiss Axiovert 200M microscope equipped with a flipping filter wheel and Axiovision software (version 4.6). Peptide and protease agonists, cat S or papain were added 15 s after initiating image acquisition and typically represented by down arrows in the figures. Images were acquired at time 0 and every 5 s thereafter for at least 90 s. All images obtained during each acquisition period were analyzed. Each experiment was

performed at least three times, and ratiometric changes were measured in at least 20 cells per acquisition with responses of three representative cells.

Primary DRGs cultured from WT, Mrgpr cluster KO and PAR2 KO mice were loaded with Fura-2 for 30 min at 37°C for ratiometric calcium imaging as described above following application of cat S and papain (5 and 20 mM, respectively). For experiments incorporating RNA interference, MrgprA3 and MrgprC11 on-target short interfering RNAs (siRNAs) were purchased from Thermo Scientific. MrgprA3 or MrgprC11 siRNA (0.175 nmol) were electroporated, respectively, into DRG neurons from Pirt-GCaMP3 mice that had been generated previously(Kim, 2014; Liu, 2009).

Electroporation of dissociated DRG neurons with Mrgpr-expression constructs was carried out using Mouse Neuron Nucleofector Kit (Amaxa Biosystems) following the manufacturer's instructions. Electroporated neurons were plated and cultured as described above and used within 72 h. Green fluorescence from genetically encoded calcium GCaMP3 was detected via single-photon Ca^{2+} imaging with a 700 Zeiss confocal microscope, using the 488-nm line of a solid-state laser for excitation of Pirt-GCaMP3 and a 488-nm laser main dichroic beam splitter and a 505–555-nm variable secondary dichroic mirror to detect the emission of green fluorescence.

Real-time quantitative PCR

Total RNA was extracted from cultured DRGs 3 days after siRNA electroporation using an Rneasy micro kit (Qiagen). Purified RNA was quantified on a Nanodrop 2000 UV spectrophotometer (Thermal Scientific) at 260 nm and assessed for purity using the 260/280-nm ratio. DNA was reverse transcribed with the Superscript First Strand Synthesis System (Invitrogen). PCR amplifications were carried out with a Step One Plus real time PCR system

(Applied Biophysics). PCR conditions were 95°C for 3min and 50 cycles of 95°C for 30 s and 60°C for 60 s.

Primers as listed below: MrgprC11-F 50-AGCATCCA CAACCCCAGAAG-30; MrgprC11-R 50-TGGAGTGCAGTTGGGATGAC-30; MrgprA3-F 50-ACACAAGCCAGCAAGCTACA-30; MrgprA3-R 50-ACTTCCAG GGATGGTTTCGT-30; Actin-F 50-CGTCGACAACGGCTCCGGCATG-30; Actin-R 50-CCACCATCACACCCTGGTGCCTAGG-30

All primers were intron spanning to avoid genomic DNA contamination. Melting curve analysis was applied to all final PCR products after the cycling protocol. Samples were run in triplicate, and threshold cycle (Ct) values from each reaction were averaged. Relative messenger RNA levels of MrgprA3 and MrgprC11 were calculated from threshold cycles and normalized to the actin level. Experiments were carried out three times with samples from different animals, and the Student's t-test was used to determine significance.

Concentration-effect measurements for cat S and papain.

HeLa cells transfected with MrgprC11 cDNA were analysed using ratiometric imaging as described above with cat S and papain at concentrations from 1 nM to 10 mM. Each of the concentration-dependent readings was performed in triplicate. Maximum intensities at each of the dilutions were calculated and plotted against concentration using GraphPad Prism software. Error bars represent s.e.m. within an experiment, although these experiments were performed multiple times with similar results. Luciferase assay. MrgprC11 plasmid DNA (10 mg) or salmon sperm as control was transfected into HeLa cells as described above and plated into 10-cm dishes. Forty-eight hours after transfection, the cells were washed with PBS, scraped and pelleted. Cells were suspended in a volume of 200 ml PBS and 100 ml were incubated with cat S (2 mM) or papain

(0.02 mM) in the presence or absence of the irreversible cysteine protease inhibitor E-64 for 10 min at room temperature. Control cells were not treated with protease.

Protease activity was quenched by adding 300 ml of complete DMEM, after which the cells were centrifuged and supernatants (50 ml) were assayed in triplicate for luminescence according to the instructions of the manufacturer (New England Biolabs). These experiments were performed multiple times with protease activity being quenched at many different time points so as to catch luminescence associated with papain, as this protease has the capacity to digest luciferase.

Western blot analysis for luciferase

HeLa cells transfected with the G. luciferase–MrgprC11 fusion construct were treated with cat S (2 mM) or papain (0.02 mM) for 10 min. Cells were pelleted and the supernatant was added directly to loading buffer to quench enzymatic activity, run on NuPAGE Novex Bis-Tris mini gels and transferred to nitrocellulose membranes. Membranes were probed with a primary rabbit anti-G. luciferase antibody followed by HRP-labelled donkey anti-rabbit antibody for reaction with the ECL substrate to identify protein bands. The results presented are representative of one of four experiments.

Western blot analysis for p-PKC (Ser660)

HeLa cells were transfected with MrgprC11 plasmid DNA as described above and plated onto three 10-cm dishes. Non-transfected HeLa cells were also plated into three other 10-cm dishes. Forty-eight hours after transfection, cells were washed with PBS and then treated with papain or cat S at 0.02 and 2 mM, respectively, for 10 min. A subset of HeLa cells that were not transfected was treated with papain, cat S or PBS alone as controls. Cells were harvested by scraping, pelleted and lysed by repetitive freeze–thaw cycles. Cell lysates were centrifuged at 4°C

for 15 min. Supernatants were collected and protein concentrations were determined by the Bradford assay. Equal amounts of cell lysates were loaded onto NuPAGE Novex Bis-Tris mini gels, electrophoresed and transferred to nitrocellulose membranes. Membranes were probed with rabbit anti-phospho-PKC (bII Ser660) followed by incubation with HRP-labelled donkey anti-rabbit antibody for reaction with the ECL substrate to identify protein bands on the membrane. The blot was re-probed with mouse anti-actin antibody to identify the control actin band (42 kDa). HRP-labelled anti-mouse antibody was used as a secondary antibody for the ECL substrate. This experiment was repeated three times and error bars represent ±s.e.m. between the individual bands between three separate experiments, with relative intensities quantified using ImageJ.

Behavioral studies

All mice used for behavioral studies were 2- to 3-month-old males (20–30 g) and were backcrossed to C57BL/6 mice for at least 10 generations. Mice were habituated for 30 min per day for 3 days prior and then at least 15 min on the day of the study. Intradermal injections of 10 μl cat S 80 mM were delivered to the cheek(Shimada and LaMotte, 2008). Scratching behavior was observed for 30 min. A scratching bout was defined as continuous scratching movements with hind paws directed at the site of injection. Scratching behavior was quantified by recording the number of scratching bouts at 5-min intervals over a 30-min observation period. Experimenters were blind to genotype. Data are presented as mean±s.e.m. n represents the number of mice analyzed or times the experiments were performed. The distribution of the variables in each experimental group was approximately normal. Statistical comparisons were conducted by two-tailed, unpaired Student's t-test. Differences were considered to be statistically significant for $P<0.05$. Representative data are from experiments that were replicated biologically at least three times with similar results.

Results

Cysteine proteases cleave the N terminus of MrgprC11

MrgprC11 plays a critical role in mediating pruriception from the periphery. These receptors are known to bind several well-recognized pruritogens, including peptides resulting from the cleavage of PARs. Whether or not proteases have any direct effect on Mrgpr receptors was not known. To address this possibility, we asked whether cysteine proteases could cleave the extracellular N-terminal portion of MrgprC11. HeLa cells were transfected with a construct encoding MrgprC11 tagged with *Gaussia luciferase* at its N terminus and then treated with cat S or papain. Receptor cleavage was assessed by measuring levels of luminescence in the supernatants (Figure 3.1). Both papain and cat S induced cleavage of the MrgprC11 N terminus as determined by luminescence (Figure 3.1A). Incubation with E-64, an irreversible cysteine protease inhibitor, blocked protease-mediated cleavage of the N termini. In separate studies, tagged MrgprC11-tranfected cells were treated with cysteine proteases. Western blots of supernatants probed with an anti-*G. luciferase*antibody revealed a dense band at ~20 kDa in cells treated with cat S or papain, consistent with the mass expected of an N-terminal peptide tagged with *G. luciferase* (Figure 3.1B). As expected, no bands were identified in controls in which transfected cells were not treated with protease. These results reveal that cysteine proteases cleave the N-terminal portion of MrgprC11.

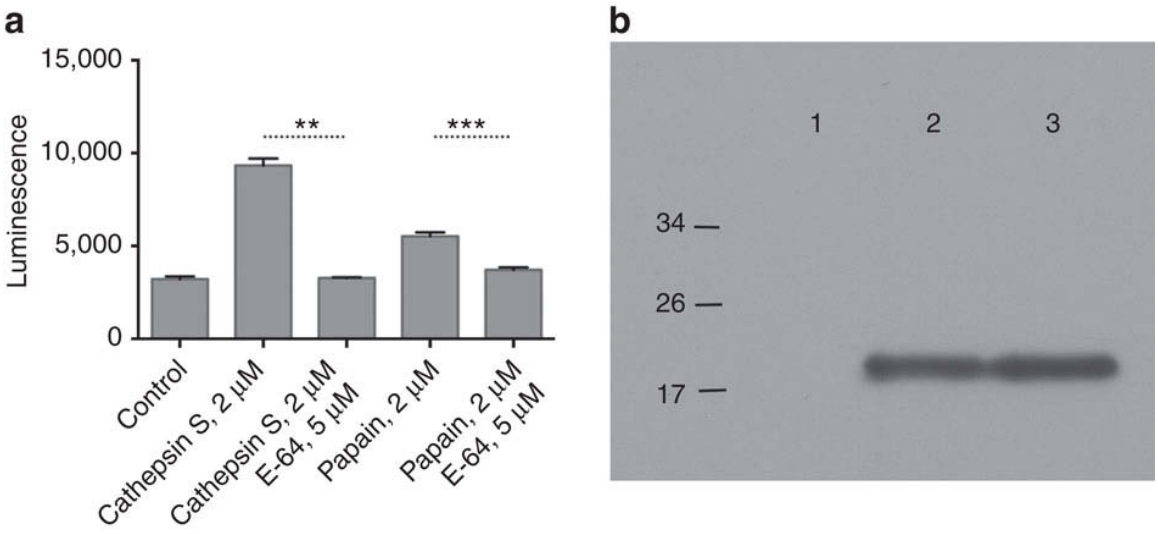

Figure 3.1 Cysteine proteases cleave near the N terminus of MrgprC11

(**A**) Luminescence was measured after treating LucMrgprC11-transfected HeLa cells with cat S (2 µM) and papain (2 µM) in the presence or absence of E-64 (5 µM). Baseline luminescence has been subtracted. The data are presented as mean±s.e.m. ***P*<0.001, ****P*<0.0005; two-tailed unpaired *t*-test from a representative experiment that was performed three times. (**B**) Western blot of LucMrgprC11 N-terminal cleavage products following treatment of transfected HeLa cells with control buffer without proteases (lane 1), papain, 0.02 µM (lane 2) and cat S, 2 µM (lane 3). The lesser amount of luminescence from papain as compared with cat S in **a** is likely a result of higher enzyme activity and a broader range of cleavage sites for papain. Similarly, for **b**, a lesser concentration of papain as compared with cat S was used for incubation times to be the same for detection of luciferase. See the Methods and Discussion sections for additional comments. Results from Dr. Ethan Lerner's group.

Cysteine proteases activate MrgprC11 *in vitro*

We next asked whether cysteine proteases were capable of activating MrgprC11. This receptor signals via Gq, resulting in phospholipase C activation and, via second messenger

recruitment, increased intracellular free Ca^{2+} and protein kinase C activation(Wilson et al., 2011). To assess receptor activation, we performed calcium imaging using the ratiometric calcium indicator Fura-2 in HeLa cells transfected with MrgprC11 following treatment with cat S or papain. Each protease elicited calcium responses (Figure 3.2A), activating MrgprC11 in a concentration-dependent manner with an effector concentration for half-maximum response of ~140 nM (Figure 3.2B). Calcium responses were ablated when cells were treated with the protease inhibitor E-64 (Figure 3.2A). In contrast to the robust responses induced by cysteine proteases, we confirmed that trypsin, a serine protease, does not activate MrgprC11(Liu, 2011). Western blotting revealed PKC phosphorylation at serine 660 (Ser660) following treatment with cat S and papain (Figure 3.2C). Quantification of the bands revealed an approximate 4.6-fold increase in p-PKC associated with protease activation relative to controls.

We next assessed whether cysteine proteases activate endogenously expressed Mrgpr receptors on dorsal route ganglion (DRG) neurons. Both cat S and papain treatment evoked calcium signals in DRGs from WT mice (Figure 3.2D). Fewer DRG neurons harvested from mice in which a cluster of *Mrgpr* genes, including *MrgprC11*, have been deleted (*Mrgpr cluster* $\Delta^{-/-}$*mice*), responded to cat S (Figure 3.2D). The lack of response of these neurons to papain is likely due to receptor inactivation by papain under the conditions used. Because cat S is known to activate PAR2 when it is expressed in heterologous cell lines(Reddy et al., 2010), we evaluated the effect of cat S on DRGs harvested from$PAR2^{-/-}$ mice. Of note, calcium responses to cat S remained intact in the absence of PAR2 receptors (Figure 3.2D). These data support a role for protease-induced MrgprC11 activation in DRGs and, importantly, identify cat S as a potential endogenous and relevant 'ligand' for this receptor. The average diameter of responsive neurons was 19.3 μm, comparable to that reported previously for Mrgpr-expressing itch neurons.

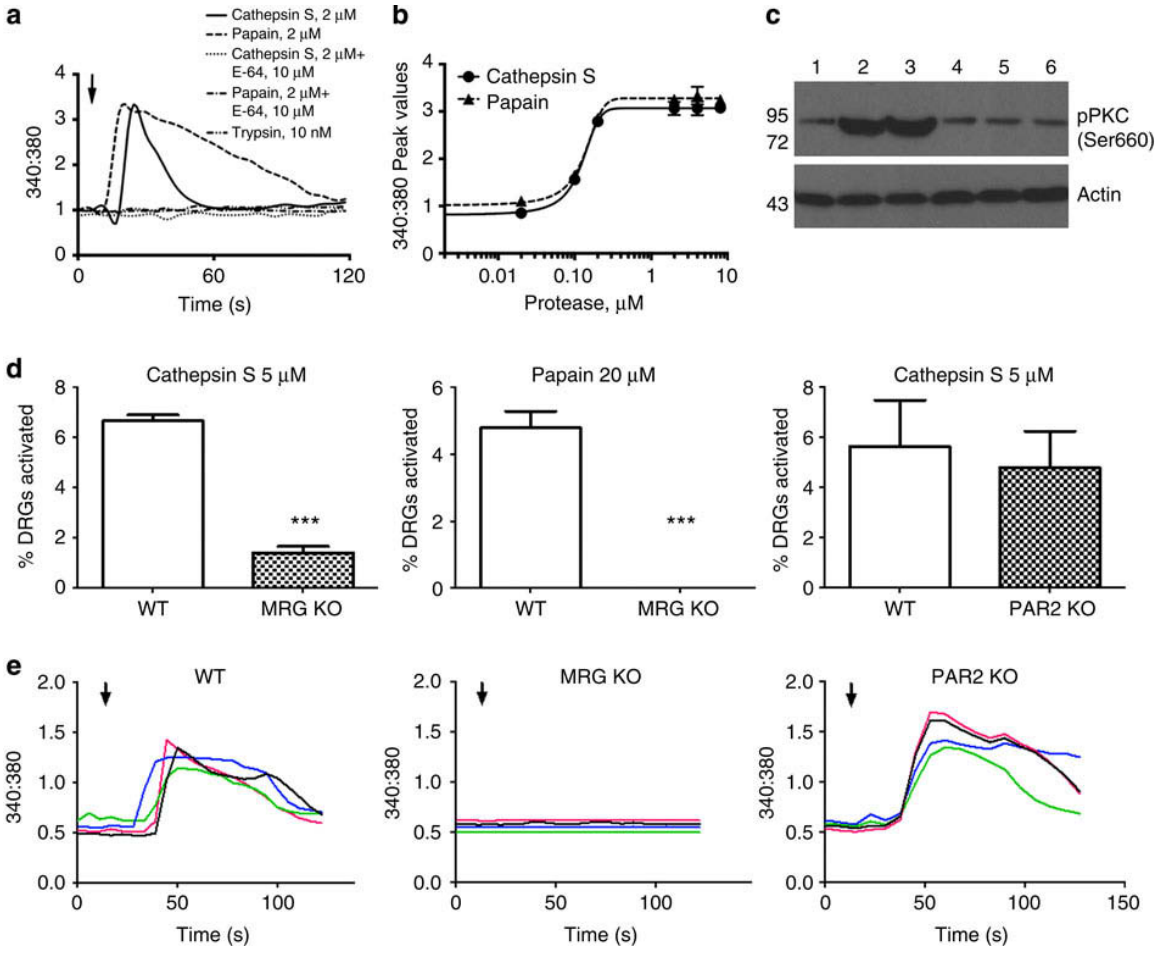

Figure 3.2 Cysteine proteases activate MrgprC11 in heterologous cells and DRG neurons and induce PKC phosphorylation

(**A**) Single-cell calcium imaging in HeLa cells transfected with MrgprC11 cDNA following treatment with cat S (2 µM, solid line), papain (2 µM, dashed line), cat S+E-64 (10 µM; dotted line), papain+E-64 (10 µM; dash-dotted line) and trypsin (10 nM) dash-double-dotted line. The concentration of trypsin is typical of that used in studies of PARs. Higher concentrations of trypsin, including those in the micromolar range, did not activate MrgprC11. (**B**) Concentration–effect curves for protease agonists cat S (squares) and papain (circles) on MrgprC11. Error bars represent ± s.e.m. from three sets of experiments. (**C**) Phosphorylation of serine 660 as a measure of second messenger is revealed by western blot. HeLa cells were transfected with MrgprC11

(lanes 1–3), or non-transfected HeLa cells (lanes 4–6) were treated with buffer alone (lanes 1 and 4), cat S (lanes 2 and 5) or papain (lanes 3 and 6). Results from Dr. Ethan Lerner's group. (**D**) The percentage of DRG neurons activated by cat S (5 μM) was significantly reduced in *Mrgpr cluster knockout* mice as compared with WT DRG neurons (n=3, P<0.001). The percentage of DRG neurons activated by papain (20 μM) was reduced to zero in *Mrgpr cluster knockout* mice as compared with WT mice (n=3, ***P<0.001; two-tailed unpaired t-test). The percentage of DRG neurons activated by cat S (5 μM) is not significantly different between WT and $PAR2^{-/-}$ mice (n=3, P=0.74). (**E**) Representative calcium traces of cat S (5 μM) in DRG neurons from WT, *Mrgpr cluster* $\Delta^{-/-}$ and $PAR2^{-/-}$ mice. Each trace represents responses from a single neuron. Arrows indicate application of cat S.

RNA interference (RNAi) knockdown of MrgC11 and closely related MrgprA3 was performed in DRG neurons (Figure 3.3). Messenger RNA levels of both genes were significantly lower as confirmed by real-time PCR (Figure 3.3D). Knockdown of MrgprC11 only abolished the calcium response to the MrgprC11 ligand cat S but not the MrgprA3 ligand chloroquine. In contrast, knockdown of MrgprA3 only affected the response to chloroquine but not the response to cat S, showing effectiveness and specificity of RNAi. Note that transient knockdown of MrgprC11 totally abolished the cat S-induced response, while knockdown of MrgprA3 only reduced the response to chloroquine. This result is consistent with the stronger knockdown effect of MrgprC11. The observation that transient knockdown eliminates the calcium response to cat S suggests that the remaining calcium response in Mrgpr cluster knockout (KO) mice may be due to an otherwise unspecified compensation mechanism in the permanent KO. In summary, these data support a role for protease-induced MrgprC11 activation in DRGs and, importantly, identify cat S as a potential endogenous and relevant 'ligand' for this receptor.

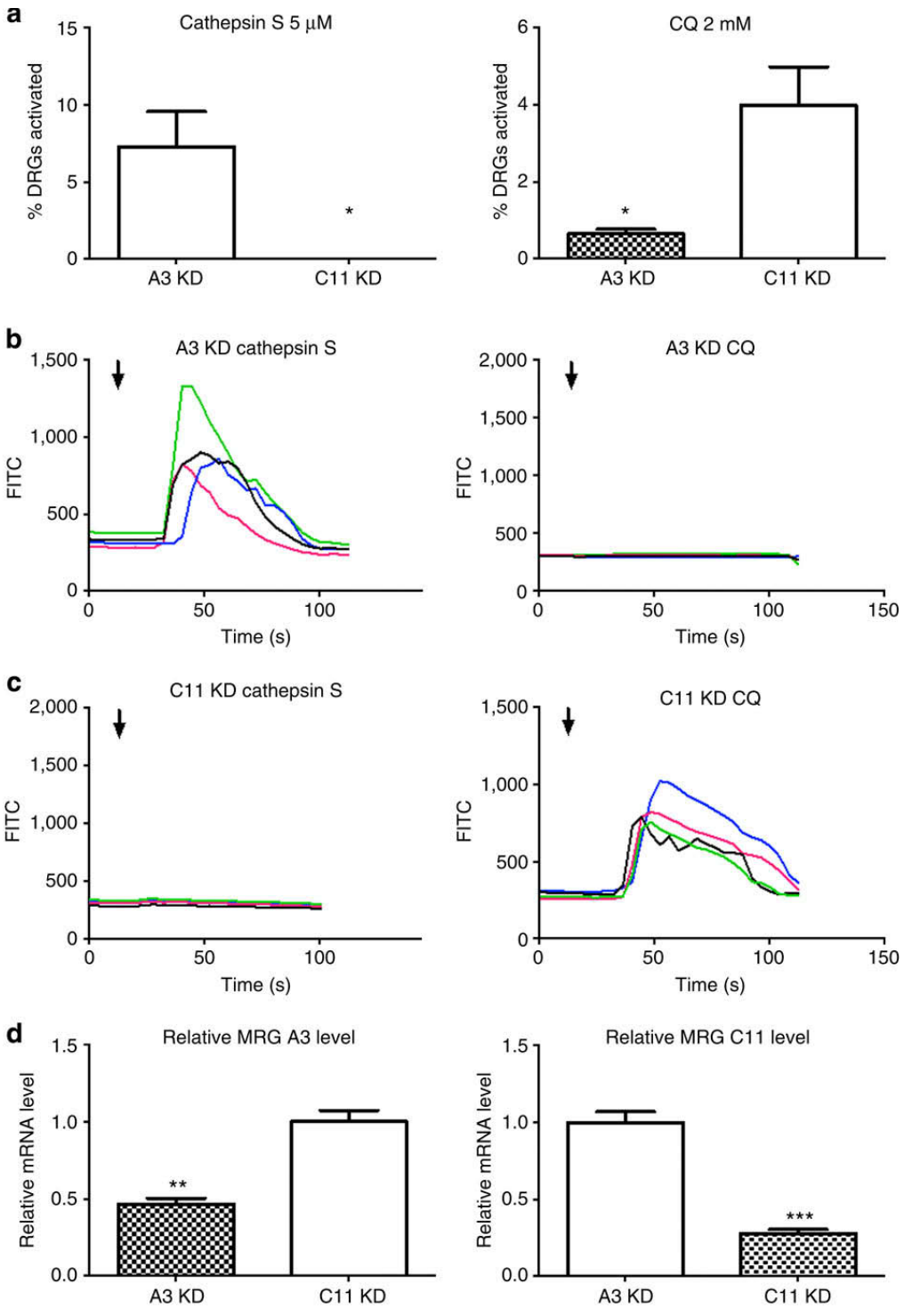

Figure 3.3 Acute knockdown of MrgprC11 abolishes DRG response to cathepsin S

(**A**) MrgprA3 knockdown DRG neurons responded normally to cat S (5 μM), while MrgprC11 knockdown DRG neurons showed no response (n=4, P<0.05). In contrast, chloroquine (CQ) (2 mM) induces calcium responses in ~4% of MrgprC11 knockdown DRGs, while knockdown of MrgprA3 markedly reduced the response to CQ (n=4, P<0.05). (**B**) Representative calcium traces from MrgprA3 knockdown DRG neurons in response to cat S and chloroquine. (**C**) Representative calcium traces from MrgprC11 knockdown DRG neurons in response to cat S and chloroquine. Each trace represents responses from a single neuron. Arrows indicate application of cat S. (**D**) Relative messenger RNA (mRNA) level of MrgprA3 and MrgprC11 in the respective knockdown DRGs as determined by real-time PCR. The data are presented as mean±s.e.m. *P<0.05, **P<0.01; ***P<0.001; two-tailed unpaired t-test.

Cathepsin S induces scratching via MrgprC11

Cat S has been shown previously to cleave and activate PAR2 *in vitro*(Reddy et al., 2010). It has been assumed, but never demonstrated clearly, that PAR2 activation is the mechanism by which cat S evokes scratching in mice and itch in humans. However, in light of our *in vitro* findings that cat S-induced calcium signalling in DRGs requires MrgprC11 but not PAR2, we sought to determine the relative importance of these two receptors, if any, to cat S-induced scratching *in vivo*. We thus compared behavioural scratching responses with intradermal injection of cat S using the mouse cheek model in WT, *Mrgpr cluster* $\Delta^{-/-}$ mice and *PAR2*$^{-/-}$ mice. Pain and itch can be readily distinguished using the cheek injection model(Shimada and LaMotte, 2008). We only observed itch associated hind-paw scratching, but not pain-related fore-paw wiping. Injection of cat S elicited robust scratching behaviour in WT mice, but was markedly reduced in *Mrgpr cluster* $\Delta^{-/-}$ mice (Figure 3.4A). Perhaps surprisingly, scratching in *PAR2*$^{-/-}$ mice was as robust as in WT littermates (Figure 3.4B). These experiments underline the pivotal role of MrgprC11 in mediating cysteine protease-induced itch.

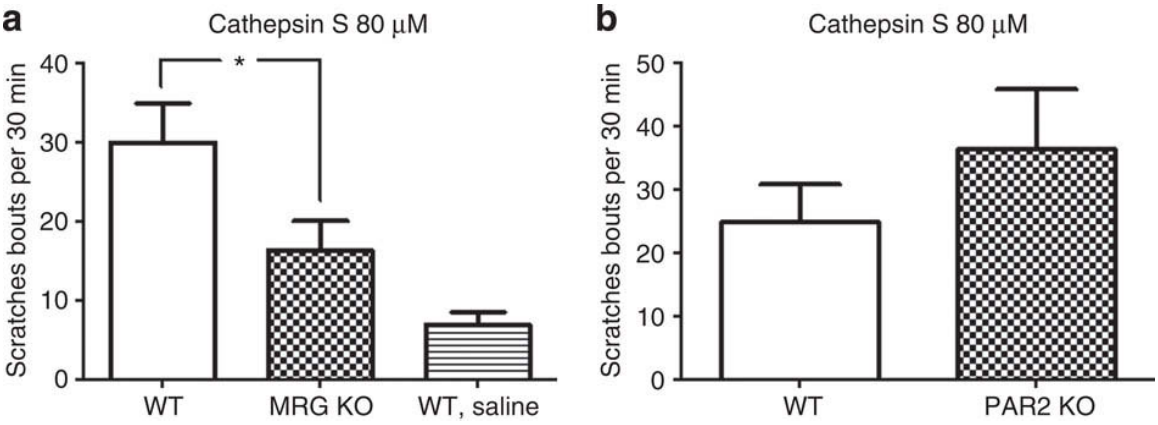

Figure 3.4 Cathepsin S-induced scratching is reduced in *Mrgpr cluster* $\Delta^{-/-}$ mice

(**A**) Scratching behaviour of WT and *Mrgpr cluster* $\Delta^{-/-}$ mice in response to cat S, n=11, P=0.04, and compared with baseline saline vehicle alone (n=9). (**B**) Scratching behaviour of WT and *PAR2*$^{-/-}$ mice in response to cat S was not significantly different, n=7, P value 0.32. The data are presented as mean±s.e.m.*P<0.05; two-tailed unpaired t-test.

MrgprC11 N-terminal cleavage sites

We next sought to determine whether cleavage of the extracellular N-terminal domain of MrgprC11 is necessary for protease-induced receptor activation, and if so, to identify the relevant cleavage sites. As per the MEROPS database, preferred amino acids for cleavage by cat S and papain include leucine at P2 and glycine, serine and aspartic acid at P1. Using site-specific mutagenesis, we generated a series of single-, double- and triple-substitution mutants near the MrgprC11 N terminus (Table 3.1). Calcium imaging of HeLa cells transfected with these mutant receptors revealed that leucine[13] was a critical residue for cat S-mediated cleavage and activation. Papain required both aspartic acid[9] and leucine[13] for receptor cleavage and activation (Table 3.1). None of the other candidate residues including glycine[14], serine[6, 7, 15] and leucine[16] were required for receptor activation by either protease.

Table 3.1 Responses of wild-type MrgprC11 or MrgprC11 N-terminal mutants following treatment with cat S, papain or SLIGRL as determined by calcium imaging

MrgprC11 N terminus: M^{1}DP TIS SHD TES TPL NET GHP NCT PIL TLS FLV^{31}			
MrgprC11 WT and mutant receptors	**Cat S, 2 µM**	**Papain, 2 µM**	**SLIGRL, 10 µM**
C11 WT	+	+	+
C11-1 ($L^{15}I$)	–	+	+
C11-2 ($G^{19}I$)	+	+	+
C11-3 ($L^{15}I$, $G^{19}I$)	–	+	+
C11-4 ($L^{15}I$, $G^{19}I$, $L^{27}I$)	–	+	+
C11-5 ($S^{30}I$)	+	+	+
C11-6 ($D^{9}I$)	+	+	+
C11-7 ($D^{9}I$, $L^{15}I$)	–	–	+
C11-8 ($S^{6}I$, $S^{7}I$)	+	+	+
C11-9 ($L^{15}R$)	–	+	+

Cat S, cathepsin S; Mrgprs, Mas-related G-protein-coupled receptors; WT, wild type. '+' indicates that the indicated receptor was activated. The indicated amino acids were each mutated to isoleucine, except for mutant MrgprC11-9 in which L^{15} was changed to R. Note that SLIGRL activated all of the receptors. Results from Dr. Ethan Lerner's group.

To determine the specific protease cleavage sites, a peptide corresponding to the 28N-terminal residues of MrgprC11 was synthesized, MDPTISSHD^{9}TESTPL^{13} NETGHPNCTPILT. The aspartic and leucine residues required for papain and cat S activity are indicated. This peptide was incubated with cat S or papain and then subjected to mass spectrometry (MS)/MS peptide sequence analysis, as described in Table 3.2, as we have done previously with cat S and PAR2(Elmariah et al., 2014). Cat S cleavage occurred between N^{16} and E^{17} with L^{15}at the P2 position, MDPTISSHD^{9}TESTPL^{15}N↓ETGHPNCTPILT, consistent with the site-directed mutagenesis approach above. Substituting arginine for leucine^{13} completely eliminated the response to cat S (Table 3.1; Figure 3.5B). Papain preferred L^{15} at the P2 position and cleavage

between N^{16} and E^{17} but no additional specificity was apparent, and cleavage otherwise occurred at multiple sites.

Table 3.2 MS/MS data from incubation of the mouse MrgprC11 N-terminal peptide

Sequence Number	Sequence	Count	Sequence Number	Sequence	Count
1	DPTISSBDTESTPLN*	4	42	MDPTISSHDTESTPLNETGHPNCTPILT	2
2	DPTISSBDTESTPLNETG	1	43	PLNETGHPN	4
3	ESTPLNETGHPN	4	44	PLNETGHPNC	2
4	ESTPLNETGHPNC	4	45	PLNETGHPNCTPILT	2
5	ESTPLNETGHPNCTPLLT	3	46	PLNETGHPNCTPILTLS	1
6	ETGHPNCTPI**	3	47	PTISSHDTE	5
7	ETGHPNCTPIL**	2	48	PTISSHDTES	3
8	ETGHPNCTPILT**	16	49	PTISSHDTESTPLN*	4
9	ETGHPNCTPILTL**	3	50	PTISSHDTESTPLNE	2
10	GHTNCTTILI	2	51	PTISSHDTESTPLNETG	5
11	HDTESTPLN*	6	52	PTISSHDTESTPLNETGHPN	5
12	HDTESTPLNE	5	53	PTISSHDTESTPLNETGHPNC	1
13	HDTESTPLNETG	8	54	PTISSHDTESTPLNETGHPNCTPILT	1
14	HDTESTPLNETGHPN	6	55	SHDTESTPLN*	4
15	HDTESTPLNETGHPNC	5	56	SHDTESTPLNE	2
16	HDTESTPLNETGHPNCTPILT	4	57	SHDTESTPLNETG	2
17	HPNCTPIL	3	58	SHDTESTPLNETGHPN	6
18	HPNCTPILT	5	59	SHDTESTPLNETGHPNC	3
19	HPNCTPILTL	3	60	SHDTESTPLNETGHPNCTPILT	4
20	HPNCTPILTLS	5	61	SSHDTESTPLN*	6
21	ISSHDILS	1	62	SSHDTESTPLNE	2
22	ISSHDILSTPLN*	2	63	SSHDTESTPLNETGHPN	4
23	ISSHDILSTPLNE	3	64	SSHDTESTPLNETGHPNC	5
24	ISSHDILSTPLNETG	1	65	SSHDTESTPLNETGHPNCTPIL	1
25	ISSHDILSTPLNETGRDN	3	66	SSHDTESTPLNETGHPNCTPILT	8
26	M*DPTISSHDTE	1	67	STPLNETGHPN	2
27	M*DPTISSHDTES	3	68	STPLNETGHPNC	2
28	M*DPTISSHDTESTPLN	1	69	STPLNETGHPNCTPILT	4
29	M*DPTISSHDTESTPLNE	3	70	TESTPLN*	2
30	M*DPTISSHDTESTPLNETG	1	71	TESTPLNE	2
31	M*DPTISSHDTESTPLNETGHPN	1	72	TESTPLNETG	2
32	MDPTISSH	3	73	TESTPLNETGHPN	1
33	MDPTISSHD	1	74	TESTPLNETGHPNC	1

34	MDPTISSHDT	1	75	TESTPLNETGHPNCTPILT	2
35	MDPTISSHDTE	6	76	TGHPNCTPILT	4
36	MDPTISSHDTES	2	77	TGHPNCTPILTL	2
37	MDPTISSHDTESTPLN	7	78	TGHPNCTPILTLS	3
38	MDPTISSHDTESTPLNE	4	79	TPLNETGHPN	5
39	MDPTISSHDTESTPLNETG	5	80	TPLNETGHPNC	3
40	MDPTISSHDTESTPLNETGHPN	5	81	TPLNETGHPNCTPILT	4
41	MDPTISSHDTESTPLNETGHPNC	9			

MDPTISSHDTESTPLNETGHPNCTPILT with papain. The peptides are listed in order beginning with the highest total ion count. Other than cleavage by papain associated with L15 at the P2 position, no cleavage preference was identified. (Sequence) represents the amino acid sequence of the peptides identified by MS/MS following incubation with papain. (count) represents the number of times this sequence was identified. * indicates the peptides in which incubation with papain results in a C-terminus with L15 at the P2 position. ** indicates the peptides in which incubation with papain results in E17 at the N-terminus, consistent with cleavage by papain with L15 at the P2 position. Results from Dr. Ethan Lerner's group.

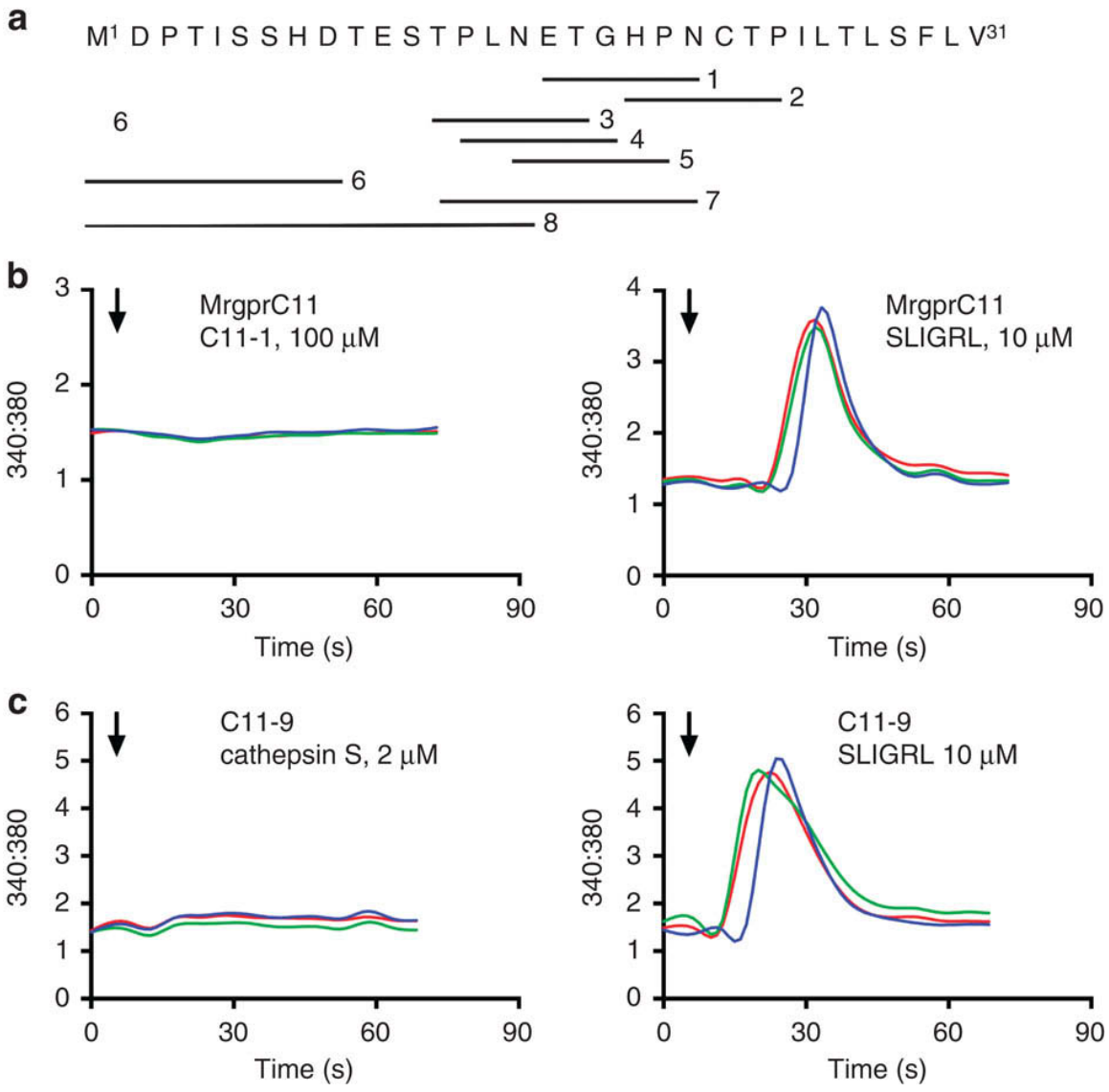

Figure 3.5 N-terminal peptides do not activate MrgprC11 and cat S requires L^{15} for activity

(**A**) A series of eight MrgprC11 N-terminal peptides was generated based on possible protease cleavage sites. (**B**) Calcium imaging of HeLa cells transfected with MrgprC11 following treatment with a representative MrgprC11 N-terminal peptide, C11-1 100 µM, the hexapeptide tethered ligand ETGHPN at the cat S cleavage site. (**C**) Cat S does not activate the MrgprC11 in which L^{15} has been changed to R. Note that SLIGRL activates the native and mutant receptors. Arrows represent addition of test reagent. Results from Dr. Ethan Lerner's group.

MrgprC11 is not activated by tethered or diffusible ligands

As conventional PARs are activated by tethered ligands generated following protease-mediated cleavage of their N-terminal domains, we sought to determine whether such peptides could activate MrgprC11. We generated a series of eight peptides (Figure 3.5A) ranging from 6 to 15 amino acids based on predicted cleavage sites near the MrgprC11 N terminus. These included the tethered hexapeptide ETGHPN that begins at the cat S cleavage site, and the diffusible peptide MDPTISSHDTESTPLN that begins at the N terminus of MrgprC11 and ends at the cat S cleavage site. In contrast to PAR2 N-terminal peptides, synthetic MrgprC11 N-terminal peptides failed to elicit calcium responses in MrgprC11-expressing cells (Figure 3.5B). These data reveal that in contrast to the activation of PARs, Mrgpr activation does not occur via generation of either a tethered or diffusible ligand.

Proteases activate β2AR and MC1R–MrgprC11 hybrid receptors

We have shown thus far that protease-mediated cleavage of MrgprC11 causes receptor activation without the formation of either a tethered or diffusible ligand. Another possible explanation of the ability of cysteine proteases to activate Mrgprs is that proteolysis of the extracellular domain results in a direct conformational change of the intracellular portion of the receptor that allows G-coupled signalling to occur. If this is the case, a mutant MrgprC11 in which the native N terminus has been substituted with the N terminus of an unrelated GPCR that can also be cleaved by cysteine proteases might be activated by proteolysis. To evaluate this possibility, we substituted the N terminus of MrgprC11 with either that of the β2-adrenergic receptor (β2AR) or the melanocortin-1 receptor (MC1R). These receptors are class A GPCRs, such as Mrgprs, but they couple primarily to Gs. We selected β2AR and MC1R because of the deep knowledge surrounding their structure and function. Each of these receptors contains residues that can be cleaved by cysteine proteases. However, biogenic amines and melanocortins,

respectively, not proteases, are their conventional ligands. As predicted, both cat S and papain treatment of HeLa cells transfected with hybrid receptors β2AR–MrgprC11 or MC1R–MrgprC11 resulted in robust calcium signalling. As controls, protease treatment did not result in calcium mobilization in HeLa cells expressing native β2AR or MC1R (Figure 3.6). Taken together with the site-specific mutagenesis results, these findings argue that cat S- or papain-mediated cleavage of specific N-terminal residues directly triggers conformational changes in the transmembrane and/or intracellular domains of the MrgprC11 receptor that lead to downstream signalling.

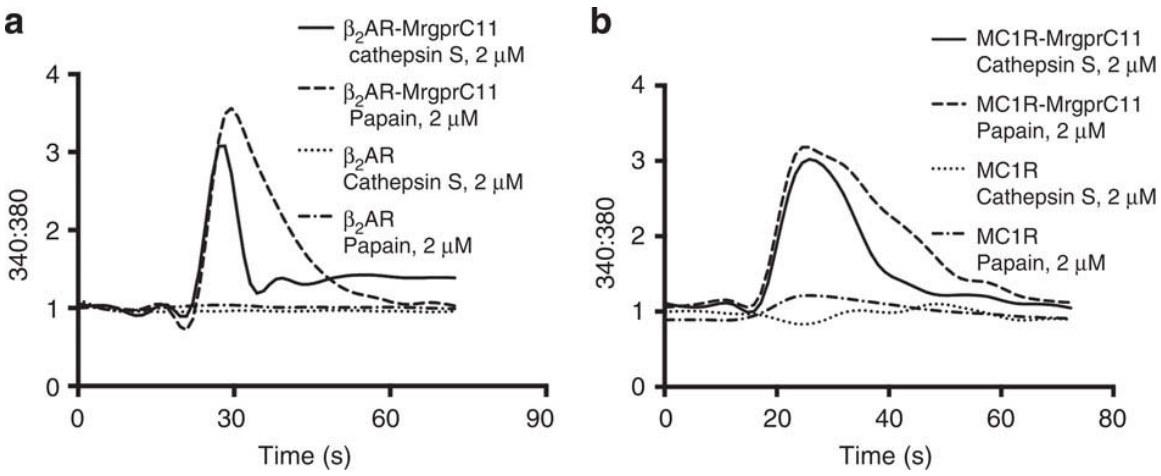

Figure 3.6 Cathepsin S and papain activate MrgprC11 downstream signalling in N-terminal exchange receptors

(**A**) Cat S and papain activate β2AR–MrgprC11 but not the WT AR as determined by calcium imaging. (**B**) Cat S and papain activate MC1R–MrgprC11 but not WT MC1R as determined by calcium imaging. Results from Dr. Ethan Lerner's group.

Effect of cysteine proteases on other Mrgprs

To determine whether cysteine protease-mediated receptor activation was specific to MrgprC11, we examined whether cat S and papain were capable of triggering calcium mobilization in HeLa cells transfected with other members of the Mrgpr family, including human MRGPRX1–4 as well as mouse MrgprA3, which mediates chloroquine-induced itch. We found that in addition to activating human PAR2 and mouse MrgprC11, cat S activated human MRGPRX2 (Table 3.3). Cat S failed to activate other human MRGPRs and mouse MrgprA3 (Table 3.3). In contrast, papain activated human MRGPRX1, but had no effect on the other human MRGPRs (Table 3.3). As expected, trypsin failed to activate these Mrgprs (Figure 3.2A; Table 3.3). These results demonstrate that cysteine proteases activate only select Mrgprs, and that cat S, in particular, activates mouse and human Mrgprs that have been implicated in itch transmission.

Table 3.3 Responses of PAR2 and Mrgprs following treatment with cat S, papain and trypsin as determined by calcium imaging

GPCR	Cat S, 2 μM	Papain, 2 μM	Trypsin, 10 nM
hPAR2	+	+	+
hMRGPRX1	–	+	–
hMRGPRX2	+	–	–
hMRGPRX3	–	–	–
hMRGPRX4	–	–	–
mMrgprC11	+	+	–
mMrgprA3	–	–	–

Cat S, cathepsin S; Mrgprs, Mas-related G-protein-coupled receptors; PAR2, protease-activated receptor-2.

'+' indicates that the indicated receptor was activated.

Discussion

Endogenous and exogenous proteases have long been implicated in the pathogenesis of many inflammatory diseases, including skin diseases(Deschamps, 2011; Reddy and Lerner, 2010; Reddy et al., 2010; Schonefuss, 2010).Our previous work showed that endogenous cat S and other proteases trigger histamine-independent itch(Reddy and Lerner, 2010; Reddy et al., 2008, 2010). Transgenic mice in which cat S is overexpressed spontaneously develop an intensely pruritic, eczematous disorder resembling atopic dermatitis(Kim et al., 2012). In addition, cat S levels are selectively upregulated in psoriatic keratinocytes(Schonefuss, 2010), a condition also associated with considerable itch(Globe et al., 2009; Gupta et al., 2008; Prignano et al., 2009). Intradermal injection of cat S elicits acute itch in human subjects as well as scratching in mice(Kim et al., 2012; Reddy and Lerner, 2010). Until now, the exact mechanism by which cysteine proteases induce itch remained elusive and was presumed to require activation of the PAR2 receptor via generation of KVDGTS, a tethered ligand distinct from SLIGRL(Elmariah et al., 2014). We demonstrate for the first time that the cysteine proteases cat S and papain directly activate MrgprC11 to evoke histamine-independent scratching behavior. The activation kinetics of MrgprC11 by papain were prolonged relative to those of cat S. The mechanism for this prolonged activation is not clear but may result from a balance of receptor activation/inactivation, calcium-induced release from intracellular stores or perhaps endosomal receptor signalling associated with papain(Tsvetanova et al., 2015; Vilardaga et al., 2014).

Consistent with protease activation of MrgprC11, scratching responses elicited by the intradermal injection of cat S were significantly reduced in *Mrgpr cluster* $\Delta^{-/-}$ mice, but remained intact in $PAR2^{-/-}$ mice. *In vitro* correlates of these *in vivo* observations were demonstrated as the capacity of cat S to activate DRG neurons from *Mrgpr cluster* $\Delta^{-/-}$ mice was markedly diminished while not significantly diminished in $PAR2^{-/-}$ DRG neurons. RNAi knockdown of

MrgprC11 specifically abolished the response of DRG neurons to cat S. In contrast, knockdown of MrgprA3 did not diminish the response of DRG neurons to cat S. It is not clear why the decrease in scratching responses in *Mrgpr cluster* $\Delta^{-/-}$ mice, while significant, was not as substantial as the decrease in Ca^{2+} signals in DRG neurons from these mice. One potential explanation is that cat S activates PAR2 on keratinocytes, resulting in the release of thymic stromal lymphopoietin, a skin-derived cytokine that has been shown to induce itch via neuronal receptors for this molecule(Wilson et al., 2013). In addition, while PAR2 does not appear to have a direct role in cat S-evoked itch in WT mice, a non-native role may be unmasked in the absence of MrgprC11. Our data also identify the cysteine protease cat S as a functional endogenous ligand for Mrgprs, currently considered as orphan receptors. Whether other endogenous cysteine proteases activate Mrgprs awaits future investigations.

Conventional PARs are GPCRs that are uniquely activated by proteolysis. In this scenario, proteases bind and specifically cleave residues in the N-terminal domain of the receptor to unmask a 'tethered' ligand that subsequently interacts with another portion of the receptor to trigger intracellular signalling. Similarly, PARs can be activated by synthetic hexapeptides that mimic the first six amino acids of the unmasked N terminus. The data presented here are the first to demonstrate that GPCRs other than PARs can be activated by proteolysis, as cysteine proteases activate MrgprC11. Site-specific mutagenesis revealed that cat S requires L^{15} and papain requires D^{9} and L^{15} for cleavage, while data from MS/MS demonstrated that cleavage occurs between residues N^{16} and E^{17}. In contrast to PARs, tethered ligands do not appear to play a role in Mrgpr activation, and synthetic Mrgpr N-terminal peptides have no apparent functional activity. These data highlight the possibility that cysteine proteases may exert effects on other 'non-PAR' GPCRs and further suggest that proteases are capable of modulating GPCRs by multiple mechanisms.

Classically, GPCRs are thought to become activated when ligands bind in a pocket formed by the transmembrane helices thereby triggering exposure of cytoplasmic domains required for coupling to heterotrimeric G-protein subunits(Ji et al., 1998). PARs, on the other hand, become activated when proteolysis allows for tethered ligands to interact with residues in the second extracellular loop, subsequently resulting in conformational changes in the transmembrane helices(Elmariah et al., 2014; Vu et al., 1991). While the exact mechanism by which proteolysis triggers activation of MrgprC11 remains unknown, we suggest that the N-terminal domain interacts with the extracellular loops of the receptor to lock it in an inactive state. Cleavage of the N terminus by cysteine proteases may release this lock, shifting transmembrane and cytoplasmic domains as suggested with traditional PARs. Our observations that calcium signalling was evoked by cathepsin-induced proteolysis of the β2AR and MC1R N-terminal exchange mutants are consistent with this hypothesis. The mechanism underlying this observation deserves further study.

It is interesting that although N-terminal MrgprC11 peptides did not activate Mrgpr signaling, SLIGRL, a PAR2 N-terminal peptide, is capable of inducing itch via activation of MrgprC11(Liu, 2011), at least at micromolar concentrations. Whether this effect occurs naturally is not clear. The concept that N-terminal peptides released into the extracellular milieu following PAR cleavage may exert a biologic effect independent of PARs has been reported. PAR1 cleavage by thrombin generates an N-terminal peptide known as parstatin, which is capable of inhibiting vascular endothelial cell growth factor- and fibroblast growth factor-induced angiogenesis *in vitro* and *in vivo*. It also plays a role in modulating platelet function(Furman, 2000; Zania, 2009). Whether protease-mediated cross-signalling between PAR2 and MrgprC11 serves a relevant role in coupling itch and inflammation *in vivo* is not known.

Cysteine proteases, in particular cysteine cathepsins, are widely expressed in mammalian tissues and have been implicated in the pathophysiology of a diverse array of inflammatory, autoimmune and allergic diseases, as well as in neuropathic pain(Cattaruzza, 2011; Clark, 2007; Gupta et al., 2008; Inaoka, 1995; Mohamed and Sloane, 2006). Recent work in murine colitis models demonstrates that macrophage- and microglial cell-derived cat S induces colonic inflammation and pain by activating PAR2 on different cell types, linking increased paracellular permeability in colonocytes with nociceptive hyper-excitability and neurogenic inflammation in primary spinal afferent neurons(Cattaruzza, 2011; Jacob, 2005; Steinhoff et al., 2000; Zhao, 2014). We suggest that cat S may similarly act as a key regulator linking itch and inflammation in the skin. Our work reveals a novel mechanism by which cat S accomplishes its diverse effects: activation of MrgprC11.

Increased cat S expression has been reported in several common inflammatory skin conditions, including atopic dermatitis, psoriasis and seborrhoeic dermatitis(Kim et al., 2012; Schonefuss, 2010; Viode, 2014). Under these conditions, cat S may simultaneously contribute to itch and propagate inflammation via different but related mechanisms. First, as we demonstrated here, cat S induces itch directly by activating MrgprC11. Second, cat S-mediated activation of PAR2 may induce itch if PAR2 N-terminal peptides bind to MrgprC11 on primary sensory nerves. In addition, PAR2 activation in keratinocytes may trigger the release of thymic stromal lymphopoietin, which in turn activates cutaneous sensory neurons that express transient receptor potential ankyrin channel A1 (TRPA1), leading to itch stimulation and neurogenic inflammation(Wilson, 2013). Recognizing that proteases can recruit multiple distinct pathways to induce itch and inflammation may help drive the development of more effective therapeutic strategies to treat inflammatory diseases, shifting the focus from blocking individual downstream

receptors to inhibiting protease–receptor complexes. This chapter is modified from previous publication(Reddy et al., 2015).

CHAPTER 4: CONCLUSION AND FUTURE DIRECTIONS

This thesis focuses on the central and peripheral mechanisms of pain and itch. We've identified a small subset of spinal interneurons receiving direct synaptic input from both pain and itch primary sensory neurons. Contrary to the current pain and itch coding theories, specific activation of these neurons intensity dependently generated robust pain and itch responses simultaneously. Such intensity dependent coding serves as a good example of currently overlooked non-monotonic coding in spinal cord circuitries. Accordingly, I proposed a "leaky gate" model, in which these neurons transmit both itch signals and weak pain signals (ensuring pain sensitivity) through the "gate", but recruit endogenous opioid systems to close the "gate" upon strong painful stimuli to prevent overwhelming pain. This "leaky gate" functions as a brake for pain pathway to prevent intense stimuli from generating debilitating pain sensation, moreover, the advantage of a "leaky" gate lies in that pain sensitivity is preserved by the high triggering threshold of this "brake". Consistent with our model, loss of these *Grp*$^{+}$ neurons increased pain responses while itch was decreased. This model provides a refined theory of pain and itch coding in spinal cord and better explains observations in human psychophysical studies.

The gate control theory of pain has yielded influential mechanistic understandings of pain circuitries over the years and provided spinal cord stimulation as an effective method of pain relief. Further research on this leaky gate model would likely lead to more detailed knowledge of complex pain and itch related spinal circuitries. Since the gate control system demonstrates maladaptive changes in chronic pain conditions, further studies of leaky gate model in

pathological conditions, such as chronic pain and chronic itch, would be a good start point. In addition, the residual itch responses and the increased pain behavior after the loss of *Grp*$^+$ neurons indicates the existence of parallel pain and itch pathways. Grp cre line as well as the MrgprA3 cre line would serve as ideal tools to map parallel circuitries and determine whether candidate subsets such as those labeled by GRPR and NK1 receive direct synaptic input from *Grp*$^+$ and *MrgprA3*$^+$ neurons. Last but not least, the input-output relationship of *Grp*$^+$ neurons was inferred by ex vivo recordings in combination with behavioral analysis. Direct examination of such relationship under physiological conditions, potentially via in vivo calcium imaging of spinal cord, could further consolidate findings presented in this thesis.

In collaboration with Dr. Ethan Lerner's group from Massachusetts General Hospital, we also discovered that cysteine proteases, including cathepsin S, cleave and activate G protein coupled receptors, MrgprC11. This is the first GPCR outside PAR family to be activated by protease cleavage. Moreover, in contrary to previous hypothesis that PAR2 mediate protease induced itch, cysteine proteases activate dorsal root ganglion neurons and trigger scratching in MrgprC11 dependent way. Interestingly, the activation of MrgprC11 involves a novel mechanism other than the generation of tethered ligand as in the case of PARs or diffusible ligands. Further study of this novel activation mechanism could expand our knowledge about GPCR signaling and might help to develop novel chemogenetic tools.

REFERENCES

Akiyama, T., and Carstens, E. (2013). Neural processing of itch. Neuroscience *250*, 697–714.

Akiyama, T., Carstens, M.I., and Carstens, E. (2009). Excitation of mouse superficial dorsal horn neurons by histamine and/or PAR-2 agonist: potential role in itch. J. Neurophysiol. *102*, 2176–2183.

Alemi, F., Kwon, E., Poole, D.P., Lieu, T., Lyo, V., Cattaruzza, F., Cevikbas, F., Steinhoff, M., Nassini, R., Materazzi, S., et al. (2013). The TGR5 receptor mediates bile acid-induced itch and analgesia. J. Clin. Invest. *123*, 1513–1530.

Alon, U. (2007). Network motifs: theory and experimental approaches. Nat. Rev. Genet. *8*, 450–461.

Andersson, D.A., Gentry, C., Moss, S., and Bevan, S. (2008). Transient receptor potential A1 is a sensory receptor for multiple products of oxidative stress. J. Neurosci. *28*, 2485–2494.

Andoh, T., and Kuraishi, Y. (2003). Nitric oxide enhances substance P-induced itch-associated responses in mice. Br. J. Pharmacol. *138*, 202–208.

Andoh, T., Nagasawa, T., Satoh, M., and Kuraishi, Y. (1998). Substance P induction of itch-associated response mediated by cutaneous NK1 tachykinin receptors in mice. J. Pharmacol. Exp. Ther. *286*, 1140–1145.

Andoh, T., Katsube, N., Maruyama, M., and Kuraishi, Y. (2001). Involvement of leukotriene B(4) in substance P-induced itch-associated response in mice. J. Invest. Dermatol. *117*, 1621–1626.

Andoh, T., Nishikawa, Y., Yamaguchi-Miyamoto, T., Nojima, H., Narumiya, S., and Kuraishi, Y. (2007). Thromboxane A2 induces itch-associated responses through TP receptors in the skin in mice. J. Invest. Dermatol. *127*, 2042–2047.

Andoh, T., Yoshida, T., Lee, J.-B., and Kuraishi, Y. (2012). Cathepsin E induces itch-related response through the production of endothelin-1 in mice. Eur. J. Pharmacol. *686*, 16–21.

Bailer, A.J., and Oris, J.T. (1997). Estimating inhibition concentrations for different response scales using

generalized linear models. Environ. Toxicol. Chem. *16*, 1554–1559.

Bailer, A.J., and Oris, J.T. (1998). Incorporating hormesis in the routine testing of hazards. Hum. Exp. Toxicol. *17*, 247–250.

Bandell, M., Story, G.M., Hwang, S.W., Viswanath, V., Eid, S.R., Petrus, M.J., Earley, T.J., and Patapoutian, A. (2004). Noxious Cold Ion Channel TRPA1 Is Activated by Pungent Compounds and Bradykinin. Neuron *41*, 849–857.

Bautista, D.M., Jordt, S.-E., Nikai, T., Tsuruda, P.R., Read, A.J., Poblete, J., Yamoah, E.N., Basbaum, A.I., and Julius, D. (2006). TRPA1 mediates the inflammatory actions of environmental irritants and proalgesic agents. Cell *124*, 1269–1282.

Bautista, D.M., Pellegrino, M., and Tsunozaki, M. (2013). TRPA1: A gatekeeper for inflammation. Annu. Rev. Physiol. *75*, 181–200.

Bell, J.K., McQueen, D.S., and Rees, J.L. (2004). Involvement of histamine H4 and H1 receptors in scratching induced by histamine receptor agonists in Balb C mice. Br. J. Pharmacol. *142*, 374–380.

Bourane, S., Duan, B., Koch, S.C., Dalet, A., Britz, O., Garcia-Campmany, L., Kim, E., Cheng, L., Ghosh, A., Ma, Q., et al. (2015a). Gate control of mechanical itch by a subpopulation of spinal cord interneurons. Science (80-.). *350*.

Bourane, S., Duan, B., Koch, S.C., Dalet, A., Britz, O., Garcia-Campmany, L., Kim, E., Cheng, L., Ghosh, A., Ma, Q., et al. (2015b). Gate control of mechanical itch by a subpopulation of spinal cord interneurons. Science (80-.). *350*, 550–554.

Bourane, S., Duan, B., Koch, S.C., Dalet, A., Britz, O., Garcia-Campmany, L., Kim, E., Cheng, L., Ghosh, A., Ma, Q., et al. (2015c). Gate control of mechanical itch by a subpopulation of spinal cord interneurons. Science (80-.). *350*, 550–554.

Braz, J., Solorzano, C., Wang, X., and Basbaum, A.I. (2014). Transmitting pain and itch messages: a

contemporary view of the spinal cord circuits that generate gate control. Neuron *82*, 522–536.

Calabrese, E.J., and Baldwin, L.A. (2003). Hormesis: the dose-response revolution. Annu. Rev. Pharmacol. Toxicol. *43*, 175–197.

Cattaruzza, F. (2011). Cathepsin S is activated during colitis and causes visceral hyperalgesia by a PAR2-dependent mechanism in mice. Gastroenterology *141*, 1864-1874-e3.

Cavanaugh, D.J., Lee, H., Lo, L., Shields, S.D., Zylka, M.J., Basbaum, A.I., and Anderson, D.J. (2009). Distinct subsets of unmyelinated primary sensory fibers mediate behavioral responses to noxious thermal and mechanical stimuli. Proc. Natl. Acad. Sci. U. S. A. *106*, 9075–9080.

Cesselin, F., Bourgoin, S., Artaud, F., and Hamon, M. (1984). Basic and Regulatory Mechanisms of In Vitro Release of Met-Enkephalin from the Dorsal Zone of the Rat Spinal Cord. J. Neurochem. *43*, 763–774.

Cesselin, F., Le Bars, D., Bourgoin, S., Artaud, F., Gozlan, H., Clot, A.M., Besson, J.M., and Hamon, M. (1985). Spontaneous and evoked release of methionine-enkephalin-like material from the rat spinal cord in vivo. Brain Res. *339*, 305–313.

Cevikbas, F., Wang, X., Akiyama, T., Kempkes, C., Savinko, T., Antal, A., Kukova, G., Buhl, T., Ikoma, A., Buddenkotte, J., et al. (2014). A sensory neuron-expressed IL-31 receptor mediates T helper cell-dependent itch: Involvement of TRPV1 and TRPA1. J. Allergy Clin. Immunol. *133*, 448–460.

Chattopadhyaya, B., Di Cristo, G., Higashiyama, H., Knott, G.W., Kuhlman, S.J., Welker, E., and Huang, Z.J. (2004). Experience and activity-dependent maturation of perisomatic GABAergic innervation in primary visual cortex during a postnatal critical period. J. Neurosci. *24*, 9598–9611.

Clark, A.K. (2007). Inhibition of spinal microglial cathepsin S for the reversal of neuropathic pain. Proc. Natl Acad. Sci. USA *104*, 10655–10660.

Davidson, S., Zhang, X., Yoon, C.H., Khasabov, S.G., Simone, D.A., and Giesler, G.J. (2007). The itch-producing agents histamine and cowhage activate separate populations of primate spinothalamic tract

neurons. J. Neurosci. *27*, 10007–10014.

Davidson, S., Zhang, X., Khasabov, S.G., Simone, D.A., and Giesler, G.J. (2009). Relief of itch by scratching: state-dependent inhibition of primate spinothalamic tract neurons. Nat. Neurosci. *12*, 544–546.

Davidson, S., Zhang, X., Khasabov, S.G., Moser, H.R., Honda, C.N., Simone, D.A., and Giesler, G.J. (2012). Pruriceptive spinothalamic tract neurons: physiological properties and projection targets in the primate. J. Neurophysiol. *108*, 1711–1723.

Deschamps, K. (2011). Genetic and pharmacological evaluation of cathepsin s in a mouse model of asthma. Am. J. Respir. Cell Mol. Biol. *45*, 81–87.

Dong, X., Han, S., Zylka, M.J., Simon, M.I., and Anderson, D.J. (2001). A diverse family of GPCRs expressed in specific subsets of nociceptive sensory neurons. Cell *106*, 619–632.

Duan, B., Cheng, L., Bourane, S., Britz, O., Padilla, C., Garcia-Campmany, L., Krashes, M., Knowlton, W., Velasquez, T., Ren, X., et al. (2014). Identification of spinal circuits transmitting and gating mechanical pain. Cell *159*, 1417–1432.

Dunford, P.J., Williams, K.N., Desai, P.J., Karlsson, L., McQueen, D., and Thurmond, R.L. (2007). Histamine H4 receptor antagonists are superior to traditional antihistamines in the attenuation of experimental pruritus. J. Allergy Clin. Immunol. *119*, 176–183.

Elmariah, S.B., Reddy, V.B., and Lerner, E.A. (2014). Cathepsin S signals via PAR2 and generates a novel tethered ligand receptor agonist. PLoS One *9*, e99702.

Entus, R., Aufderheide, B., and Sauro, H.M. (2007). Design and implementation of three incoherent feed-forward motif based biological concentration sensors. Syst. Synth. Biol. *1*, 119–128.

Fernandes, E.S., Vong, C.T., Quek, S., Cheong, J., Awal, S., Gentry, C., Aubdool, A.A., Liang, L., Bodkin, J. V, Bevan, S., et al. (2013). Superoxide generation and leukocyte accumulation: key elements in the mediation of leukotriene B_4-induced itch by transient receptor potential ankyrin 1 and transient receptor

potential vanilloid 1. FASEB J. *27*, 1664–1673.

Fleming, M.S., Ramos, D., Han, S.B., Zhao, J., Son, Y.-J., and Luo, W. (2012). The majority of dorsal spinal cord gastrin releasing peptide is synthesized locally whereas neuromedin B is highly expressed in pain- and itch-sensing somatosensory neurons. Mol. Pain *8*, 52.

Von frey, M. (1922). Zur Physiologie der Juckempfindung.

Fukushima, T., Tsuda, M., Kofuji, T., and Hori, Y. (2011). Physiological properties of enkephalin-containing neurons in the spinal dorsal horn visualized by expression of green fluorescent protein in BAC transgenic mice. BMC Neurosci. *12*, 36.

Furman, M.I. (2000). The cleaved peptide of PAR1 results in a redistribution of the platelet surface GPIb-IX-V complex to the surface-connected canalicular system. Thromb. Haemost. *84*, 897–903.

Globe, D., Bayliss, M.S., and Harrison, D.J. (2009). The impact of itch symptoms in psoriasis: results from physician interviews and patient focus groups. Heal. Qual. Life Outcomes *7*, 62.

Gomes, L.O., Hara, D.B., and Rae, G.A. (2012). Endothelin-1 induces itch and pain in the mouse cheek model. Life Sci. *91*, 628–633.

Gong, S., Zheng, C., Doughty, M.L., Losos, K., Didkovsky, N., Schambra, U.B., Nowak, N.J., Joyner, A., Leblanc, G., Hatten, M.E., et al. (2003). A gene expression atlas of the central nervous system based on bacterial artificial chromosomes. Nature *425*, 917–925.

Grudt, T.J., and Perl, E.R. (2002). Correlations between neuronal morphology and electrophysiological features in the rodent superficial dorsal horn. J. Physiol. *540*, 189–207.

Gupta, S., Singh, R.K., Dastidar, S., and Ray, A. (2008). Cysteine cathepsin S as an immunomodulatory target: present and future trends. Expert Opin. Ther. Targets *12*, 291–299.

Han, L., Ma, C., Liu, Q., Weng, H.-J., Cui, Y., Tang, Z., Kim, Y., Nie, H., Qu, L., Patel, K.N., et al. (2013). A subpopulation of nociceptors specifically linked to itch. Nat. Neurosci. *16*, 174–182.

Han, S.-K., Mancino, V., and Simon, M.I. (2006). Phospholipase Cbeta 3 mediates the scratching response activated by the histamine H1 receptor on C-fiber nociceptive neurons. Neuron *52*, 691–703.

Han, Z.S., Zhang, E.T., and Craig, A.D. (1998). Nociceptive and thermoreceptive lamina I neurons are anatomically distinct. Nat. Neurosci. *1*, 218–225.

Handwerker, H.O. (1992). Pain and allodynia, itch and alloknesis: An alternative hypothesis. APS J. *1*, 135–138.

Handwerker, H.O., Forster, C., and Kirchhoff, C. (1991). Discharge patterns of human C-fibers induced by itching and burning stimuli. J. Neurophysiol. *66*, 307–315.

Hashimoto, T., Ohata, H., and Momose, K. (2004). Itch-scratch responses induced by lysophosphatidic acid in mice. Pharmacology *72*, 51–56.

Ikoma, A., Steinhoff, M., Ständer, S., Yosipovitch, G., and Schmelz, M. (2006). The neurobiology of itch. Nat. Rev. Neurosci. *7*, 535–547.

Imamachi, N., Park, G.H., Lee, H., Anderson, D.J., Simon, M.I., Basbaum, A.I., and Han, S.-K. (2009). TRPV1-expressing primary afferents generate behavioral responses to pruritogens via multiple mechanisms. Proc. Natl. Acad. Sci. U. S. A. *106*, 11330–11335.

Inaoka, T. (1995). Molecular cloning of human cDNA for cathepsin K: novel cysteine proteinase predominantly expressed in bone. Biochem. Biophys. Res. Commun. *206*, 89–96.

Jacob, C. (2005). Mast cell tryptase controls paracellular permeability of the intestine. Role of protease-activated receptor 2 and beta-arrestins. J. Biol. Chem. *280*, 31936–31948.

Jansen, N.A., and Giesler, G.J. (2015). Response characteristics of pruriceptive and nociceptive trigeminoparabrachial tract neurons in the rat. J. Neurophysiol. *113*, 58–70.

Ji, T.H., Grossmann, M., and Ji, I. (1998). G protein-coupled receptors. I. Diversity of receptor-ligand interactions. J. Biol. Chem. *273*, 17299–17302.

Kaplan, S., Bren, A., Dekel, E., and Alon, U. (2008). The incoherent feed-forward loop can generate non-monotonic input functions for genes. Mol. Syst. Biol. *4*, 203.

Kardon, A.P., Polgár, E., Hachisuka, J., Snyder, L.M., Cameron, D., Savage, S., Cai, X., Karnup, S., Fan, C.R., Hemenway, G.M., et al. (2014). Dynorphin acts as a neuromodulator to inhibit itch in the dorsal horn of the spinal cord. Neuron *82*, 573–586.

Kasraie, S., Niebuhr, M., Baumert, K., and Werfel, T. (2011). Functional effects of interleukin 31 in human primary keratinocytes. Allergy *66*, 845–852.

Kim, Y.S. (2014). Central terminal sensitization of TRPV1 by descending serotonergic facilitation modulates chronic pain. Neuron *81*, 873–887.

Kim, B.M., Lee, S.H., Shim, W.S., and Oh, U. (2004). Histamine-induced Ca(2+) influx via the PLA(2)/lipoxygenase/TRPV1 pathway in rat sensory neurons. Neurosci. Lett. *361*, 159–162.

Kim, D.-K., Kim, H.-J., Kim, H., Koh, J.-Y., Kim, K.-M., Noh, M.-S., Kim, J.-J., and Lee, C.-H. (2008a). Involvement of serotonin receptors 5-HT1 and 5-HT2 in 12(S)-HPETE-induced scratching in mice. Eur. J. Pharmacol. *579*, 390–394.

Kim, H.J., Kim, D.K., Kim, H., Koh, J.Y., Kim, K.M., Noh, M.S., Lee, S., Kim, S., Park, S.H., Kim, J.J., et al. (2008b). Involvement of the BLT2 receptor in the itch-associated scratching induced by 12-(S)-lipoxygenase products in ICR mice. Br. J. Pharmacol. *154*, 1073–1078.

Kim, N., Bae, K.B., Kim, M.O., Yu, D.H., Kim, H.J., Yuh, H.S., Ji, Y.R., Park, S.J., Kim, S., Son, K.-H., et al. (2012). Overexpression of cathepsin S induces chronic atopic dermatitis in mice. J. Invest. Dermatol. *132*, 1169–1176.

LaMotte, R.H., Shimada, S.G., and Sikand, P. (2011). Mouse models of acute, chemical itch and pain in humans. Exp. Dermatol. *20*, 778–782.

LaMotte, R.H., Dong, X., and Ringkamp, M. (2014). Sensory neurons and circuits mediating itch. Nat. Rev.

Neurosci. *15*, 19–31.

Lee, J., Kim, T., Hong, J., Woo, J., Min, H., Hwang, E., Lee, S.J., and Lee, C.J. (2012). Imiquimod enhances excitability of dorsal root ganglion neurons by inhibiting background (K(2P)) and voltage-gated (K(v)1.1 and K(v)1.2) potassium channels. Mol. Pain *8*, 2.

Lembo, P.M. (2002). Proenkephalin A gene products activate a new family of sensory neuron--specific GPCRs. Nat. Neurosci. *5*, 201–209.

Lewis, T., Grant, R.T., and Marvin, H.M. (1927). Vascular reactions of the skin to injury. Part X The intervention of a chemical stimulus illustrated especially by the flare. The response to faradism - Google Search.

Liang, J., Kawamata, T., and Ji, W. (2010). Molecular signaling of pruritus induced by endothelin-1 in mice. Exp. Biol. Med. (Maywood). *235*, 1300–1305.

Lieu, T., Jayaweera, G., Zhao, P., Poole, D.P., Jensen, D., Grace, M., McIntyre, P., Bron, R., Wilson, Y.M., Krappitz, M., et al. (2014). The bile acid receptor TGR5 activates the TRPA1 channel to induce itch in mice. Gastroenterology *147*, 1417–1428.

Liu, Q. (2009). Sensory neuron-specific GPCR Mrgprs are itch receptors mediating chloroquine-induced pruritus. Cell *139*, 1353–1365.

Liu, Q. (2011). The distinct roles of two GPCRs, MrgprC11 and PAR2, in itch and hyperalgesia. Sci. Signal. *4*, ra45.

Liu, Q. (2012). Mechanisms of itch evoked by beta-alanine. J. Neurosci. *32*, 14532–14537.

Liu, T., and Ji, R.-R. (2012). Oxidative stress induces itch via activation of transient receptor potential subtype ankyrin 1 in mice. Neurosci. Bull. *28*, 145–154.

Liu, Q., Tang, Z., Surdenikova, L., Kim, S., Patel, K.N., Kim, A., Ru, F., Guan, Y., Weng, H.-J., Geng, Y., et al. (2009). Sensory neuron-specific GPCR Mrgprs are itch receptors mediating chloroquine-induced

pruritus. Cell *139*, 1353–1365.

Liu, Q., Sikand, P., Ma, C., Tang, Z., Han, L., Li, Z., Sun, S., LaMotte, R.H., and Dong, X. (2012). Mechanisms of itch evoked by β-alanine. J. Neurosci. *32*, 14532–14537.

Liu, T., Xu, Z.-Z., Park, C.-K., Berta, T., and Ji, R.-R. (2010). Toll-like receptor 7 mediates pruritus. Nat. Neurosci. *13*, 1460–1462.

McMahon, S.B., and Koltzenburg, M. (1992). Itching for an explanation. Trends Neurosci. *15*, 497–501.

Melzack, R., and Wall, P.D. (1965). Pain mechanisms: a new theory. Science *150*, 971–979.

Milo, R., Shen-Orr, S., Itzkovitz, S., Kashtan, N., Chklovskii, D., and Alon, U. (2002). Network motifs: simple building blocks of complex networks. Science *298*, 824–827.

Min, H., Lee, H., Lim, H., Jang, Y.H., Chung, S.J., Lee, C.J., and Lee, S.J. (2014). TLR4 enhances histamine-mediated pruritus by potentiating TRPV1 activity. Mol. Brain *7*, 59.

Mishra, S.K., and Hoon, M.A. (2013). The Cells and Circuitry for Itch Responses in Mice. Science (80-.). *340*, 968–971.

Mishra, S.K., Tisel, S.M., Orestes, P., Bhangoo, S.K., Hoon, M.A., Abrahamsen, B., Zhao, J., Asante, C., Cendan, C., Marsh, S., et al. (2011). TRPV1-lineage neurons are required for thermal sensation. EMBO J. *30*, 582–593.

Mohamed, M.M., and Sloane, B.F. (2006). Cysteine cathepsins: multifunctional enzymes in cancer. Nat. Rev. Cancer *6*, 764–775.

Morita, T., McClain, S.P., Batia, L.M., Pellegrino, M., Wilson, S.R., Kienzler, M.A., Lyman, K., Olsen, A.S.B., Wong, J.F., Stucky, C.L., et al. (2015). HTR7 Mediates Serotonergic Acute and Chronic Itch. Neuron *87*, 124–138.

Nakatsuka, T., Ataka, T., Kumamoto, E., Tamaki, T., and Yoshimura, M. (2000). Alteration in synaptic

inputs through C-afferent fibers to substantia gelatinosa neurons of the rat spinal dorsal horn during postnatal development. Neuroscience *99*, 549–556.

Neuman, B., Wiedermann, C.J., Fischer-Colbrie, R., Schober, M., Sperk, G., and Winkler, H. (1984). Biochemical and functional properties of large and small dense-core vesicles in sympathetic nerves of rat and ox vas deferens. Neuroscience *13*, 921–931.

Nicolson, T.A., Bevan, S., and Richards, C.D. (2002). Characterisation of the calcium responses to histamine in capsaicin-sensitive and capsaicin-insensitive sensory neurones. Neuroscience *110*, 329–338.

Norrsell, U., Finger, S., and Lajonchere, C. (1999). Cutaneous sensory spots and the "law of specific nerve energies": history and development of ideas. Brain Res. Bull. *48*, 457–465.

Ochoa, J., and Torebjörk, E. (1989). Sensations evoked by intraneural microstimulation of C nociceptor fibres in human skin nerves. J. Physiol. *415*, 583–599.

Oh, M.-H., Oh, S.Y., Lu, J., Lou, H., Myers, A.C., Zhu, Z., and Zheng, T. (2013). TRPA1-dependent pruritus in IL-13-induced chronic atopic dermatitis. J. Immunol. *191*, 5371–5382.

Patel, K.N., and Dong, X. (2010). An itch to be scratched. Neuron *68*, 334–339.

Prignano, F., Ricceri, F., Pescitelli, L., and Lotti, T. (2009). Itch in psoriasis: epidemiology, clinical aspects and treatment options. Clin. Cosmet. Investig. Dermatol. *2*, 9–13.

Ramachandran, R., and Hollenberg, M.D. (2008). Proteinases and signalling: pathophysiological and therapeutic implications via PARs and more. Br. J. Pharmacol. *153*, S263–S282.

Rawlings, N.D., Barrett, A.J., and Bateman, A. (2012). MEROPS: the database of proteolytic enzymes, their substrates and inhibitors. Nucleic Acids Res. *40*, D343–D350.

Reddy, V.B., and Lerner, E.A. (2010). Plant cysteine proteases that evoke itch activate protease-activated receptors. Br. J. Dermatol. *163*, 532–535.

Reddy, V.B., Iuga, A.O., Shimada, S.G., LaMotte, R.H., and Lerner, E.A. (2008). Cowhage-evoked itch is mediated by a novel cysteine protease: a ligand of protease-activated receptors. J. Neurosci. *28*, 4331–4335.

Reddy, V.B., Shimada, S.G., Sikand, P., Lamotte, R.H., and Lerner, E.A. (2010). Cathepsin S elicits itch and signals via protease-activated receptors. J. Invest. Dermatol. *130*, 1468–1470.

Reddy, V.B., Sun, S., Azimi, E., Elmariah, S.B., Dong, X., and Lerner, E.A. (2015). Redefining the concept of protease-activated receptors: cathepsin S evokes itch via activation of Mrgprs. Nat. Commun. *6*, 7864.

Schmelz, M., Schmidt, R., Bickel, A., Handwerker, H.O., and Torebjork, H.E. (1997). Specific C-Receptors for Itch in Human Skin. J. Neurosci. *17*, 8003–8008.

Schmelz, M., Schmidt, R., Weidner, C., Hilliges, M., Torebjork, H.E., and Handwerker, H.O. (2003). Chemical response pattern of different classes of C-nociceptors to pruritogens and algogens. J. Neurophysiol. *89*, 2441–2448.

Schonefuss, A. (2010). Upregulation of cathepsin S in psoriatic keratinocytes. Exp. Dermatol. *19*, e80–e88.

Shimada, S.G., and LaMotte, R.H. (2008). Behavioral differentiation between itch and pain in mouse. Pain *139*, 681–687.

Shimizu, Y., Morikawa, Y., Okudaira, S., Kimoto, S., Tanaka, T., Aoki, J., and Tokumura, A. (2014). Potentials of the circulating pruritogenic mediator lysophosphatidic acid in development of allergic skin inflammation in mice: role of blood cell-associated lysophospholipase D activity of autotaxin. Am. J. Pathol. *184*, 1593–1603.

Sikand, P., Shimada, S.G., Green, B.G., and LaMotte, R.H. (2009). Similar itch and nociceptive sensations evoked by punctate cutaneous application of capsaicin, histamine and cowhage. Pain *144*, 66–75.

Sikand, P., Dong, X., and LaMotte, R.H. (2011a). BAM8-22 peptide produces itch and nociceptive sensations in humans independent of histamine release. J. Neurosci. *31*, 7563–7567.

Sikand, P., Dong, X., and LaMotte, R.H. (2011b). BAM8-22 peptide produces itch and nociceptive

sensations in humans independent of histamine release. J. Neurosci. *31*, 7563–7567.

Solorzano, C., Villafuerte, D., Meda, K., Cevikbas, F., Bráz, J., Sharif-Naeini, R., Juarez-Salinas, D., Llewellyn-Smith, I.J., Guan, Z., and Basbaum, A.I. (2015). Primary afferent and spinal cord expression of gastrin-releasing peptide: message, protein, and antibody concerns. J. Neurosci. *35*, 648–657.

Spike, R.C., Puskár, Z., Andrew, D., and Todd, A.J. (2003). A quantitative and morphological study of projection neurons in lamina I of the rat lumbar spinal cord. Eur. J. Neurosci. *18*, 2433–2448.

Ständer, S., Weisshaar, E., Mettang, T., Szepietowski, J.C., Carstens, E., Ikoma, A., Bergasa, N. V, Gieler, U., Misery, L., Wallengren, J., et al. (2007). Clinical classification of itch: a position paper of the International Forum for the Study of Itch. Acta Derm. Venereol. *87*, 291–294.

Steinhoff, M., Vergnolle, N., Young, S.H., Tognetto, M., Amadesi, S., Ennes, H.S., Trevisani, M., Hollenberg, M.D., Wallace, J.L., Caughey, G.H., et al. (2000). Agonists of proteinase-activated receptor 2 induce inflammation by a neurogenic mechanism. Nat. Med. *6*, 151–158.

Sun, S., and Dong, X. (2016). Trp channels and itch. Semin. Immunopathol. *38*, 293–307.

Sun, Y.-G., and Chen, Z.-F. (2007). A gastrin-releasing peptide receptor mediates the itch sensation in the spinal cord. Nature *448*, 700–703.

Sun, Y.-G., Zhao, Z.-Q., Meng, X.-L., Yin, J., Liu, X.-Y., and Chen, Z.-F. (2009). Cellular basis of itch sensation. Science *325*, 1531–1534.

Thurmond, R.L., Gelfand, E.W., and Dunford, P.J. (2008). The role of histamine H1 and H4 receptors in allergic inflammation: the search for new antihistamines. Nat. Rev. Drug Discov. *7*, 41–53.

Todd, A.J. (2010). Neuronal circuitry for pain processing in the dorsal horn. Nat. Rev. Neurosci. *11*, 823–836.

Todd, A.., Spike, R.., and Polgár, E. (1998). A quantitative study of neurons which express neurokinin-1 or somatostatin sst2a receptor in rat spinal dorsal horn. Neuroscience *85*, 459–473.

Todd, A.J., Spike, R.C., Russell, G., and Johnston, H.M. (1992). Immunohistochemical evidence that Met-enkephalin and GABA coexist in some neurones in rat dorsal horn. Brain Res. *584*, 149–156.

Trentin, P.G., Fernandes, M.B., D'Orléans-Juste, P., and Rae, G.A. (2006). Endothelin-1 causes pruritus in mice. Exp. Biol. Med. (Maywood). *231*, 1146–1151.

Tsvetanova, N.G., Irannejad, R., and von Zastrow, M. (2015). G protein-coupled receptor (GPCR) signaling via heterotrimeric G proteins from endosomes. J. Biol. Chem. *290*, 6689–6696.

Tuckett, R.P. (1982). Itch evoked by electrical stimulation of the skin. J. Invest. Dermatol. *79*, 368–373.

Usoskin, D., Furlan, A., Islam, S., Abdo, H., Lönnerberg, P., Lou, D., Hjerling-Leffler, J., Haeggström, J., Kharchenko, O., Kharchenko, P. V, et al. (2014). Unbiased classification of sensory neuron types by large-scale single-cell RNA sequencing. Nat. Neurosci. *18*, 145–153.

Vilardaga, J.P., Jean-Alphonse, F.G., and Gardella, T.J. (2014). Endosomal generation of cAMP in GPCR signaling. Nat. Chem. Biol. *10*, 700–706.

Viode, C. (2014). Cathepsin S, a new pruritus biomarker in clinical dandruff/seborrhoeic dermatitis evaluation. Exp. Dermatol. *23*, 274–275.

Vong, L., Ye, C., Yang, Z., Choi, B., Chua, S., and Lowell, B.B. (2011). Leptin action on GABAergic neurons prevents obesity and reduces inhibitory tone to POMC neurons. Neuron *71*, 142–154.

Vu, T.K., Hung, D.T., Wheaton, V.I., and Coughlin, S.R. (1991). Molecular cloning of a functional thrombin receptor reveals a novel proteolytic mechanism of receptor activation. Cell *64*, 1057–1068.

Wall, P.D. (1978). The gate control theory of pain mechanisms. A re-examination and re-statement. Brain *101*, 1–18.

Wang, S., Dai, Y., Fukuoka, T., Yamanaka, H., Kobayashi, K., Obata, K., Cui, X., Tominaga, M., and Noguchi, K. (2008). Phospholipase C and protein kinase A mediate bradykinin sensitization of TRPA1: a molecular mechanism of inflammatory pain. Brain *131*, 1241–1251.

Wickersham, I.R., Lyon, D.C., Barnard, R.J.O., Mori, T., Finke, S., Conzelmann, K.-K., Young, J.A.T., and Callaway, E.M. (2007). Monosynaptic restriction of transsynaptic tracing from single, genetically targeted neurons. Neuron *53*, 639–647.

Wilson, S.R. (2013). The epithelial cell-derived atopic dermatitis cytokine TSLP activates neurons to induce itch. Cell *155*, 285–295.

Wilson, S.R., Gerhold, K.A., Bifolck-Fisher, A., Liu, Q., Patel, K.N., Dong, X., and Bautista, D.M. (2011). TRPA1 is required for histamine-independent, Mas-related G protein-coupled receptor-mediated itch. Nat. Neurosci. *14*, 595–602.

Wilson, S.R., Thé, L., Batia, L.M., Beattie, K., Katibah, G.E., McClain, S.P., Pellegrino, M., Estandian, D.M., and Bautista, D.M. (2013). The epithelial cell-derived atopic dermatitis cytokine TSLP activates neurons to induce itch. Cell *155*, 285–295.

Yamaguchi, T., Nagasawa, T., Satoh, M., and Kuraishi, Y. (1999). Itch-associated response induced by intradermal serotonin through 5-HT2 receptors in mice. Neurosci. Res. *35*, 77–83.

Zania, P. (2009). Parstatin, the cleaved peptide on proteinase-activated receptor 1 activation, is a potent inhibitor of angiogenesis. J. Pharmacol. Exp. Ther. *328*, 378–389.

Zhao, P. (2014). Cathepsin S causes inflammatory pain via biased agonism of PAR2 and TRPV4. J. Biol. Chem. *289*, 27215–27234.

SHUOHAO SUN

725 North Wolfe Street | Department of Neuroscience | ssun10@jhmi.edu

WBSB 908, Baltimore, MD, 21205 | Johns Hopkins University | 443-562-1484

EDUCATION

Johns Hopkins University, Baltimore, MD

PhD in Neuroscience 2010 - Present

- Thesis Advisor: Dr. Xinzhong Dong
  Professor, Johns Hopkins University School of Medicine

  Investigator, Howard Hughes Medical Institute

  E-mail: xdong2@jhmi.edu

Tsinghua University, Beijing, China

Bachelor of Science, Biology 2006 - 2010

RESEARCH EXPERIENCE

Graduate Research Projects

- Coding of pain and itch in the spinal cord: a small subset of spinal interneurons positively codes for itch, while forms a leaky gate to negatively regulate pain transmission. These neurons pass through weak pain signals to ensure pain sensitivity, while close the "gate" to strong painful stimuli with endogenous opioids to prevent overwhelming pain responses.
- Proteases induced itch: proteases induce itch by direct proteolytic cleavage and activation of G protein coupled receptors, Mrgprs.

Undergrad Research Project

- Visual memory and working memory in drosophila

RESEARCH SKILLS

Molecular biology, Mouse genetics, Calcium imaging, Mouse behavior, ChR2 assisted circuit mapping, rabies viral circuit tracing, Electrophysiology

TEACHING EXPERIENCE

School of Medicine, **Johns Hopkins University, Baltimore, MD**

Teaching Assistant **(**2014)

- Nervous Systems and Special Senses (neuroanatomy course for medical students)

HONORS & AWARDS

William and Mary Drescher Endowment Fund for Graduate Medical Research, Johns Hopkins University 2011

National Scholarship for Academic Performance, The Government of China
2007 - 2009

Scholarship for social work, Tsinghua University
2008

PUBLICATIONS

Sun S, Dong X. (2015) Trp channels and itch. Seminars in immunopathology, 1-15.

Reddy VB*, **Sun S***, Azimi E, Elmariah SB, Dong X, Lerner EA. (2015) Redefining the concept of protease-activated receptors: cathepsin S evokes itch via activation of Mrgprs. Nature communications, 6:7864. **contributed equally to this work*.

Kim YS, Chu Y, Han L, Li M, Li Z, Lavinka PC, **Sun S**, Tang Z, Park K, Caterina MJ, Ren K, Dubner R, Wei F, Dong X. (2014) Central terminal sensitization of TRPV1 by descending serotonergic facilitation modulates chronic pain. Neuron, 81(4):873-87.

Liu Q, Sikand P, Ma C, Tang Z, Han L, Li Z, **Sun S**, LaMotte RH, Dong X. (2012) Mechanisms of itch evoked by β-alanine. J Neurosci.3509-12.